AFGL-TR-79-0236

LEVEL II

12

ADAPTIVE HF PROPAGATION PATH UTILIZATION

A.K. Gupta
M.D. Grossi

Smithsonian Astrophysical Observatory
60 Garden Street
Cambridge, Massachusetts 02138

Final Report
11 June 1979 - 30 September 1979

30 June 1980

Approved for public release; distribution unlimited

AIR FORCE GEOPHYSICS LABORATORY
AIR FORCE SYSTEMS COMMAND
UNITED STATES AIR FORCE
HANSCOM AFB, MASSACHUSETTS 01731

Unclassified

SECURITY CLASSIFICATION OF THIS PAGE (When Data Entered)

REPORT DOCUMENTATION PAGE

READ INSTRUCTIONS BEFORE COMPLETING FORM

1. REPORT NUMBER	2. GOVT ACCESSION NO.	3. RECIPIENT'S CATALOG NUMBER
AFGL-TR-79-0236	AD-A090 023	

4. TITLE (and Subtitle)

ADAPTIVE HF PROPAGATION PATH UTILIZATION

5. TYPE OF REPORT & PERIOD COVERED

Final Report
June 11, 1979–Sept. 30, 1979

6. PERFORMING ORG. REPORT NUMBER

7. AUTHOR(s)

A. K. Gupta
M. D. Grossi

8. CONTRACT OR GRANT NUMBER(s)

F19628-79-C-0137

9. PERFORMING ORGANIZATION NAME AND ADDRESS

Smithsonian Astrophysical Observatory
60 Garden Street
Cambridge, MA 02138

10. PROGRAM ELEMENT, PROJECT, TASK AREA & WORK UNIT NUMBERS

62101F
464304CF

11. CONTROLLING OFFICE NAME AND ADDRESS

Air Force Geophysics Laboratory
Hanscom AFB, Massachusetts 01731
Monitor/Richard S. Allen/PHP

12. REPORT DATE

30 June 1980

13. NUMBER OF PAGES

108

14. MONITORING AGENCY NAME & ADDRESS (if different from Controlling Office)

Final Rept.
11 Jun 79 - 30 Sep 79

15. SECURITY CLASS. (of this report)

Unclassified

15a. DECLASSIFICATION/DOWNGRADING SCHEDULE

16. DISTRIBUTION STATEMENT (of this report)

Approved for public release; distribution unlimited.

17. DISTRIBUTION STATEMENT (of the abstract entered in Block 20, if different from Report)

18. SUPPLEMENTARY NOTES

19. KEY WORDS (Continue on reverse side if necessary and identify by block number)

Adaptive communications
Adaptive HF
Ionospheric link
Spread-spectrum communications
Adaptive signalling
Time and frequency spread channels
Adaptivity
Diversity
Coding

20. ABSTRACT (Continue on reverse side if necessary and identify by block number)

Detailed knowledge of the characteristics of HF propagation paths is an essential requirement to a better utilization of these paths in reliable communications.

Recent advances in HF path characterization as well as in communication equipment, coding schemes, and microprocessor technology make it possible to conceive approaches of adaptive utilization of HF propagation that promise

DD FORM 1 JAN 73 1473 EDITION OF 1 NOV 65 IS OBSOLETE

Unclassified

SECURITY CLASSIFICATION OF THIS PAGE (When Data Entered)

20. Abstract (Continued)

a substantial improvement upon present-day HF circuit performance.

This recently acquired expertise includes the following advances:

a) better understanding of the multipath spread and Doppler spread characteristics of HF propagation paths in several path configurations (midlatitude paths, transequatorial paths, transauroral paths, etc.);

b) availability of frequency-agile HF transmitters and receivers;

c) Availability of high-speed sounding techniques, such as the digisonde approach;

d) availability of microprocessor logics for real-time evaluation of channel performance, for making decisions on the required diversity and for carrier frequency selection;

e) availability of coding schemes, such as the M-ary codes, that maximize the data rate for the selected signalling approach.

This report illustrates an adaptive method that makes it possible to transmit a data rate of 24 kilobits/sec with an error rate of 10^{-4} (therefore suitable for high-quality digital voice) in a single-hop ionospheric path established in midlatitude or across the aurora belt.

The proposed adaptive approach is based on path sounding, channel probing, FSK or MFSK signalling, and waveform diversity, with the sounding and probing functions used to provide the initial information for the working of the adaptivity control loops.

Preface

This report is submitted to the USAF Electronic Systems Division in fulfillment of the obligations of the Smithsonian Astrophysical Observatory (SAO) on Contract F19628-79-C-0137.

This report illustrates the study activity on adaptive utilization of HF propagation paths performed under USAF-ESD sponsorship by SAO scientists Dr. Mario D. Grossi, Principal Investigator, and by Dr. Ashok K. Gupta.

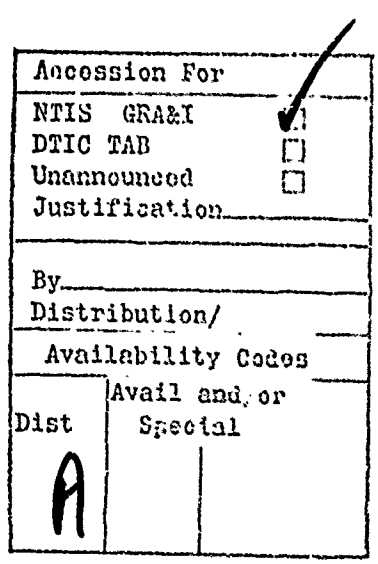

Contents

Contents

Illustrations

Contents

Illustrations

Tables

Adaptive HF Propagation Path Utilization

1. INTRODUCTION

HF propagation paths are time-spread and frequency-spread channels, and are characterized by severe variability in the time domain of all their properties, inclusive of path losses.

Improvements over a present-day HF link's performance in terms of circuit reliability, data rate, and error rate can be achieved only through the use of adaptive schemes that in principle appear to be able to cope with the channel variability, if the necessary penalty in terms of equipment complexity is willingly accepted.

Real-time oblique ionospheric sounding between the two terminals of the link and the channel probing simultaneously performed between them are the data-gathering operations that provide the inputs on which to base the adaptive control of the link's performance parameters.

For the sake of illustration, we have assumed in this report that the link has 1125 to 3375 carriers, respectively for a midlatitude and a transauroral path, available in the HF band between 3 MHz and 30 MHz.

A sounding scan lasts 100 to 160 seconds and is repeated every 300 to 480 seconds. The master station of the link, where the sounding transmitter is located, also generates the waveform for channel probing and includes a complete

(Received for publication

terminal for two-way digital communications. During the pauses of the emissions, measurements of noise and interference levels are performed at both the master and the slave station of the link, for use by decision-making microprocessors and control units. At each terminal, the transmitting and the receiving facility could have separate units for sounding/probing and for communicating, or these functions could be performed by the same equipment in different modes of operation. In the latter case, the equipment at the two terminals could be identical and the assignment of the master and slave roles would be dictated by operational requirements.

By processing the data obtained by sounding and probing, it will be possible to select automatically the group of frequencies to be used for communicating. At each sounding cycle, information about the frequency selection and about the waveform to be employed is exchanged between terminals and used locally to achieve adaptivity. During the next sounding scan (they are performed at a rate of one every 5 to 8 minutes) the group of frequencies that were selected for communicating are excluded from the sounding frequency plan. Instead, information on the changing status of the group of communicating frequencies is obtained from measurements performed on the coded waveform that is part of the communications bit stream.

2. TECHNICAL DISCUSSION

2.1 General

During the course of this study we have evaluated two basic configurations for the link:

1. a two-way, high-data-rate, high-capacity, adaptive exchange between the two terminals of the HF link, with adaptivity based on path sounding and channel probing, with feedback acknowledgement;

2. a one-way link for relatively reliable information transfer, although characterized by lack of feedback acknowledgement and lack of adaptivity.

In this report, Configuration 1 is illustrated in more detail. Configuration 2 is treated in Section 2.7, as an application of M-ary codes with a large value of M.

2.2 Pertinent Properties of HF Ionospheric Propagation Paths

2.2.1 GENERAL REMARKS

The HF propagation paths of interest in this study are single-hop paths established in midlatitude or across the auroral zone. The properties of interest are:

1. path losses;
2. noise and interference spectral density;
3. multipath spread;
4. Doppler spread.

Of these properties, it would be relevant to know accurately the time variability and the related statistics. Unfortunately, this is known only in particular cases, so that a reliable experimental investigation on the properties above is thus far an unfulfilled requirement. In general, we can say that these ionospheric channels exhibit time fadings that are important in determining the design of the signal and, in addition, show long-term variations due to large-scale fluctuations of the medium. Such slow effects have a time constant significantly greater than 5 to 10 minutes, an interval of time selected (as will be seen in the following sections) as the basic sounding/probing periodicity. Adaptive approaches to the communication problem are required to circumvent this long-term variability in propagation conditions.

In this study, we will make the usual distinction between path sounding and channel probing, with the former devoted to the measurement of path losses and of noise and interference levels, and with the latter devoted to measurement of such parameters as multipath spread and Doppler spread. The following criteria were adopted in our study:

1. The link is assumed reciprocal, except for the noise and interference levels at each terminal. Therefore, the decision on the frequencies to be used (this decision is the output of the sounding operation) is based on the measurement of interference and noise both at the master and at the slave station, and on the one-way measurement of the path losses between the two.

2. Processing of multipath spread and Doppler spread (the basic operation of the channel probing activity) is performed at the slave station and the results are transmitted back to the master station, for use in the final selection of the frequencies to be used in communicating.

3. Channel probing is to be undertaken only at the best frequencies put in evidence by the path sounding, in order to shorten the overall cycle sounding/probing.

2.2.2 HF IONOSPHERIC PATHS CHARACTERIZATION AND MEASUREMENT

2.2.2.1 General Considerations

Due to the propagation mechanism of radio waves in the ionosphere, various mathematical models can be formulated to identify its measureable parameters. These models (or characterization) are also useful in selecting measurement techniques for the channel parameters. The selection of channel parameters itself depends upon the particular application and upon the receiver structure. In

Section 2.2.2.6, we have summarized the general principles involved in randomly modeling time-variant channels. These models are the multipath transmission models and the composite filter models. The two types of models may be distinguished initially. A "multipath transmission" view is suggested by identifiable mechanisms or "paths" of propagation between input and output terminals The "composite-filter" view is a view whereby channel output is related to input by means of a linear mathematical operation involving a suitably defined system function.

The HF ionospheric channel, by virtue of energy propagating over many paths of different propagation delays, exhibits time dispersion (or frequency selective fading), and by virtue of time variations of individual phase-path lengths, exhibits frequency dispersion (or time-selective fading).

For most communication problems, it is usually valid to assume that the channel is linear, with nonlinear effects, if any, being relatively negligible. This suggests modeling the channel as a time-variant linear (TVL) filter in terms of a time-variant transfer function.

2.2.2.2 The Basic Signal Models Employed in the HF Channel Characterization (Multipath View)

These can be described as linear combinations of the responses of three types of propagation paths; namely,

1. the ground-wave propagation as modeled by a steady specular path.
2. a random scatter mechanism of propagation as generally modeled by a diffuse path.
3. long-term variabilities of ionospheric paths, often as simulated by a quasi-specular model which is characterized by a log-normal envelope and Gaussian phase probability density functions. In quasi-specular type of propagation, the observed fluctuations in envelope and phase are caused by fluctuating attenuation and electric path length over the traversed path.

The output of a given medium may actually consist of a linear combination of non-diffuse and diffuse components, and different combinations may be necessary to describe the output of the same medium at different times. For example, the sum of a few quasi-specular paths, each of which fluctuates slowly relative to the fluctuations of the resultant signal, is modeled by a sample function of a Gaussian process plus a specular component. Such a combination may be encountered over HF links.

The representation of a channel output in terms of a linear combination of non-diffuse and diffuse signal models with stationary statistics transforms the characterization of the channel into the specification of:

1. A multipath structure,

2. The relative intensities, and average delay and Doppler differences of the various distinguishable paths,

3. The statistical characteristics of individual path delays and delay spread, and path Doppler shifts and Doppler spread.

4. The constitution and properties of the fine structure of each distinguishable path (that is, its possible decomposition into the sum of non-diffuse (specular or quasi-specular) and diffuse components) including the relative characteristics of the components, and the statistical properties of their parameters.

When modeled by a "composite filter", the variable multipath nature of the propagation process over HF channels causes a number of effects of great importance in the evaluation of the signal transmission performance of the "equivalent" filter.

First, the group delay differences among the various paths cause the overall channel-composite filter attenuation and delay characteristics to vary with frequency. If the delay spread of the significant paths is not a very small fraction of the reciprocal of the bandwidth occupied by the signal, the various components of the signal will experience non-uniform attenuation and delay, which results in signal waveform distortion. The characteristics of this distortion will be random for a randomly time-variant linear channel.

Second, the fluctuations in the relative characteristics of the various paths cause each frequency component in the signal to acquire a modulation of envelope and phase (and, hence, frequency). This multipath-induced modulation causes the signal level to fluctuate up and down, which raises the possibility of signal outages or dropouts, each resulting from a "fade" or drop of the received-signal strength below the threshold of acceptable performance in the presence of independent additive disturbances. In addition, a non-zero delay spread among the various paths limits the bandwidth over which the fluctuations experienced by signal components at different frequencies will maintain the necessary degree of mutual coherence to keep the resultant signal distortion below tolerable bounds.

Finally, the fluctuation rate induced by the channel in a particular parameter of the carrier sets a non-zero limit on the frequency content in the baseband spectrum that can be used to modulate that particular carrier parameter if interference between the channel fluctuations and the desired signal baseband waveform is to remain negligible.

If the "composite" filter model is used, the time, frequency and/or statistical behavior of a channel-characteristic system function offers the basis for the definition of the gross parameters for describing the gross aspects of the channel response. The gross transmission parameters of principal importance in characterizing the effects of a randomly time-variant medium upon broad classes of

signals are discussed in Section 2.2.2.7. In the next section, we will first discuss the system functions for fading dispersive linear channels (or randomly time-variant channels), then we will outline in Section 2.4, the measurement techniques of the gross transmission parameters summarized in Section 2.2.2.7.

2.2.2.3 System Functions for Fading Dispersive Linear Channels

The system functions for radio channels have been extensively studied in the past[1, 2, 3, 4, 5, 6]. Below we will briefly summarize the results in a way as to identify important channel parameters.

Radio channels can generally be represented by randomly time-variant linear (RTVL) filters. System functions can then be defined for representing RTVL channels in the same manner as is done with other types of linear filters. There are four ways in which the output of this filter y(t) or its Fourier transforms $Y(j\omega)$ can be expressed in terms of the input x(t) or $X(j\omega)$; namely

y(t) in terms of an operation on x(t)

y(t) in terms of an operation on $X(j\omega)$

$Y(j\omega)$ in terms of an operation on x(t)

$Y(j\omega)$ in terms of an operation on $X(j\omega)$.

The required expressions are given in Table 1, where $h(t, \xi)$ is also called a delay-spread function and $H(j\omega, t)$ is the Fourier transform of $h(t, \xi)$. In the treatment of a channel as a signal-distorting filter with randomly time-variant characteristic parameters, extremely useful analytical and structural models can be deduced (as for a time-variant linear filter) by examining the consequences of the dependence of $h(t, \xi)$ upon ξ and/or of $H(j\omega, t)$ upon ω, holding t fixed. Therefore, in the subsequent discussion, t will be dropped. Based upon these two approaches (time and frequency domain approximation) two different representations of the signal-distorting medium have been developed by the investigators. These are the sampling model of a signal-distorting filter and the paired-echo model.

---

1. Baghdady, E.J. (1969) Principles of simulation of randomly time-varying channels, IEEE International Conference Communications, Boulder, Colorado, June 9-11, pp. 40-3 to 40-18.

2. Price, R. and Green, P.E. (1958) A communication technique for multipath channels, Proc. IRE, pp. 555-570.

3. Kailath, T. (1959) Sampling Models for Linear Time-Variant Filters, MIT-RLE Report No. 352, Cambridge, Mass.

4. Daly, R.F. (1964) On the Modeling of Time-Varying Frequency-Selective Radio Channels, SRI Project No. 4172, Contract DA 36-039SC-90859.

5. Esposito, R. and Grossi, M.D. (1971) Channel Characterization for Digital Communications in Ground-to-Space HF Paths, 11th Technical Meeting of the Joint Satellite Study Group (JSSG), Florence, Italy, October 4-9.

6. Grossi, M.D. (1971) Experimental HF Back-Up/Emergency Communications System for Space Shuttle/Space Station, Raytheon Prop. ER70-4333.

Table 1. System Parameters

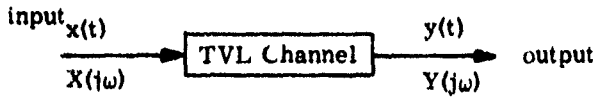

1. Time-smear, or multipath-spread function, $h(t, \xi)$

$$y(t) = \int_{-\infty}^{+\infty} x(t - \xi)\, h(t, \xi)\, d\xi$$

= Σ responses to variously delayed and weighted replicas of x(t).

2. Frequency-smear, or Doppler-spread function $M(\omega, \xi)$

$$Y(j\omega) = \int_{-\infty}^{+\infty} X(j\omega - j\xi)\, M(\omega, \xi)\, d(\xi/2\pi)$$

= Σ responses to variously frequency-shifted and weighted replicas of $X(j\omega)$.

3. Time-dependent, frequency selective function, $H(j\omega, t)$

$$y(t) = \int_{-\infty}^{+\infty} X(j\omega)\, H(j\omega, t)\, e^{j\omega t}\, d(\omega/2\pi)$$

= Σ responses to $X(j\omega)\, e^{j\omega t}$ time components.

4. Frequency-dependent, time-selective function $m(t, \omega)$

$$Y(j\omega) \int_{-\infty}^{+\infty} x(t)\, m(t, \omega)\, e^{-j\omega t}\, dt$$

= Σ responses to $x(t)\, e^{-j\omega t}$ frequency components

2.2.2.4 Sampling Model

Restriction[1] of the frequency range of interest in the analysis of a filter response can be interpreted as equivalent to replacing the actual filter by the same filter in cascade with a rectangular filter, as shown in Figure 1. The frequency-response function $H(j\omega)$ of the filter is thus replaced by $H(j\omega)p_{rect,\,\Omega_x}(\omega)$, where $p_{rect,\,\Omega_x}(\omega)$ represents the rectangular amplitude characteristic shown in Figure 1. The resulting amplitude characteristic is of course strictly physically unrealizable and hence the corresponding models may not be strictly physically realizable. However, in practice, this need not cause any difficulty because of approximations in the necessary number of paths in the model.

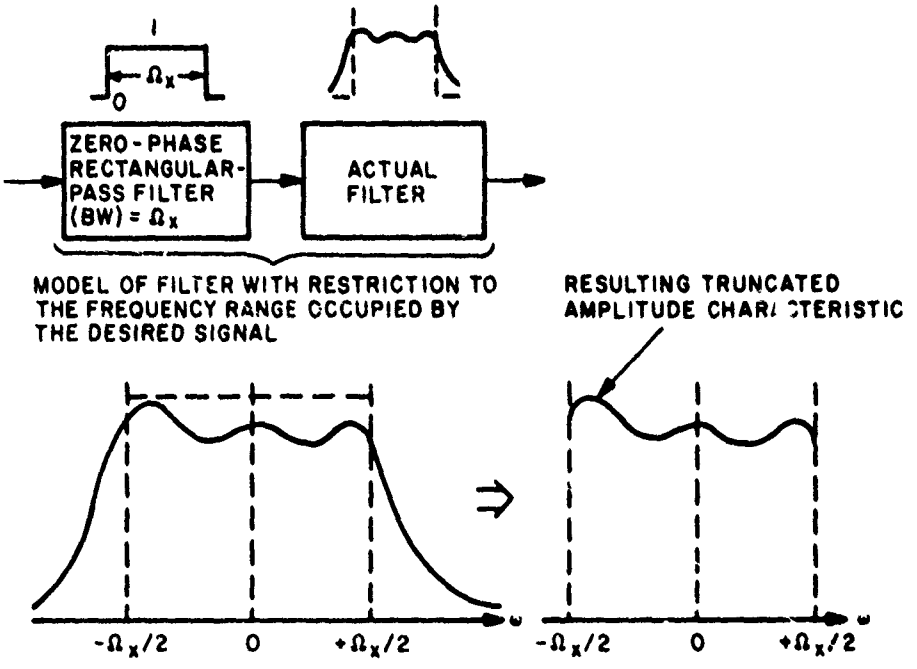

Figure 1. Truncation of a Filter Transfer Function by Restriction of the Input Spectrum to the Range Occupied by the Input Signal

We now observe that since the model frequency-response function, $H(j\omega)$ $p_{rect,\,\Omega_x}(\omega)$ is zero for $|\omega| > \Omega_x/2$, its inverse Fourier transform (by the sampling theorem) can be expressed as

$$h_{model}(t) \sum_{n=-\infty}^{\infty} h_{model}\left(n\,\frac{2\pi}{\Omega_x}\right) \frac{\sin\left[\left(\frac{\Omega_x}{2}\right)\left(t - \frac{n2\pi}{\Omega_x}\right)\right]}{\left(\frac{\Omega_x}{2}\right)t - n2\pi/\Omega_x)} \qquad (1)$$

This suggests the parallel-path representation shown in Figure 2. For a finite number of paths all with positive delays, the filter can also be modeled by a tapped delay line preceded by a rectangular filter as shown in Figure 3. The path gains, and hence the tap gains, are determined from

$$h_{model}(t) = \frac{\Omega_x}{2\pi} h(\tau) \frac{\sin\left(\frac{\Omega_x}{2}\right)\tau}{\left(\frac{\Omega_x}{2}\right)\tau} \tag{2}$$

by taking sample values spaced uniformly $2\pi/\Omega_x$ seconds apart.

2.2.2.5 Paired-Echo Model

In practical applications, one is usually concerned with how well the actual filter characteristics can be approximated by a given number of paths, or "taps", in the parallel-path or tapped delay-line model. To minimize the number of taps required, Baghdady[1] proposed the paired-echo model which approximates the system function in frequency domain. This approximation determines the number of necessary paths and the explicit interrelations among the tap gains. This is in contrast to the sampling approach where the approximation is made in the time domain with no explicit quantitative indication of how well the result approximates the frequency-domain characteristics. The paired-echo model, discussed below, is of practical value in computations of distortion only when the number of parallel signal paths in the resulting model is not too large. The method also becomes impractical if the nonlinearity of the phase characteristic is quite severe.

In the paired-echo approach, the starting point is $H(j\omega)$ which is the low-pass analog of the bandpass filter relative to the reference frequency of the signal. For convenience, let

$$H(j\omega) = A(\omega)\, e^{-j\phi(\omega)} \tag{3}$$

where $A(\omega)$ and $\phi(\omega)$ are both real functions of ω, known respectively as the amplitude and phase characteristics of the filter. As is well-known, the filter does not introduce signal distortion if $A(\omega)$ is constant and $\phi(\omega)$ is linear over the frequency range occupied by the input-signal spectrum. Distortion results from departures in $A(\omega)$ and/or $\phi(\omega)$ from these conditions. These deviations $A(\omega) - A(o)$ and $\phi(\omega) - \omega\tau_{gd}(o)$ may be expressed as the sums of approximately chosen and weighted trigonometric terms within the frequency range occupied by the signal spectrum in Fourier series. Thus, if W denotes the width of the band occupied by the input signal, then one can write

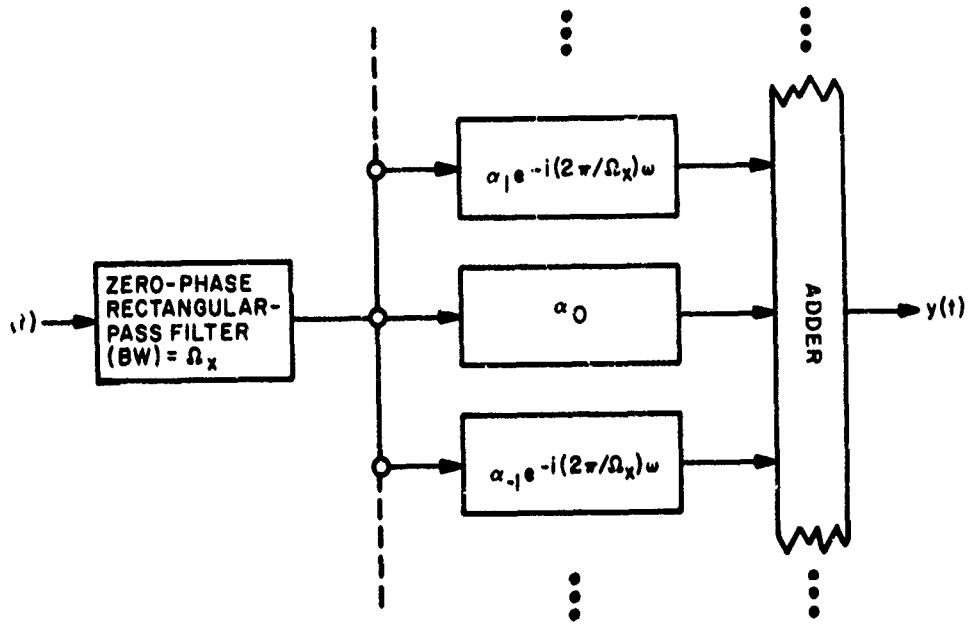

Figure 2. Parallel-Path Representation of $h_{model}(t)$

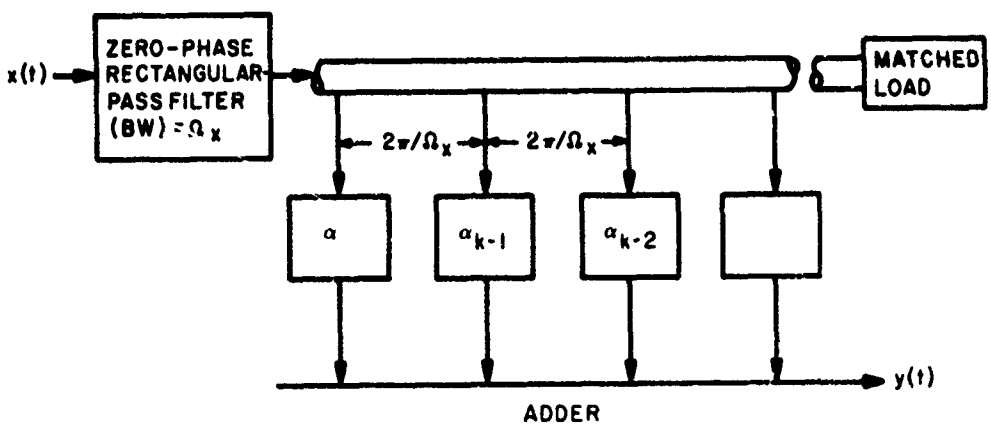

Figure 3. Tapped Delay-Line Representation of $h_{model}(t)$

$$A(\omega) - A(o) = \sum_{\substack{n=-\infty \\ n\neq o}}^{\infty} a_n e^{jn(2\pi/W)\omega} \tag{4}$$

and

$$\phi(\omega) - \omega\tau_{gd}(o) = \sum_{\substack{m=-\infty \\ m\neq o}}^{\infty} b_m e^{jm(2\pi/W)\omega} = \sum_{m=1}^{\infty} C_m \sin\left[m\left(\frac{2\pi}{W}\right)\omega + \vartheta_m\right] \tag{5}$$

where we have set $|b_m| \triangleq C_m$ and $\vartheta_m \triangleq \measuredangle b_m + \pi/2$. The Fourier coefficients a_n and b_m are obtained in the usual manner with W as the basic averaging interval.

Using the Fourier expansions of Eqs. (4) and (5), we can write from Eq. (3)

$$H(j\omega) = \left[A(o) + \sum_{n=-\infty}^{\infty} a_n e^{jn(2\pi/W)\omega}\right]\left\{\prod_{m=1}^{\infty} e^{-jC_m \sin[m(2\pi/W)\omega + \vartheta_m]} \cdot e^{-j\omega\tau_{gd}(o)}\right\} \qquad \text{for } |\omega| \leq \frac{W}{2} \tag{6}$$

Each term in the product within braces can in turn be expanded in an infinite series as

$$e^{-jC_m \sin[m(2\pi/W)\omega + \vartheta_m]} = \sum_{k=-\infty}^{\infty} J_k(C_m)\, e^{-jK[m(2\pi/W)\omega + \vartheta_m]} \tag{7}$$

where $J_k(C_m)$ is the Bessel function of the first kind, order K, and argument C_m. From Eqs. (6) and (7) and collecting terms having identical exponentials, we obtain

$$H(j\omega) = e^{-j\omega\tau_{gd}(o)} \sum_{K=-\infty}^{\infty} |\alpha_K|\, e^{j[K(2\pi/W)\omega + \measuredangle \alpha_K]} \tag{8}$$

where α_K is a complex coefficient. Various mathematical models from Eqs. (6) and (8) can be obtained. In Figure 4, we have shown a model, derived from Eq. (8), which connects the input and output terminals by a multiplicity of parallel

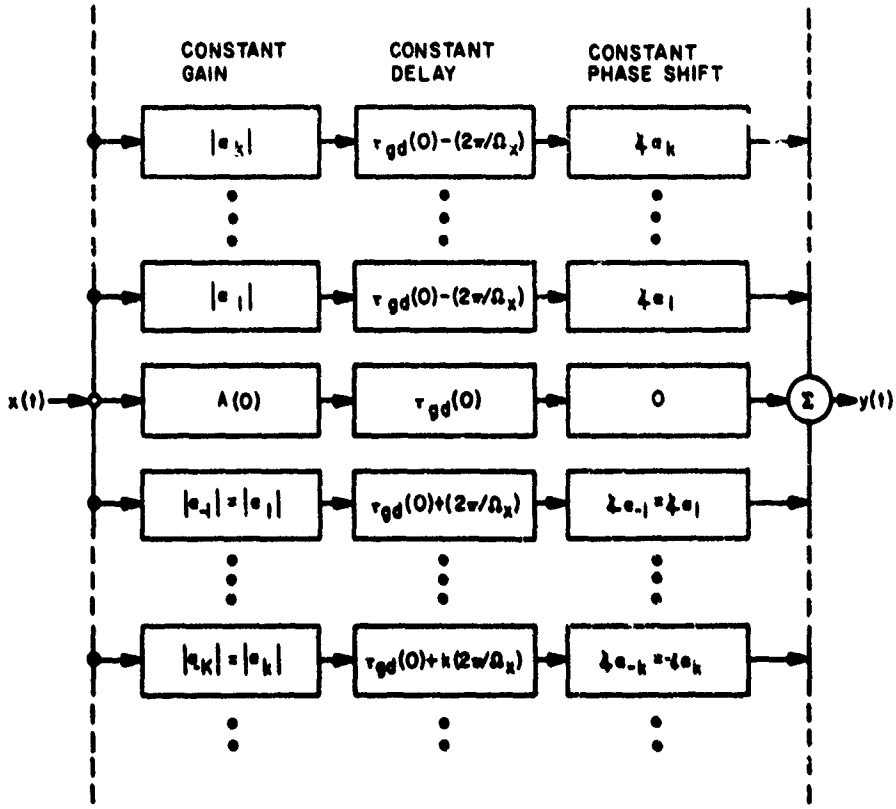

Figure 4. Block Diagram Representation of $H(j\omega)$

branches, each providing a separate transmission path for the signal between input and output. The individual paths pass the signal without distortion; only pure delays and constant attenuation and carrier-reference phase shifts are introduced. It is also important to note the symmetry of paths about K = 0; that is, the paths for +K and -K have conjugate complex transmission "gains", but the delay of the +K path exceeds $\tau_{gd}(o)$ by the same amount that the delay of the -K path is less than $\tau_{gd}(o)$. Symmetrical path pairs about the K = o are thus said to contribute "paired echoes"[1, 7] of the input signal in the output. Each trigonometric term in the expansion for $A(\omega)$ contributes, in the absence of any distortion from $\phi(\omega)$, only one pair of echoes, a precursory echo (corresponding to (+)ve n in Eq. (4)) and a successory echo (for (-)ve n in Eq. (4)). But in the expansion of $\phi(\omega)$ in Eq. (6), each term gives rise to an infinite number of uniformly spaced precursory and

---

7. Bello, P.A. and Esposito, R. (1970) Measurement techniques for time-varying dispersive channels, Alta Frequenza, No. II, Vol. XXXIX, pp. 980-996.

successory echoes. From Eq. (8) and Figure 4, the quantity $\tau_{gd}(o) - K(2\pi/W)$ will become negative for $K > W\,\tau_{gd}(o)/2\pi$, unless $\tau_{gd}(o)$ (the slope of $\phi(\omega)$ at $\omega = o$) is infinite. The representation in Figure 4 therefore is a physically unrealizable structure. Therefore, Fourier expansions of $A(\omega) - A(o)$ and $\phi(\omega) - \omega\,\tau_{gd}(o)$ that converge rapidly are of course most desirable from the viewpoint of truncation of the series to fewer terms. Filters with very smooth and low ripple in $A(\omega)$ and $\phi(\omega)$ may also be represented by a much smaller number of pure-delay, all-pass paths. When the number of parallel paths in Figure 4, or in the model for Figure 5, is finite and the corresponding delays are all positive, the signal-distorting filter model can also be redrawn in terms of a tapped delay line as shown in Figure 6. Such a model may be physically conceived to consist of a lossless delay line with taps whose number and spacing are chosen equal to the number and delay differences of the parallel-path model.

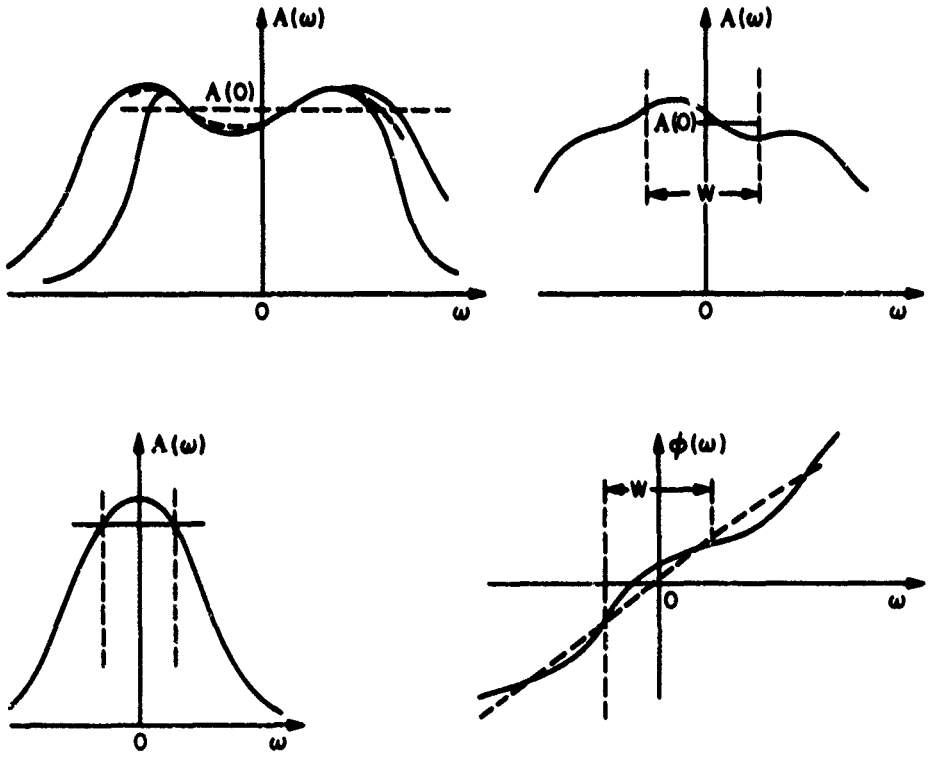

Figure 5. Amplitude and Phase Ripples Each of Which Can Be Approximated by $H(j\omega)$ in Eq. (8) and Figure 4

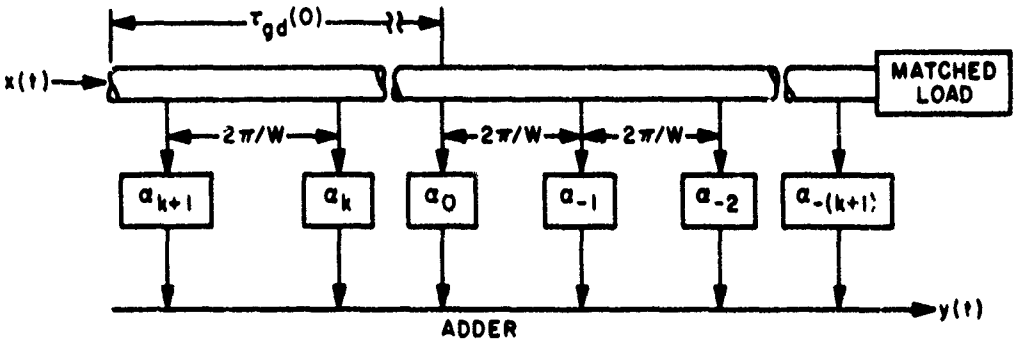

Figure 6. Tapped Delay-Line Representation of H(jω)

2.2.2.6 Statistical Characterization of Random Time-Variant Linear (RTVL) Transmission Channels

The randomness of the channel results from the variation with time of the properties of its active propagation mechanisms and therefore is reflected in the characterization of time-dependent system functions h(t, ξ) and H(jω, t). The statistical characteristics of the response of a RTVL channel depends upon the time duration in which the observations are made of the channel response for the statistical characterization of the channel-induced fluctuations. The selection of averaging time intervals, dependent on fading rate, is normally aimed at establishing time intervals over which the generally nonstationary statistical process of interest can be modeled approximately by a statistically stationary process. If the nominal fluctuation rate or fading bandwidth is denoted by Bfad, then the "instantaneous" averaging time, due to detection circuits, is taken as less than one tenth of the reciprocal of Bfad. The time interval, which is long enough to include a "typical" pattern of the instantaneous channel-induced fluctuations, is normally greater than 1000 times the reciprocal of Bfad. Traditionally, this time interval is chosen on the basis of the time interval that yields received envelope statistics in response to a test sinusoidal carrier with a best fit to the Rayleigh distribution function. This time interval is important in the sense that H(jω, t) can be treated as wide-sense stationary.

A combined time-shift and frequency-shift correlation function of H(jω, t) is defined as

$$R_{HH}(\Omega, \tau) = \text{time and frequency average of } \{H(j\omega, t)\, H(-j\omega - j\Omega, t + \tau)\} \quad . \quad (9)$$

A double Fourier transformation of $R_{HH}(\Omega, \tau)$ over Ω and τ yields

$$S(\tau_d, f_d) = \int_{-\infty}^{\infty} \int_{-\infty}^{\infty} R_{HH}(\Omega, \tau)\, e^{j\Omega\tau_d}\, e^{-j2\pi f_d \tau}\, d\left(\frac{\Omega}{2\pi}\right) d\tau \qquad (10)$$

If the variables τ_d and f_d are interpreted as time-delay and Doppler-shift variables, then $S(\tau_d, f_d)$ is called the channel-scattering function. Since $S(\tau_d, f_d)$ and $R_{HH}(\Omega, \tau)$ $R_{HH}(\Omega, \tau)$ are Fourier transforms of each other with

$$\Omega \longleftrightarrow \tau_d \quad \text{and} \quad \tau \longleftrightarrow f_d \ ,$$

the spread of $R_{HH}(\Omega, \tau)$ in the Ω variable is inversely proportional to the spread of $S(\tau_d, f_d)$ in the delay variable τ_d. The spread of $R_{HH}(\Omega, \tau)$ in the τ variable is inversely proportional to the spread of $S(\tau_d, f_d)$ in the Doppler-shift variable, f_d.

The scattering function in Eq. (10) can also be obtained from the tap-gain correlation function which, for WSSUS (wide-sense stationary uncorrelated scatters) channel, is defined as

$$R(\zeta, \tau) = \langle h^*(t, \xi)\, h(t + \tau, \xi) \rangle \ , \qquad (11)$$

where $h(t, \xi)\, d\xi$ denotes the complex gain associated with scatters in the interval $(\xi, \xi + d\xi)$. It is called the input delay spread function. The Fourier transform of the time-varying impulse response $h(t, \zeta)$ with respect to ξ is $H(j\omega, t)$ which is also called the time-variant transfer function.

From the Fourier transform of the $R(\xi, \tau)$ with respect to τ, one obtains $S(\tau d, fd)$ and if one Fourier transforms $R(\xi, \tau)$ with respect to the multipath variable ξ, one obtains $R(\Omega, \tau)$, defined as

$$R(\Omega, \tau) = \int R(\xi, \tau) \exp(-j2\pi\Omega\xi)\, d\xi \ . \qquad (12)$$

$R(\Omega, \tau)$ is called the time-frequency correlation function. This is the cross-correlation function between received carriers spaced Ω H_z apart at transmission.

2.2.2.7 Summary of Gross Channel Parameters

In light of above discussions, the gross transmission parameters, important in characterizing the effects of a RTVL medium upon broad classes of signals, are:

1. The outage (dropout or fadeout) is the fraction of time in an interval in which the characteristics of the useful signal parameters do not change significantly.

The signal parameter most frequently examined is the envelope, and the threshold is determined by signal-relative-to-noise considerations.

2. The delay spread is a measure of the duration of the channel impulse response, or of the maximum delay difference between the first and last significant paths.

3. The coherence bandwidth is the maximum frequency range over which all frequency components of a signal would maintain substantially fixed relative amplitude and phase relationships and fluctuate practically in step if they were contained within the coherence bandwidth. The channel signal-distortion effects upon link performance would thus be negligible. The bandwidth is inversely proportional to the delay spread.

4. The diversity (or the decorrelation) bandwidth is the minimum frequency separation between two input carriers that result in the correlation coefficient of 1/e or less between the corresponding envelopes. The diversity bandwidth is about 10 to 50 times the coherence bandwidth.

5. The fading rate (or Doppler spread) is a measure of the nominal width of the dispersion in frequency experienced by each individual frequency component in the transmitted signal.

6. The diversity (or decorrelation) time is a measure of the time separation that must exist between two impulse excitations to yield a correlation coefficient of 1/e or less between the output envelopes. The decorrelation time is inversely proportional to the fading bandwidth.

7. The instantaneous channel function $h(t, \xi)$ which is discussed earlier.

8. The second-order channel functions which are discussed earlier.

These parameters are not all independent because, except for outage probability, they are determined by $R_{HH}(\Omega, \tau)$ and $S(\tau_d, f_d)$ of Eqs. (9) and (10). Some of the interrelationships are already discussed earlier. The nominal spread of $S(\tau_d, f_d)$ in τ_d dimension is a measure of the multipath-delay spread of the multipath channel or of the delay spread of single path. The nominal spread of $S(\tau_d, f_d)$ in the f_d dimension is a measure of the fading rate. The nominal spread of $R_{HH}(\Omega, \tau)$ in the Ω dimension is a measure of (a) the low-distortion transmission bandwidth, when the delay difference between two paths is greater than the delay spreads of the individual path (see Figure 7)[8]; (b) the coherence bandwidth of paths with overlapping delay spreads (see Figure 8).[8] The nominal spread of $R_{HH}(\Omega, \tau)$ in the τ dimension is a measure of the channel-decorrelation time.

---

8. Lomax, J.B. (1970) HF propagation dispersion, in Phase and Frequency Instabilities in Electromagnetic Wave Propagation, K. Davies, editor, pp. 497-510, AGARD Conference Proceedings No. 33, Technivision Services Slough, England.

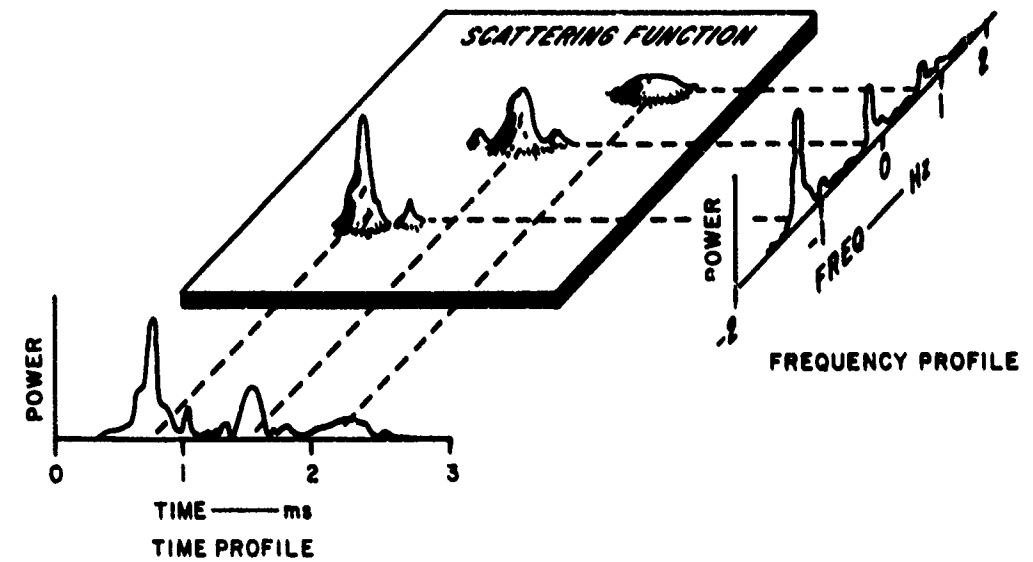

Figure 7. Scattering Function Showing That the Delay Difference Between Two Paths Is Greater Than the Delay Spreads of an Individual Path

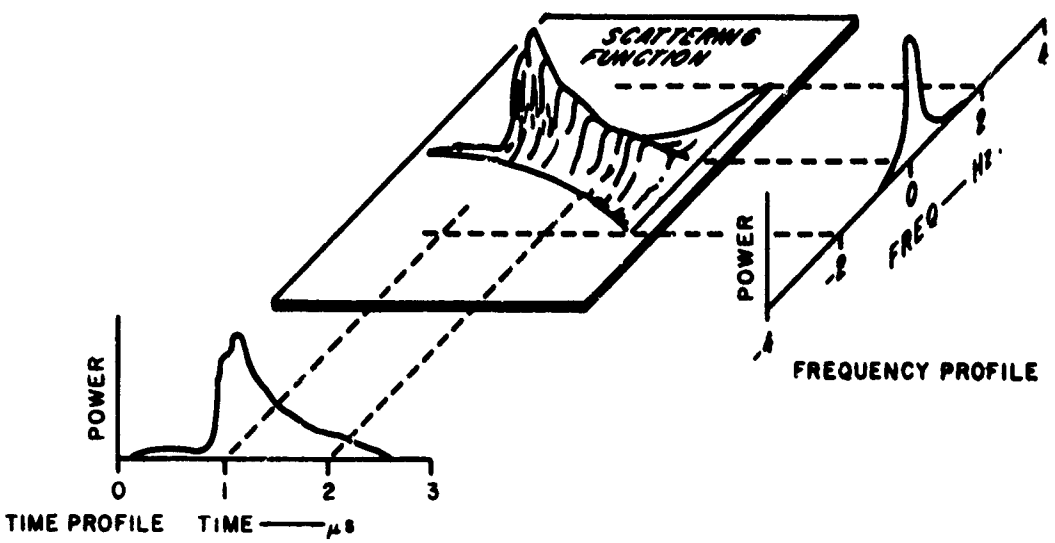

Figure 8. Scattering Function Showing Paths With Overlapping Delay Spreads

In Section 2.4, we will discuss the measurement techniques for these channel parameters. In the following section, we will develop[9] the time-frequency plane model (or "diversity model") used in signal design in Section 2.5, from the scattering function $S(\tau_d, f_d)$.

2.2.2.8 Derivation of the Time-Frequency Plane Model from the Canonical Channel Model

In this section, we will derive the time-frequency plane model from the scattering function which is useful in signal design, we will also demonstrate the various shapes of the possible delay-Doppler occupancy patterns.

If x(t) is the input and y(t) is the output, then

$$y(t) = \int\int x(t - \tau_d) \exp\, j2\pi f_d(t - \tau_d)\ \ v(\tau_d, f_d)\, d\tau_d\, df_d \quad . \tag{13}$$

where $V(\tau_d, f_d) = \int h(\tau_d, t)\, e^{-j2\pi f_d t}\, dt$ is called the Doppler-delay spread function.

If the input to a channel is confined by a time gate to the time interval $0 < t < T$ and the output spectrum is confined by a bandpass filter to the frequency interval $-\frac{1}{2}W < \omega < \frac{1}{2}W$, then in place of the actual channel with Doppler-delay spread function $V(\tau_d, f_d)$ one may use a channel whose Doppler-delay spread function $\bar{v}(\tau_d, f_d)$ has the singular form

$$\bar{V}(\tau_d, f_d) = \sum_{m,\,n} V_{mn}\, \delta\left(f_d - \frac{m}{T}\right) \delta\left(\tau_d - \frac{n}{W}\right) \tag{14}$$

where $\delta(\ )$ is the unit impulse,

$$V_{mn} = \int\int \exp\left[j\pi T\left(\frac{f_d - m}{T}\right)\right] \operatorname{sinc}\left[\tau\left(f_d - \frac{m}{T}\right)\right]$$

$$\operatorname{sinc}\left[W\left(\tau_d - \frac{n}{W}\right)\right]\ \ v(\tau_d, f_d)\, d\tau_d\, df_d \tag{15}$$

and

$$\operatorname{sinc} x = \frac{\sin \pi x}{\pi x}$$

---

9. Bello, P.A. (1969) Measurement of random time-var ant linear channels, IEEE Trans. on Info. Th., Vol. IT-25, No. 4, July.

Examination of Eq. (15) shows that $\{V_{mn}\}$ are essentially two-dimensional sampled versions of the original scattering function, the sampling taking place with "pulses" of width of the order of 1/T in the fd direction and 1/W in the τd direction.

The discrete channel model, which consists of a finite set of delays and Doppler shifts is shown in Figure 9, where $\text{rect}(x) = \begin{cases} 1 \; ; \; |x| < \frac{1}{2} \\ 0 \; ; \; |x| \geq \frac{1}{2} \end{cases}$. The output y(t) in Eq. (13) can therefore be written as

$$y(t) = \sum_m \sum_n \text{rect}\left(\frac{t - \frac{n}{W} - \frac{T}{2}}{T} \right) \times \left(t - \frac{n}{W} \right) \exp\left[j2\pi \frac{m}{T} \left(t - \frac{n}{W} \right) \right] V_{mn} \tag{16}$$

It is known[9] that the Doppler-delay spread function $V(\tau_d, f_d)$ and the scattering function $S(\tau_d, f_d)$ are related as

$$\overline{V^*(\tau_d, f_d)\, V(\tau_d, f_d)} = S(\tau_d, f_d) \tag{17}$$

or

$$\overline{V^*_{mn} V_{rs}} \begin{cases} = S\left(\frac{n}{W}, \frac{m}{T} \right) \Big/ TW \quad , \quad \text{for } m = r, \; n = s \\ = 0 \quad , \quad \text{for } m \neq r, \; n \neq s \end{cases} \tag{18}$$

that is, the scattering function varies very little for changes in τd of the order of 1/W and changes in fd of the order of 1/T. Thus the gains of the discrete point "scatterers" become uncorrelated, and the strength of the reflection from a particular scatterer becomes proportional to the amplitude of the scattering function at the same value of delay and Doppler shift. For T $\gg$ than the multipath delay spread and W $\gg$ than the fading bandwith, the number of V_{mn} coefficients significantly different from zero will be determined by how many rectangles of dimension 1/T W can be fit into the delay-Doppler occupancy pattern, that is into regions of the τ_d, f_d plane over which $V(\tau_d, f_d)$ is significantly different than zero. Such regions are shown in Figure 10. If S_A is the area of one such region, then the number of coefficients of significant amplitude can be expressed as

$$N\text{coef} = TW\, S_A \quad . \tag{19}$$

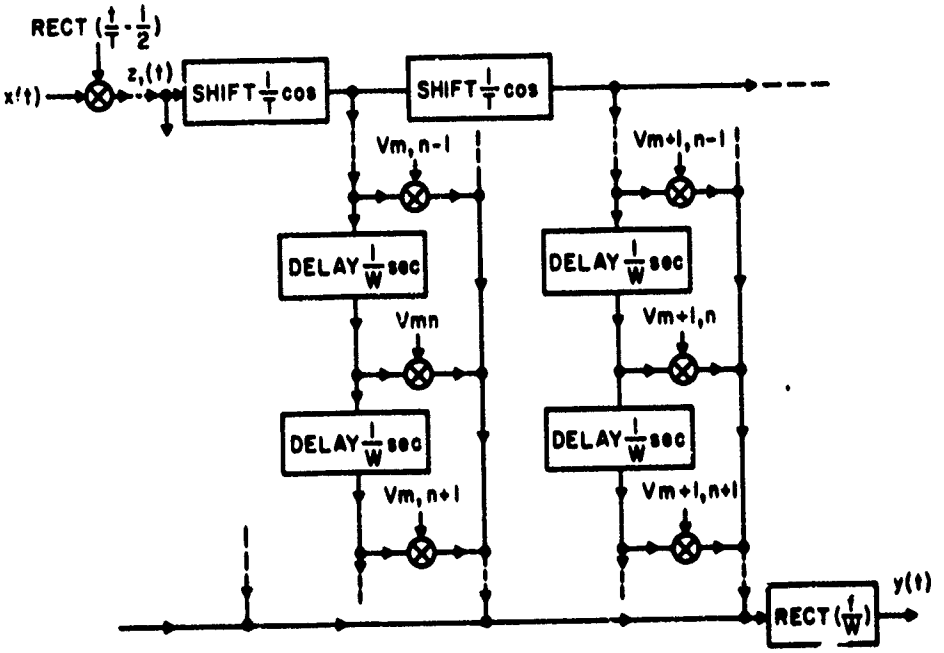

Figure 9. Canonical Channel Model for Input-Time Output-Frequency Constraint

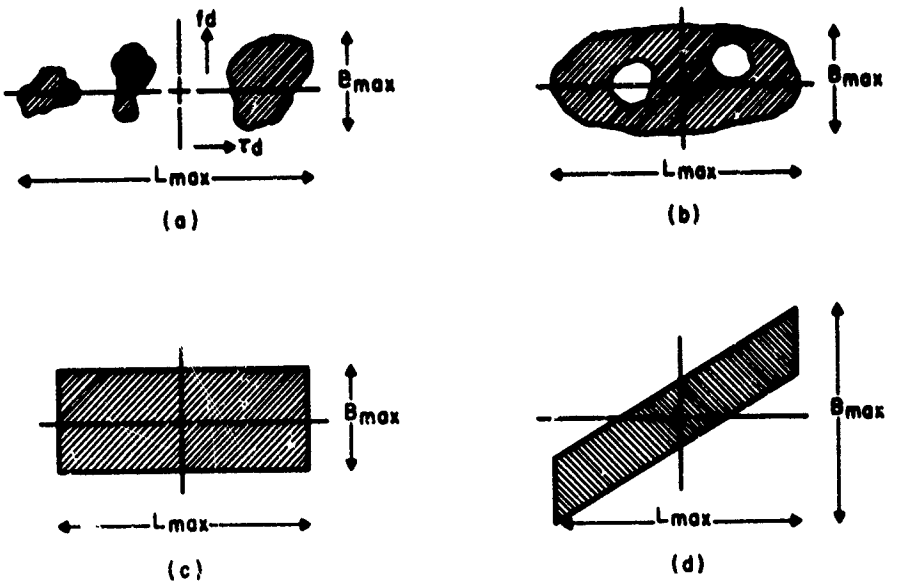

Figure 10. Examples of Possible Delay-Doppler Occupancy Patterns

2.2.2.9 Noise and Interference

The levels of noise and interference at the two terminals of the link will not be the same, therefore these measurements must be performed at both stations.

Receiver front-end noise will be negligible at HF with respect to background noise (atmospheric and galactic) and with respect to man-made interference. Table 2 provides an estimate in dB above KTB of the atmospheric and galactic noise level at 20 MHz, for various seasons and hours of the day.

Table 2. Atmospheric and Galactic Noise (dB above KTB)

Hours		20 MHz	
		Atmo.	Galactic
Winter	0000-0400	22	22
	0400-0800	24	22
	0800-1200	28	22
	1200-1600	42	22
	1600-2000	37	22
	2000-2400	30	22
Spring	0000-0400	30	22
	0400-0800	25	22
	0800-1200	34	22
	1200-1600	45	22
	1600-2000	37	22
	2000-2400	39	22
Summer	0000-0400	22	22
	0400-0800	25	22
	0800-1200	25	22
	1200-1600	36	22
	1600-2000	34	22
	2000-2400	30	22
Autumn	0000-0400	25	22
	0400-0800	20	22
	0800-1200	36	22
	1200-1600	38	22
	1600-2000	40	22
	2000-2400	36	22

Interference into the receivers of the link from nearby transmitters, or from co-channel emissions, either at close range or at a distance, as well as man-made noise will be the predominant factors in establishing the overall signal-to-(noise + interference) ratio at a given carrier of the HF link. As it will be discussed later on in this report, the adaptive scheme that we propose will use a waveform characterized by the presence of numerous spectral lines and the noise + interference level at each one of them will be verified in order to exclude the most interfered ones.

After review of CCIR Report No. 65, we have adopted in our analysis two values for the level of noise + interference; +30 dB and +45 dB above KTB.

2.2.2.10 Estimates of the Path Losses and of the Time/ Frequency Spreads

Ideally, we would like to provide reliable estimates of all the parameters indicated in Figures 11, 12 and 13 for each path of interest in our study. They are the quantities B_d, B_o, B_m, $S(\xi, \nu)$. Actually it would be sufficient to simplify the scattering function to a group of N gaussoides, with $B_o = 0$, $B_d = 0$, and to reduce therefore the scattering function to the one shown in cross-section in Figures 14 and 15, where the analytical expression of $S(\xi, \nu)$ becomes

$$S(\xi, \nu) = \sum_{i=1}^{N} P_i (2\pi B L_i)^{-1} \exp \left\{ -\frac{1}{2} \left[\frac{(r - r_i)^2}{L_i^2} + \left(\frac{f}{B} \right)^2 \right] \right\} \qquad (20)$$

In this formula, the parameter N represents the number of paths in the structure, r_i and L_i are the mean delay and the multipath spread, B is the Doppler spread of the path, and P_i denotes the relative strength of the i^{th} path.

Further simplification can be achieved by representing the scattering function $S(\xi, \nu)$ as a single gaussoid, whose amplitude is a function of the path losses and whose widths L_{tot} and B_{tot} are respectively the total time spread and the total Doppler spread.

Because of the time variability of the path, we also require the knowledge of the statistical properties of all these parameters, so that we can compute their median values and plot the curves that provide the percentage of the time (y-axis) during which path losses, the multipath spread and the Doppler spread exceed the value of the abscissa (x-axis). Unfortunately only fragmentary data exist that are usable to this end.

First, let's review the case of a one-hop HF path in midlatitude. Davies[10] gives a step-by-step procedure that can be easily followed and leads to a reliable estimate of the path losses. For a path with a length 2.5 megameters working

10. Davies, K. (1965) Ionospheric Radio Propagation, NBS Monograph No. 80.

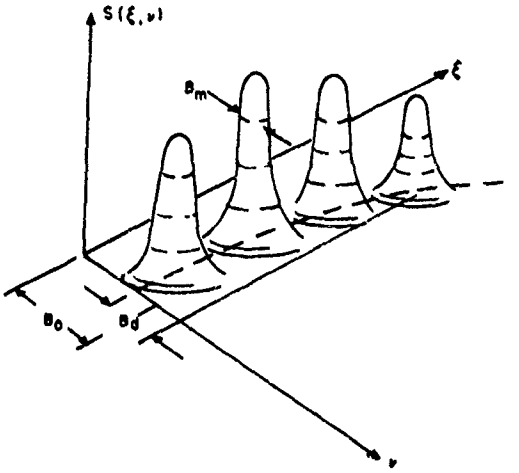

Figure 11. Multimodal Scattering Function

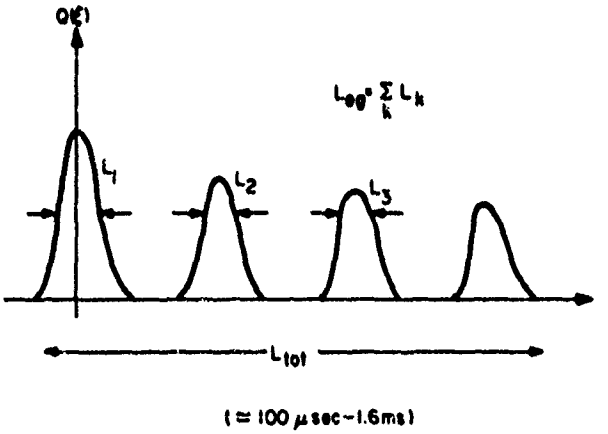

Figure 12. Multimodal Delay Power Spectrum

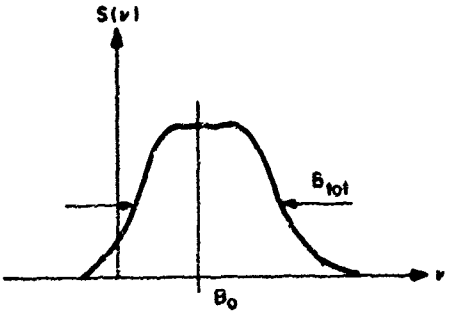

Figure 13. Doppler Power Spectrum

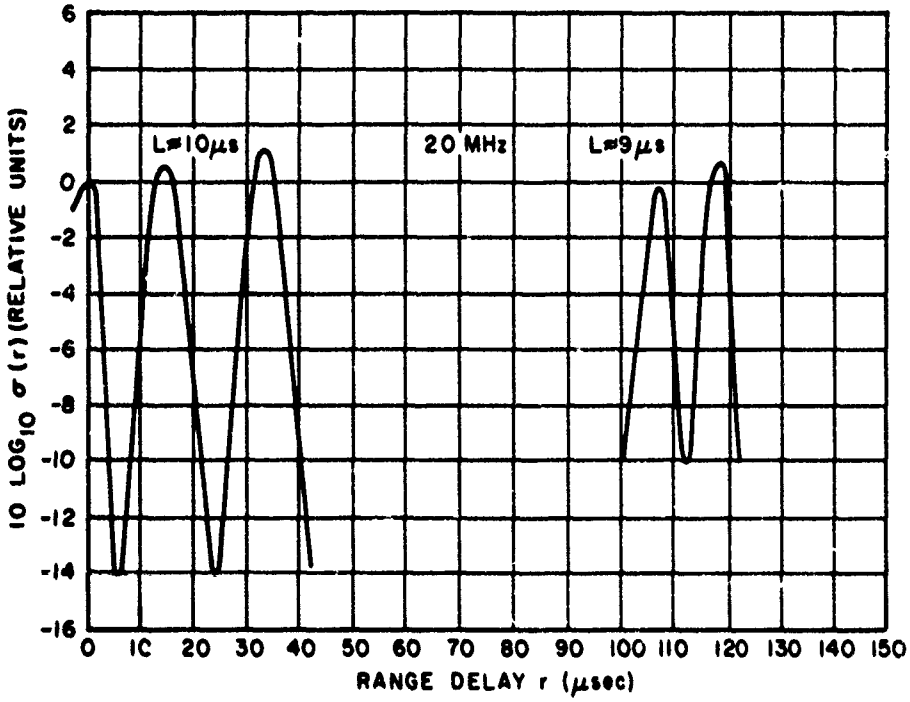

Figure 14. Range Scattering Function σ(r) of a One-Hop Ionospheric Path in Midlatitude

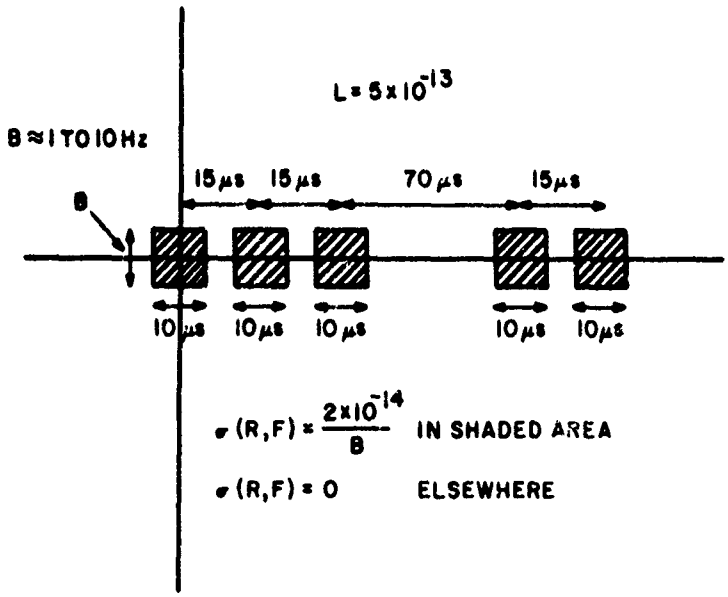

Figure 15. Cross-Section of the Scattering Function of the Ionospheric Path in Figure 14

at such a frequency f that 0.85 MUF4000 < f < MUF4000, a typical value of path losses (inclusive of absorption losses and of antenna gains) is 130 dB. Few theoretical formulations and even fewer experimental data are available on the multipath spread and Dopper spread of single-hop HF paths in midlatitude. Bailey[11] investigated the HF multipath spread phenomenon and its dependence upon operating frequency (specifically, upon its ratio to the MUF). He also included in his analysis the dependence of multipath spread on path length, link location, local time as well as season. This analysis shows that in a 2.5 megameter path, when using a working frequency of 0.9-MUF4000, the time spread L ≅ 100 microsec. Reliable statistics on the time spread are unavailable. Concerning now the Doppler spread of a midlatitude one-hop HF path, we can estimate a median value of 0.1 Hz. For this parameter too, a reliable statistic is an unfulfilled requirement.

Let's review now the case of a transauroral path. Lomax,[12] Shaver et al,[13] and Shepherd and Lomax[14] have reported on experimental measurements of high-latitude HF propagation characteristics, specifically for the frequency of 7.366 MHz. These authors found that winter propagation (inclusive of "normal" and "off-path" rays) is characterized by a time spread of approximately 1200 microseconds and by a Doppler spread of approximately 1 Hz. Summer propagation shows Doppler spread up to 20 Hz, although most of the signal energy was received within 0.5 Hz from the carrier. Data on transauroral-path losses at HF are scant, although these are certainly larger than in midlatitude paths. In our study we have assumed two values for this parameter, 150 dB and 165 dB. An estimate of the percentage of time during which these values will be exceeded is, however, lacking.

Table 3 summarizes the channel properties that we have assumed as educated guesses for our study of adaptive HF propagation path utilization.

---

11. Bailey, D.K. (1959) The effect of multipath distortion on the choice of operating frequencies for HF communications circuits, IRE Trans. Antenna and Propagation, AP-7, 398.

12. Lomax, J.B. (1970) HF propagation dispersion, in Phase and Frequency Instabilities in Electromagnetic Wave Propagation, K. Davies, editor, pp. 497-510, AGARD Conference Proceedings No. 33, Techvision Services, Slough, England.

13. Shaver, H.N., Tupper, B.C., and Lomax, J.B. (1967) Evaluation of a Gaussian HF channel model, IEEE Trans. on Communications Technology, Vol. 15, No. 1, pp. 79-88.

14. Shepherd, R.A. and Lomax, J.B. (1967) Frequency spread in ionospheric radio propagation, IEEE Trans. on Communications Technology, Vol. 15, No. 2, pp. 268-275.

Table 3. HF Channel Properties

	Midlatitude Path	Transauroral Path
Multipath Spread	100 μsec	1500 μsec
Doppler Spread	0.1 Hz	10 Hz
Path Losses	130 dB	150 dB 165 dB
Noise + Interference (above KTB)	30 dB 45 dB	30 dB 45 dB

2.3 Path Sounding

Path sounding has the scope of measuring path losses at an adequate number of spot frequencies in the band of interest (3 MHz to 30 MHz) and of measuring at the same time noise and interference levels, at the same frequencies and at both ends of the link.

Table 4 gives the parameters of the proposed sounding scan. The master station radiates sequentially 1125 to 3750 carriers to cover the 3-MHz to 30-MHz band, in a time interval 100 to 160 seconds (88 milliseconds to 47 milliseconds per carrier). Of the two numbers given above for each sounding parameter, the first applies to a midlatitude path, the second to a transauroral path. The scan is repeated every 5 to 8 minutes.

Once a set of frequencies has been chosen for communicating, it is automatically excluded from next sounding cycle. However, information on the channel status for each one of the frequencies thus excluded from sounding and probing is still updated once every 5 to 8 minutes by measurements performed on the communication waveform. Frequency switching is preceded by a "tone" of notification and takes place even while communications go on, for the case in which the channel deteriorates and another set of frequencies is found more suitable for carrying out the communications.

The block diagram in Figure 16 has been worked out for Link Configuration 1 (two-way adaptive link) and illustrates the various functions of the two terminals of the link. Here, one-way sounding and probing is achieved from the master station to the slave station. Acknowledgement is from the slave to the master station. Finally, communication is a two-way exchange between the stations.

Table 4. Sounding/Probing Scan Parameters

	Midlatitude Path	Transauroral Path
Band covered	3 MHz-30 MHz	3 MHz-30 MHz
Number of spot frequencies	1125	3375
Separation between two adjacent spot frequencies	24 KHz	8 KHz*
Sounding scan time	100 seconds	160 seconds
Rate of sounding scan repetition	one every 300 seconds	one every 480 seconds
Dwelling time per spot frequency	88 millisec	47 millisec
Nominal bandwidth of sounding receiver	24 KHz	8 KHz
Width of sounding pulse	41.5 microsec	125 microsec
Pulse repetition frequency	100 pps	100 pps
Pulses per dwelling time	8 pulses	4 pulses
PRF duty cycle	10^{-3}	$1.25\ 10^{-2}$
Noise and interference measurements integration time, for each spot frequency	53 millisec	4. millisec
Overall noise and interference measurement time	60 seconds	160 seconds

*This value is chosen because 8 KHz is the bandwith of the signal waveform selected for the transauroral link. The path coherent bandwidth is only 666 Hz.

Midlatitude link

Step 1 - 100 seconds devoted to sounding operation.

Step 2 - 60 seconds devoted to measurement of noise and interference at both terminals of the link.

Step 3 - 20 seconds devoted to computations, taking into account the need of accumulating at a single terminal (the slave station) the information pertaining to noise and interference at both terminals. During this step, the microprocessor at the slave station selects the frequencies and designates them to the master station.

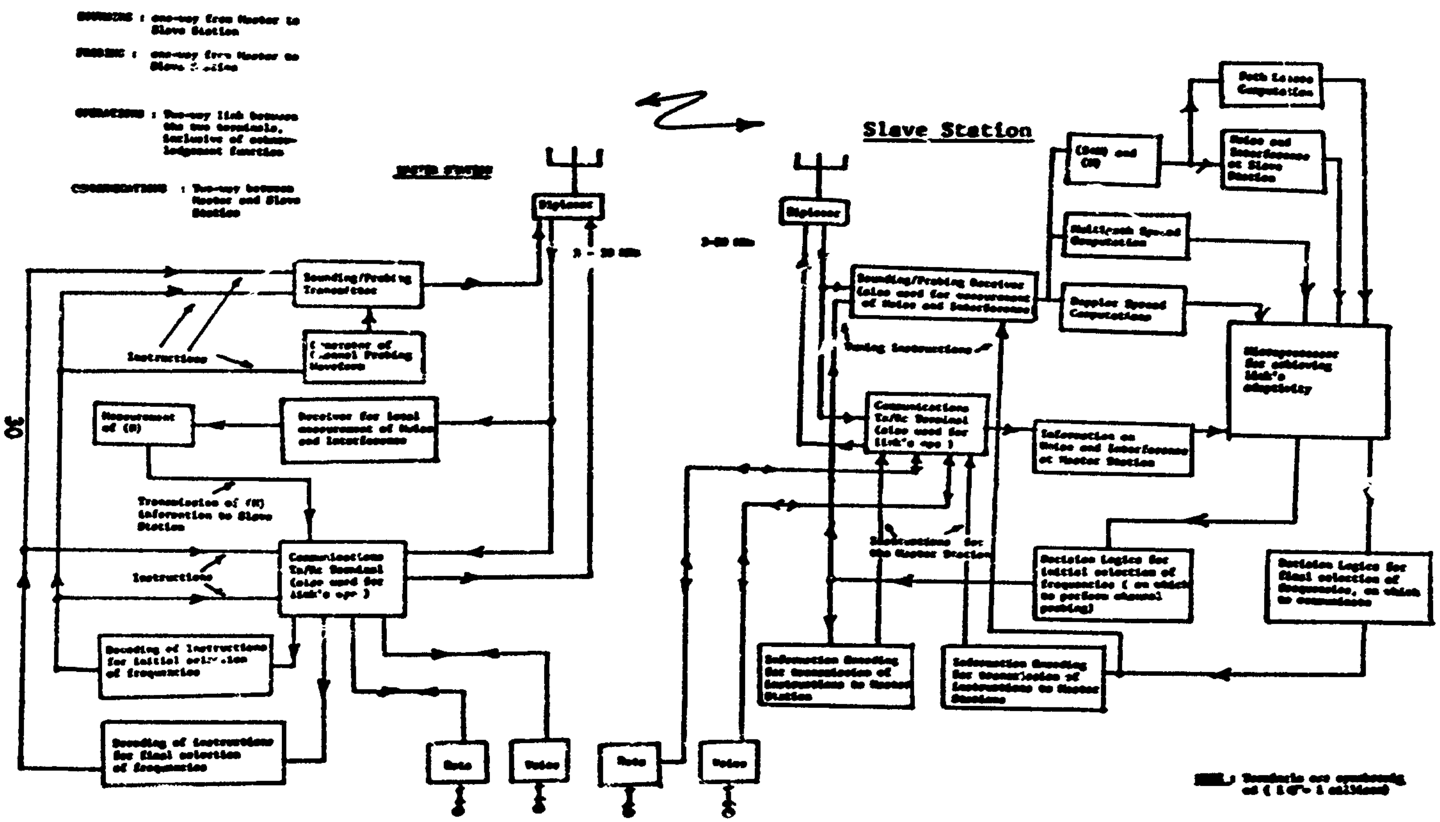

Figure 16. Simplified Block Diagram of Link's Terminals

Step 4 - 100 seconds devoted to channel probing, to be performed only at the frequencies designated by Step 3.

Step 5 - 20 seconds devoted to computations, acknowledgement and information exchange between the two terminals, in order to perform the final selection of frequencies to be used in communications, by taking into account the data on multipath spread and Doppler spread.

Step 6 - The two terminals are now ready to initiate communications. The frequencies finally adopted for communications are excluded from next sounding/ probing cycle (one every 300 seconds), although they continue to be monitored by measurements on the modulation waveform.

Transauroral link

Step 1 - 160 seconds

Step 2 - 160 seconds

Step 3 - 20 seconds

Step 4 - 120 seconds

Step 5 - 20 seconds

Step 6 - The two terminals are now ready to initiate communications. The sounding/probing cycle is repeated every 8 minutes (480 seconds).

Communications are therefore inhibited only in the first 300 (or 480 seconds) of link operation. After this initial adaptive adjustments of the link's terminals, any readjustment is performed without requiring a discontinuation of communications.

2.4 Channel Probing

The importance of time- and frequency-dispersive effects in HF propagation has been amply treated in the literature and there is no doubt that such effects are determining factors in the conceptual design of an adaptive system. Channel probing is aimed at gathering information on these effects, after the path sounding has determined path losses and noise plus interference levels at the available spectral lines, and has identified the frequencies promising enough to be worthy of the channel-probing effort. All these functions are slowly varying functions, so that one sample every 5 to 8 minutes is adequate.

The measurement of multipath spread and of the Doppler spread can be achieved with a variety of methods, either based on the direct measurement of these two quantities or on indirect measurements such as the ones based on the fact that, at a given frequency, the reciprocal of the Doppler spread gives the e.m. wave-fading period or that the reciprocal of the multipath spread, at a given instant in time, gives the frequency interval within which carriers fade coherently. Because the

amount of time required to process the information on the dispersive properties of each channel is not trivial, we propose to perform these measurements only for those frequencies for which path sounding has indicated acceptable path losses and affordable noise and interference levels. Therefore channel probing has to follow, in time, the sounding operation, as was illustrated in Section 2.3.

In the following sections we will review applicable measurement techniques.

2.4.1 MEASUREMENT TECHNIQUES OF TRANSMISSION PARAMETERS

The measure of communication channels is important in digital communications because high-speed digital data transmission requires considerable knowledge and equalization of channel characteristics. Kailath[3] pointed out that the problem of the measurement of system functions (see Section 2.2.2.6) of random time-variant channels differs from the corresponding problem for time-variant channels in that, even in the absence of noise, the random system function may be unmeasurable. Kailath introduced a channel parameter called a "spread factor" as the measurability criterion. This parameter is the product of B_{max}, the maximum rate of variation of the system in H_z, and L_{max}, the maximum multipath spread of the channel in seconds. According to Kailath, the system functions of a linear channel cannot be measured if the "rectangular spread factor" of the channel, S_R ($= B_{max} L_{max}$) > 1 and if no further information than B_{max}, L_{max} is known about the channel. However, he was careful to point out that additional channel knowledge would generally allow exact channel measurement even though $B_{max} L_{max} > 1$. Based upon the discrete representations of the channel (Figure 9), corresponding to input-time and output-bandwidth constraints, Bello[9] proposed the region of the non-zero delay-Doppler occupancy pattern (Figure 10) being less than unity as the less stringent measurability criterion. This new channel parameter is called the area spread factor of the channel S_A. Another method of evaluating the 'spread factor' of the channel is to define the spread factor as the ratio of the bandwidth of the fast fluctuations and the correlation bandwidth of the channel being measured. Fortunately except for certain esoteric radio channels (for example, the orbital radio channels), the spread factor is less than unity and thus the measurement techniques described below are generally quite useful.

These measurement techniques for a random dispersive channel are analyzed[7] in three levels of increasing complexity:

1. The measurement of multipath spread and Dopper spread, and Doppler shift and spectral skewness.
2. the measurement of second-order channel functions;
3. the measurement of instantaneous channel functions.

For the parameters in (1), measurement techniques used are based upon differentiation, level-crossing and correlation. For (2), the techniques used are

correlation technique, multitone technique, pulse-pair technique and the chirp technique. For the measurement of the instantaneous valves of the channel functions, the cross-correlation, multitone and pulse-pair techniques are used.

2.4.2 MEASUREMENT OF DOPPLER SPECTRUM PARAMETERS

In this section, we will summarize the techniques of the real-tir measurement of the centroid, rms bandwidth and skewness of the Doppler spectrum of the complex envelope of the narrowband process. Due to the Doppler spreading characteristics of the channel, the received process is narrowband when a CW tone is transmitted. The importance of the rms bandwidth (or second central moment of the spectrum) in signal design and in probability of error computations is well known in the literature. In Appendix B, we have outlined the effect of centroid (first moment) and the skewness of the spectrum on the probability of error computations and the equivalent signal-to-noise ratio (S/N). This S/N parameter is important in evaluating the number of frequencies required in combatting the fading and inter-symbol interference (see Section 2.5). In that section, the probability of error expression only accounts for the additive noise in the channel and neglects the fading of the channel. However, we propose that by using the equivalent signal-to-noise ratio in the probability-of-error expression, the fading effect of the channel can also be accounted for. Gupta[15] has recently developed techniques to compute the spectral moments of the complex envelope of the narrowband process. The main results are summarized here:

"General expressions of the spectral moments of any order (specifically the first four) are derived by the author in the time domain and their derivations do not require the computation of the power spectrum. In order to simplify the signal processing of the spectral moment estimators, the author proposed a general class of these estimators of an undistorted complex envelope which are obtained from one or both distorted quadrature components of the complex process. The components are distorted by means of memoryless nonlinear devices (MLNLD), such as the hard-clipper. By making use of the previous results of Bussgang (cross-correlation theorem) and Van Vleck (arcsin law), interesting results are obtained. For example, it is shown that odd (even) spectral moments of an undistorted complex process can be obtained when both quadrature components are distorted by even (odd) MLNLD and that even (odd) moments cannot be obtained if both components are hard-clipped (even-linearly rectified). However, the spectral moments of any order can be computed in the time domain when only one of the two components is distorted by arbitrary MLNLD."

---

15. Gupta, A.K. (1979) Dissertation abstract, IEEE Trans. Info. Theory, p. 760, November.

Mathematically, if S(f) is the power spectrum of a received carrier, the central spectral moments are defined as

$$m_n = \frac{\int (f - M_1)^n S(f)\, df}{\int S(f)\, df} \tag{21}$$

and the simple spectral moments M_n are obtained by replacing $(f - \mu_1)^n$ by f^n. It is simple to obtain the relationship between μ_n and m_n. μ_1 is called the centroid, m_2 and m_3 are second and third central spectral moments respectively. Skewness is defined by Gupta[15] as

$$s_k = \frac{m_3}{m_2^{3/2}} \tag{22}$$

If g(t) is the complex envelope of the received process and is given by $g(t) = \alpha(t) + j\beta(t)$, then for the case of undistorted components

$$\mu_1 = \left(\frac{1}{2\pi}\right) \frac{\langle \alpha\dot{\beta} - \beta\dot{\alpha} \rangle}{\langle \alpha^2 + \beta^2 \rangle} = \frac{\langle \alpha\dot{\beta} \rangle}{\langle \alpha^2 \rangle} = -\frac{\langle \beta\dot{\alpha} \rangle}{\langle \beta^2 \rangle} \tag{23}$$

$$\mu_2 = \left(\frac{1}{2\pi}\right)^2 \frac{\langle \dot{\alpha}^2 + \dot{\beta}^2 \rangle}{\langle \alpha^2 + \beta^2 \rangle} = \left(\frac{1}{2\pi}\right)^2 \frac{\langle \dot{\alpha}^2 \rangle}{\langle \alpha^2 \rangle} = \left(\frac{1}{2\pi}\right)^2 \frac{\langle \dot{\beta}^2 \rangle}{\langle \beta^2 \rangle} \tag{24}$$

$$\mu_3 = \left(\frac{1}{2\pi}\right)^3 \frac{\langle \ddot{\alpha}\beta - \dot{\beta}\dot{\alpha} \rangle}{\langle \alpha^2 + \beta^2 \rangle} = \left(\frac{1}{2\pi}\right)^3 \frac{\langle \ddot{\alpha}\beta \rangle}{\langle \alpha^2 \rangle} = -\left(\frac{1}{2\pi}\right)^3 \frac{\langle \dot{\beta}\dot{\alpha} \rangle}{\langle \beta^2 \rangle} \tag{25}$$

and

$$m_2 = \mu_2 - \mu_1^2 \text{ and } m_3 = \mu_3 - 3\mu_1\mu_2 + 2\mu_1^3 \quad . \tag{26}$$

the rms bandwidth or Doppler spread (D) is given by twice $\sqrt{m_2}$. α and β are $\alpha(t)$ and $\beta(t)$ respectively, "." denotes differentiation and "$\langle\ \rangle$" denotes ensemble averaging.

The inphase and quadrature components $\alpha(t)$ and $\beta(t)$ can be determined by multiplying the received carrier by both a local carrier and a 90° shifted local carrier at the same frequency as the received carrier (or as near to the same frequency as possible) and then extracting the low-frequency components. Strictly

speaking $D(=2\sqrt{m_2})$ and skewness (s_k) are independent of centroid, and thus precise knowledge of the received carrier frequency is not necessary. However, as the local carrier frequency departs from the received carrier frequency, the extracted $\alpha(t)$ and $\beta(t)$ increase in bandwidth, necessitating larger bandwidth filters and passing more noise. Thus, from the point of view of maximizing signal-to-noise ratio, it is desirable to keep the local carrier frequency as near as possible to the received signal frequency.

We consider now a simpler technique for the measurement of Doppler spread that uses only the envelope or, more generally, any well-behaved nonlinear function of the envelope of the received carrier. For the technique proposed to be strictly correct, it is necessary to assume that the transmission of a carrier results in the reception of a narrowband Gaussian process. However, slight departures from Gaussianity should not affect the measured parameter significantly.

It is demonstrated[7] that if e(t) is some nonlinear fuction (K) of the envelope $\alpha^2 + \beta^2$ of the received carrier, the rms Doppler spread is then given by

$$D = \frac{1}{\pi a} \sqrt{\frac{\langle (\dot{e}(t))^2 \rangle}{\langle (e(t))^2 \rangle}} \tag{27}$$

where a is a constant dependent upon the nonlinear device and is given by

$$a = \sqrt{\frac{2 \int_0^\infty r e^{-r} \left[\frac{dk(r)}{dr}\right]^2 dr}{\int_0^\infty e^{-r} k^2(r)\, dr}} \tag{28}$$

In the case of a linear envelope detector $a = 1/\sqrt{2}$ and for a square-law detector $a = 1$. The formation of the derivatives of the envelope from the sampled data requires some care. In Bello,[16] some attention has been given to this problem.

Fading rates have also been determined by measuring the average number of times/unit time the envelope of the received carrier crossed a specified level. Rice (see ref. in Bello[7]) has shown that for a narrowband Gaussian process the number of times (n) the envelope crosses a level R is simply related to a rms bandwidth measure. If the level is the rms of the envelope, then

$$n = \frac{\sqrt{\pi}}{2e} D \ . \tag{29}$$

---

16. Bello, P.A. (1965) On the rms bandwidth of non-linearly envelope detected narrowband Gaussian noise, IEEE Trans. on Info. Theory, pp. 236-239.

Another approach is to compute the zero crossings of the inphase (or quadrature) component of the narrowband Gaussian process. If m is the number of zero crossings then

$$m = D \ . \tag{30}$$

Various methods of estimating centroid, skewness, and Doppler spread are discussed by Gupta.[15]

2.4.3 MULTIPATH SPREAD MEASUREMENTS

The multipath spread parameter is a measure of the dispersion in path delays suffered by a process propagated through a random channel (see Figures 3, 7 and 8). If $Q(\xi)$ is the delay power spectrum which describes the distribution of power in the various path delays, the rms multipath spread is given by (similar to Eqs. (21) and (26))

$$M_2 = 2 \sqrt{\frac{\int (\xi - M_1)^2 \, Q(\xi) \, d\xi}{\int Q(\xi) \, d\xi}} \tag{31}$$

where

$$M_1 = \frac{\int \xi \, Q(\xi) \, d\xi}{\int Q(\xi) \, d\xi} \tag{32}$$

is the centroid of $Q(\xi)$ (similar to μ_1 in Eq. (21)). Although the following analysis does not differentiate the discrete scattering function (Figure 7) and continuous scattering function (Figure 8), the future work will develop new methods of defining multipath spread in two different situations.

From a strictly mathematical point of view, the multipath-spread measurement problem is entirely analogous (dual) to the Doppler-spread measurement problem. The function $Q(\xi)$ is the "power spectrum" of the instantaneous channel transfer function $G(f)$. Thus, if a very narrow pulse of spectrum $H(f)$ is transmitted, $W(f)$ the complex amplitude spectrum of the received transient is found to be

$$W(f) = H(f) \, G(f) \ . \tag{33}$$

If $H(f)$ is chosen to be essentially constant over a band of frequencies sufficiently large compared to the correlation bandwidth, then sufficient values of $G(f)$ can be determined from $W(f)$ to perform frequency-domain averaging. If similar to

g(t), one defines G(f) as $G(f) = \alpha(f) + j\beta(f)$, then one obtains[15] from Eqs. (24) and (26) that

$$M_2 = \frac{1}{\pi} \sqrt{\frac{\left\{\left(\frac{d\alpha}{df}\right)^2 + \left(\frac{d\beta}{df}\right)^2\right\}}{\{\alpha^2(f) + \beta^2(f)\}} - \left| \frac{\left\{\alpha(f)\,\frac{d\beta(f)}{df} - \beta(f)\,\frac{d\alpha(f)}{df}\right\}^2}{\{\alpha^2(f) + \beta^2(f)\}} \right|} \tag{34}$$

where "{ }" denotes frequency-domain averaging similar to the relationships in Eqs. (23) through (25). The authors of this report point out that M_2 can also be simplified to

$$\begin{aligned} M_2 &= \frac{1}{\pi} \sqrt{\frac{\left\{\left(\frac{d\alpha}{df}\right)^2\right\}}{\{\alpha^2(f)\}} - \left| \frac{\left\{\alpha(f)\,\frac{d\beta(f)}{df}\right\}}{\{\alpha^2(f)\}} \right|^2} \\ &= \frac{1}{\pi} \sqrt{\frac{\left\{\left(\frac{d\beta}{df}\right)^2\right\}}{\{\beta^2(f)\}} - \left| \frac{\left\{\beta(f)\,\frac{d\alpha(f)}{df}\right\}}{\{\beta^2(f)\}} \right|^2} \end{aligned} \tag{35}$$

Similar to Eq. (27), one can also obtain M_2 from the envelope as

$$M_2 = \frac{1}{\pi a} \sqrt{\frac{\left\{\left(\frac{dE}{df}\right)^2\right\}}{\{E^2(f)\}}} \quad , \tag{36}$$

where E(f) is some nonlinear function $K(\alpha^2(f) + \beta^2(f))$ of the frequency squared envelope.

Similar to Eqs. (29) and (30), multipath spread can also be obtained, from (by using time-frequency duality) the average number of times per hertz the transfer function envelope G(f) crosses its rms value and from the number of times per hertz the real or imaginary part of the channel-transfer function crosses zero.

2.4.4 SIMULTANEOUS MEASUREMENTS OF DOPPLER SPREAD AND MULTIPATH SPREAD

In earlier sections, techniques for the instantaneous measurement of Doppler and multipath spread, which require either the extraction of complex envelopes or envelopes of the received carriers. In this section, we will simultaneously measure both the parameters from the envelopes of the received carriers. FM and SSB

(single sideband) techniques have been discussed in Bello.[17] In this section we will discuss the SSB technique only.

In the SSB technique two carriers separated by F H_z are transmitted. Letting the received detected envelopes be represented as D_t (f + F) and E_t(f), the normalized difference in Eq. (36) is

$$\frac{dE_t(f)}{df} = \frac{E_t(f + F) - E(f)}{F} \tag{37}$$

where subscript 't' denotes that E(f) is also function of time. Assuming stationary scatter statistics, time and frequency averaging can be interchanged. Thus in Eq. (36)

$$\left\{\left(\frac{dE_t(f)}{dt}\right)^2\right\} = \left\langle \left| \frac{E_t(f + F) - E_t(f)}{F} \right|^2 \right\rangle \tag{38}$$

Figure 17 shows the block diagram implementation of Eqs. (27) and (36) with Eq. (38) using the SSB technique. Note M_2 and D are simultaneously measured.

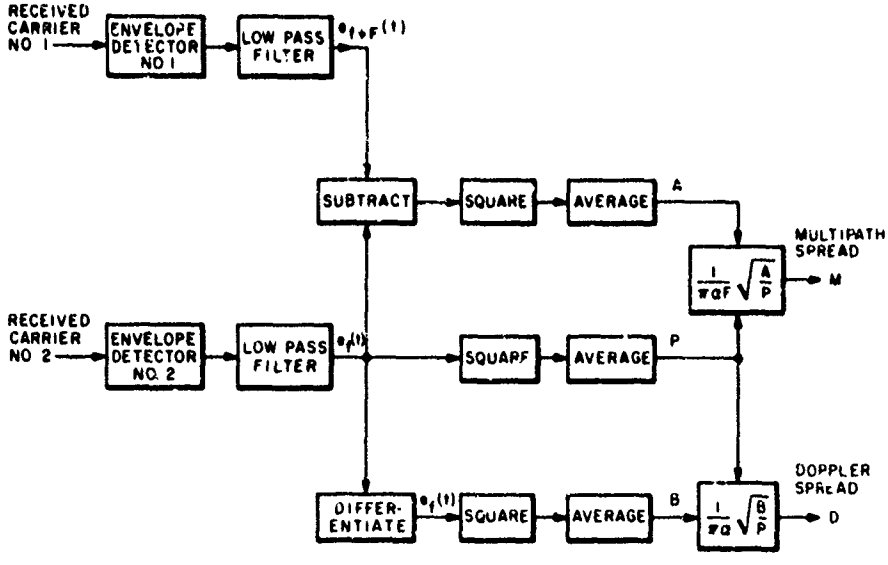

Figure 17. Simultaneous Measurement of Doppler Spread and Multipath Spread Using Envelopes Only by the SSB Technique

---

17. Bello, P.A. (1965) Some techniques for the instantaneous real-time measurement of multipath and Doppler spreads, IEEE Trans. on Comm. Tech., Vol. 13, No. 3, pp. 155-192.

2.4.5 MULTIPATH MEASUREMENTS

2.4.5.1 Incoherent Pulse Probe

A suitable signal for estimating the delay power spectrum $Q(\xi)$ is a short pulse of width Δ, which is narrow compared with the characteristic variations in $Q(\xi)$. Consider the signal,

$$z(t) = p(t)$$

$$p(t) = \begin{cases} 0 & |t| > \Delta/2 \\ 1 & |t| \leq \Delta/2 \end{cases}$$

$$\Delta \leq \text{mode width (for example, } 5\ \mu\text{sec)} \tag{39}$$

An estimate can be formed by square-law detecting the observed process and subtracting off a noise bias. Thus, for the response to one of the pulses in the train we have

$$\hat{Q}(t) \equiv |r(t)|^2 - \overline{|n(t)|^2}$$

$$= \left|\sqrt{A}\int g(\xi)\, p(t-\xi)\, d\xi + n(t)\right|^2 - \sigma_n \tag{40}$$

The properties of this estimator can be listed as follows:

Mean

$$\hat{Q}(t) = A\iint \overline{g(\xi_1)\, p(t-\xi_1)\, g^*(\xi_2)\, p(t-\xi_2)\, d\xi_1\, d\xi_2} + \overline{|n(t)|^2} - \sigma_n$$

$$= A\int Q(\xi)\left|p(t-\xi)\right|^2 d\xi$$

$$\equiv E\tilde{Q}(t) \tag{41}$$

where

E is the equivalent pulse energy, that is,

$$E = A\int |p(t)|^2\, dt \approx A\Delta$$

Thus, Q(t) will be a filtered version of the true function if enough averaging is carried out. The resolution is determined by the signal properties, so that the

pulse width must be narrower than the mode widths of $Q(\xi)$ to give an adequate estimate.

Variance

Since r(t) is a complex Gaussian process,

$$\overline{|r(t)|^4} = 2\left[\overline{|r(t)|^2}\right]^2$$

Thus,

$$\begin{aligned}
\mathrm{Var}\{\hat{Q}(t)\} &= \overline{\left[|r(t)|^2 - \sigma_n\right]^2} - \left[\hat{Q}\right]^2 \\
&= \overline{|r(t)|^4} - 2\sigma_n \overline{|r(t)|^2} + \sigma_n^2 - \overline{[\hat{Q}]} \\
&= 2\left[E\tilde{Q}(t) + \sigma_n\right]^2 - 2\sigma_n\left[E\tilde{Q}(t) + \sigma_n\right] + \sigma_n^2 - \left[E\tilde{Q}(t)\right]^2 \\
&= \left[E\tilde{Q}(t)\right]^2 + 2\sigma_n E\tilde{Q}(t) + \sigma_n^2 \qquad (42)
\end{aligned}$$

The ratio of standard deviation to mean is

$$\begin{aligned}
\frac{\text{s.d. } (\hat{Q}(\xi))}{\text{mean } (\hat{Q}(\xi))} &= \frac{\left[EQ(\xi) + \sigma_n\right]}{E\tilde{Q}(\xi)} \\
&= 1 + \frac{\sigma_n}{E\tilde{Q}(\xi)} \qquad (43)
\end{aligned}$$

It is a simple matter to show that when N_{eq} <u>independent</u> "snapshots" of the channel response are processed in this way and averaged by overlapping, the ratio of standard deviation to mean is reduced by $1/\sqrt{N_{eq}}$, that is,

$$\frac{\text{s.dev.}}{\text{mean}} = \frac{1}{\sqrt{N_{eq}}}\left[1 + \frac{\sigma_n}{E\tilde{Q}(\xi)}\right]$$

For a required ratio of 0.2 this implies

$$N_{eq} = \left(\frac{1}{0.2}\right)^2 \left[1 + \frac{\sigma_n}{E\hat{Q}(\xi)}\right]$$

$$= 25 \left[1 + \frac{\sigma_n}{E\tilde{Q}(\xi)}\right]$$

$$\geq 25$$

Note that even in the absence of noise there is a basic limitation to the attainable accuracy for a given measurement time. The maximum number of independent pulse responses which can be obtained in 1 minute is

$$N_{eq} = 60 \Big/ \frac{1}{B_{tot}} \qquad B_{tot} = \text{Doppler spread} \tag{44}$$

$$\approx 60$$

The ratio of standard deviation to mean for this zero-noise case is found to be:

$$\frac{\text{s.dev. } (\hat{Q}(\xi))}{\text{mean } (\hat{Q}(\xi))} = \frac{1}{\sqrt{N_{eq}}} \tag{45}$$

$$\approx 0.13$$

In the next few sections, which include additive-noise calculations, a performance index ρ will be used, where

$$\rho \equiv \left(1 + \frac{\sigma_n}{E\tilde{Q}(\xi)}\right) \tag{46}$$

Examples

Consider a multimodal form for $\tilde{Q}(\xi)$ with M equal energy modes of width L_o (see Figure 13). Then

$$\tilde{Q}(\xi) \approx \frac{1}{ML_o} \qquad \text{(for each mode)} \tag{47}$$

Since

$$\int Q(\xi)\, d\xi = 1$$

$$\rho = \left[1 + \frac{\sigma_n}{A\Delta\left(\frac{1}{ML_o}\right)}\right]$$

$$= \left[1 + \frac{ML_o\,\sigma_n}{A\Delta}\right] \tag{48}$$

Because the noise level varies with frequency and several different multipath structures are expected, it will be necessary to consider several sets of parameters.

Some allowance must be made for accurate measurement of the low-level detail of $\tilde{Q}(\xi)$, so that this single pulse scheme appears unsuitable because of low signal-to-noise properties.

2.4.5.2 Coherent Processing Using a Coded Sequence

An alternative estimate scheme follows if coherent processing can be carried out at the receiver. Let $z(t)$ be a pseudo-random sequence of period T which is used to phase modulate the carrier (bit length = Δ).

When the sequence is periodic it can be assumed to have the following useful property

$$\int_0^T z(t)\, z^*(t - \tau)\, dt = \phi(\tau) \tag{49}$$

with

$$\phi(\tau) = \begin{cases} \phi(o) & \tau = 0 \\ \dfrac{\phi(o)}{\sqrt{N}} & |\tau| \geq \Delta \end{cases} \tag{50}$$

where

$$\begin{aligned} N &= \text{sequence length} \\ &= T/\Delta \\ &= 2^n - 1 \end{aligned} \tag{51}$$

and $\phi(o)$ is the energy in one period.

However, we are interested in transmitting only a single period before switching to a different channel. Thus, for a particular channel

$$z_o(t) = \begin{cases} 0 & 0 > t > T \\ z(t) & \text{otherwise} \end{cases} \tag{52}$$

The autocorrelation for this aperiodic $z_o(t)$ sequence has been shown to have properties similar to those for a periodic sequence, that is,

$$\begin{aligned} \phi_o(\tau) &= \int_{-\infty}^{\infty} z_o(t)\, z_o(t-\tau)\, dt \\ &\approx \begin{cases} \phi_o(0) & \tau = 0 \\ \dfrac{\phi_o(0)}{\sqrt{N}} & |\tau| \geq \Delta \end{cases} \end{aligned} \tag{53}$$

We now consider an estimate of the form

$$\hat{Q}(\tau) = \left| \int_{-\infty}^{\infty} r(t)\, z_o^*(t-\tau)\, dt \right|^2 - b \tag{54}$$

b is a bias term which will be discussed subsequently. Then

$$\bar{\tilde{Q}}(\tau) = \overline{A \int_{-\infty}^{\infty} g(\xi) z_o(t - \xi)\, g^*(\tau)\, z_o^*(t - \tau)\, d\xi\, dt^2}$$

$$+ \overline{\left| \int_{-\infty}^{\infty} n(t) z_o^*(t - \tau)\, dt \right|^2} - b$$

$$= \overline{A \left| \int g(\xi) \phi_o(\tau - \xi)\, d\xi \right|^2}$$

$$= A \int_{-\infty}^{\infty} Q(\xi) \left| \phi_o(\tau - \xi) \right|^2 d\xi \qquad (55)$$

$$b \equiv \overline{\left| \int_{-\infty}^{\infty} n(t)\, z_o^*(t - \tau)\, dt \right|^2}$$

$$\approx \frac{\sigma_n}{W} \int_{-\infty}^{\infty} \left| z_o^*(t - \tau) \right|^2 dt$$

$$\approx \Delta \sigma_n \phi_o(o) \qquad (56)$$

where b has been chosen so that the second term in the expression above is removed. Using the relationships of Eqs. (55) and (53) it can be seen that

$$\bar{\tilde{Q}}(t) = A \int Q(\xi) \left| \phi_o(\tau - \xi) \right|^2 d\xi$$

$$\approx A \int Q(\xi) \left| p(\xi - \tau) \right|^2 d\xi + C_o$$

$$\approx A \Delta \phi_o^2(0)\, \tilde{Q}(\xi) + C_o \qquad (57)$$

where C_o is a bias term due to the sidelobe structure of $|\phi_o(\tau)|^2$, and $|p(\tau)|^2$ represents $|\phi(\tau)|^2$ in the vicinity of the origin (that is, for $|\tau| < \Delta$).

$\tilde{Q}(\xi)$ as it is defined above is the convolution of $Q(\xi)$ with a pulse of unit area, so that this notation is consistent with previous analysis. The bias term C_o can be bounded using Eq. (53).

$$C_o \approx A \int Q(\xi) \left(\frac{\phi_o(0)}{\sqrt{N}} \right)^2 d\xi$$

$$= \frac{A\phi_o^2(0)}{N} \int Q(\xi)\, d\xi$$

$$= \frac{A\phi_o^2(0)}{N} \tag{58}$$

For a true function $Q(\xi)$ with modes of height,

$$Q(\xi) = \frac{1}{ML_o} \tag{59}$$

the ratio of the average measured mode height to the bias C_o will be of the order,

$$\frac{Q(\tau)}{C_o} = \frac{A\Delta\phi^2(0)/ML_o}{A\phi^2(0)/N}$$

$$= (N\Delta/ML_o) \tag{60}$$

The worst bias effects will occur when $A(\tau)$ is spread, so that the modes are of low magnitude.

Finally, it should be observed that although it is theoretically possible to remove this bias by subtraction, since it appears to depend only on known parameters, in practice the bias will be a function of τ because of variations in the sidelobe structure of $\phi_o(\tau)$.

Variance

$$\mathrm{Var}[\hat{Q}(\xi)] = \overline{\left| \int r(t) z_o^*(t - \xi)\, dt \right|^4} - 2b \overline{\left| \int r(t) z_o^*(t - \xi)\, dt \right|^2} + b^2 - [Q]^2 \tag{61}$$

Denote

$$f(\xi) = \overline{\left| \int r(t) z_o^*(t - \xi)\, dt \right|^2} \tag{62}$$

Then

$$\begin{aligned} \mathrm{Var}[\hat{Q}(\xi)] &= 2f^2(\xi) - 2bf(\xi) + b^2 - [\bar{Q}]^2 \\ &= 2(\bar{Q} + b)^2 - 2b(\bar{Q} + b) + b^2 - [\bar{Q}] \\ &= \bar{Q}(\xi)^2 + 2b\bar{Q}(\xi) + b^2 \\ &= [\bar{Q}(\xi) + b]^2 \end{aligned} \tag{63}$$

$$\text{Standard dev. } (\hat{Q}(\xi)) = \bar{Q}(\xi) + b$$

$$\approx A\Delta\phi_o^2(0)\, \tilde{Q}(\xi) + \Delta\sigma_n\phi_o(0) \tag{64}$$

This approximation follows from Eqs. (56) and (57) with the sidelobe bias neglected. Thus,

$$\rho = \frac{\text{standard deviation } (\hat{Q}(\xi))}{\text{mean } (\hat{Q}(\xi))}$$

$$= \frac{A\Delta\phi_o^2(0)\tilde{Q}(\xi) + \Delta\sigma_n\phi_o(0)}{A\Delta\phi_o^2(0)\tilde{Q}(\xi)}$$

$$= \left[1 + \frac{\sigma_n}{A\phi_o(0)\tilde{Q}(\xi)} \right] \tag{65}$$

This equation has exactly the same form as Eq. (46) except that the equivalent energy is now increased due to compression of the coded sequence, that is,

$$E = A \int_{-\infty}^{\infty} |z(t)|^2 \, dt$$

$$= A\phi_c(0)$$

$$= AT \qquad (66)$$

Note that in computing, the CW power output of the transmitter must be used, rather the peak power.

2.4.5.3 IMPLEMENTATION

The integral of Eq. (54) can be implemented by multiplying the original sequence, which can be generated using phase-reversal keying thus implying that z(t) is real, against the inphase and quadrature components of the received waveform. This is followed by a square-law detector (or possibly linear detection) and an integrate and dump procedure using a low-pass filter with a time constant greater than T. To implement the scheme for a set of τ values requires parallel processing and possibly the use of a tapped delay line. The number of taps depends on the product of the signal bandwidth and the range of delay (τ) to be observed. Figures 18 to 22 indicate the basic structure of the receiver and of the transmitter. Not included is the logic required to switch through the set of frequencies to be measured.

2.4.5.4 Doppler Spectrum Measurements

The Doppler-spreading characteristics of the channel are best observed using a CW source. However, the fading rate is relatively low, so that efficient Doppler measurements on a set of channels requires the use of a sequential sampling approach. Earlier in this report, it was noted that individual channels had to be probed periodically at intervals of T_o ($T_o \geq 1/B_{tot}$) to give useful estimates. By probing at a faster rate than required ($T_o < 1/B_{tot}$), information is obtained that is redundant in terms of the delay power spectrum estimate (or signal level) but which may be useful for Doppler-spectrum estimation.

Consider the sequence of outputs $\{f(nT_o)\}$ obtained when Eq. (54) is implemented. For a particular τ,

$$f(nT_o) = \hat{Q}_{nT_o}(\tau) \qquad \text{(estimate at } nT_o\text{)} \qquad (67)$$

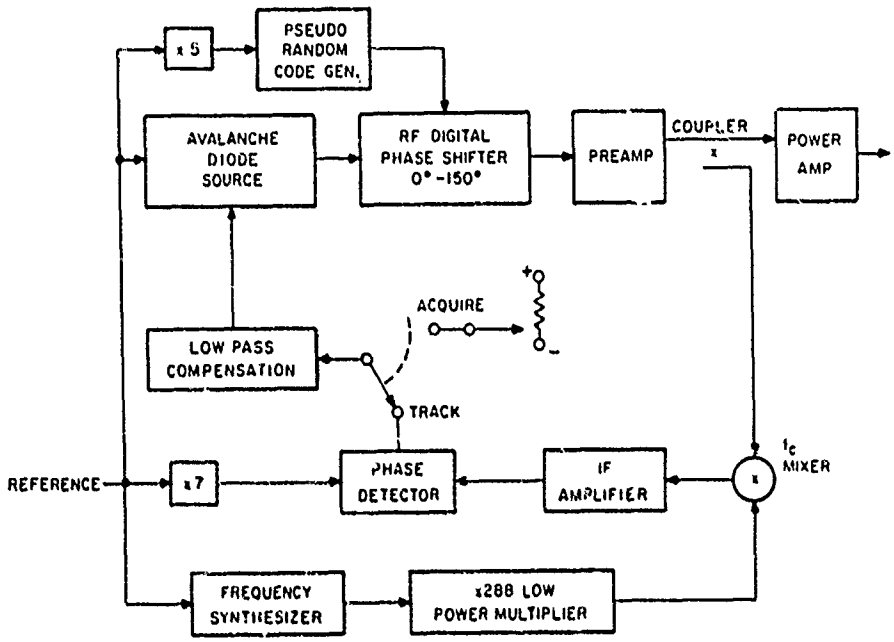

Figure 18. Transmitter System

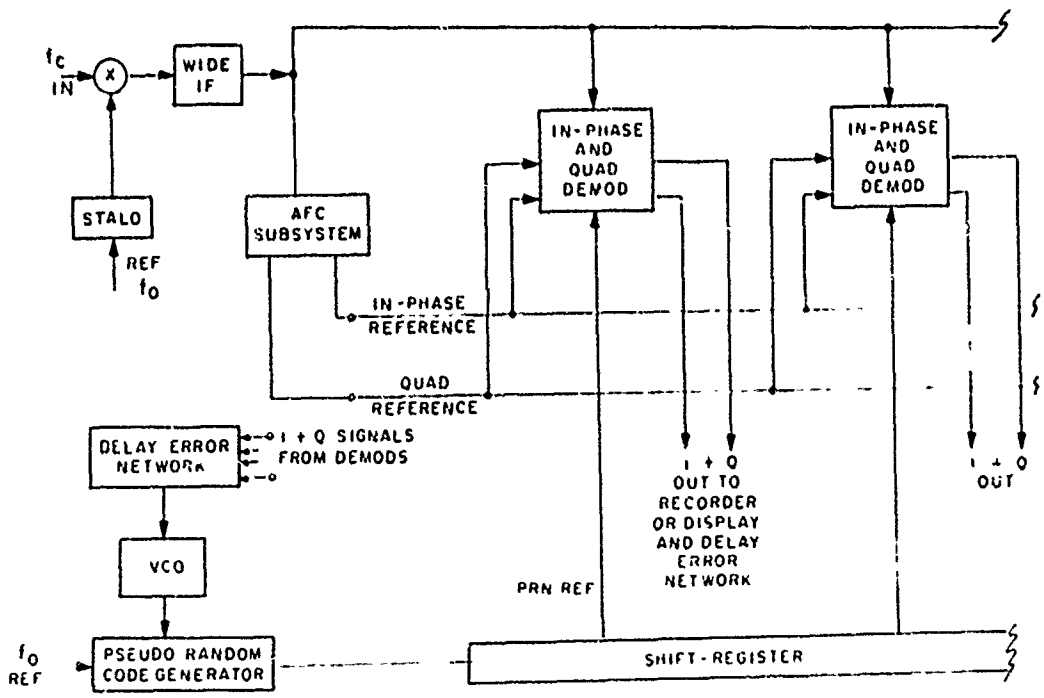

Figure 19. Receiver Overall Block Diagram

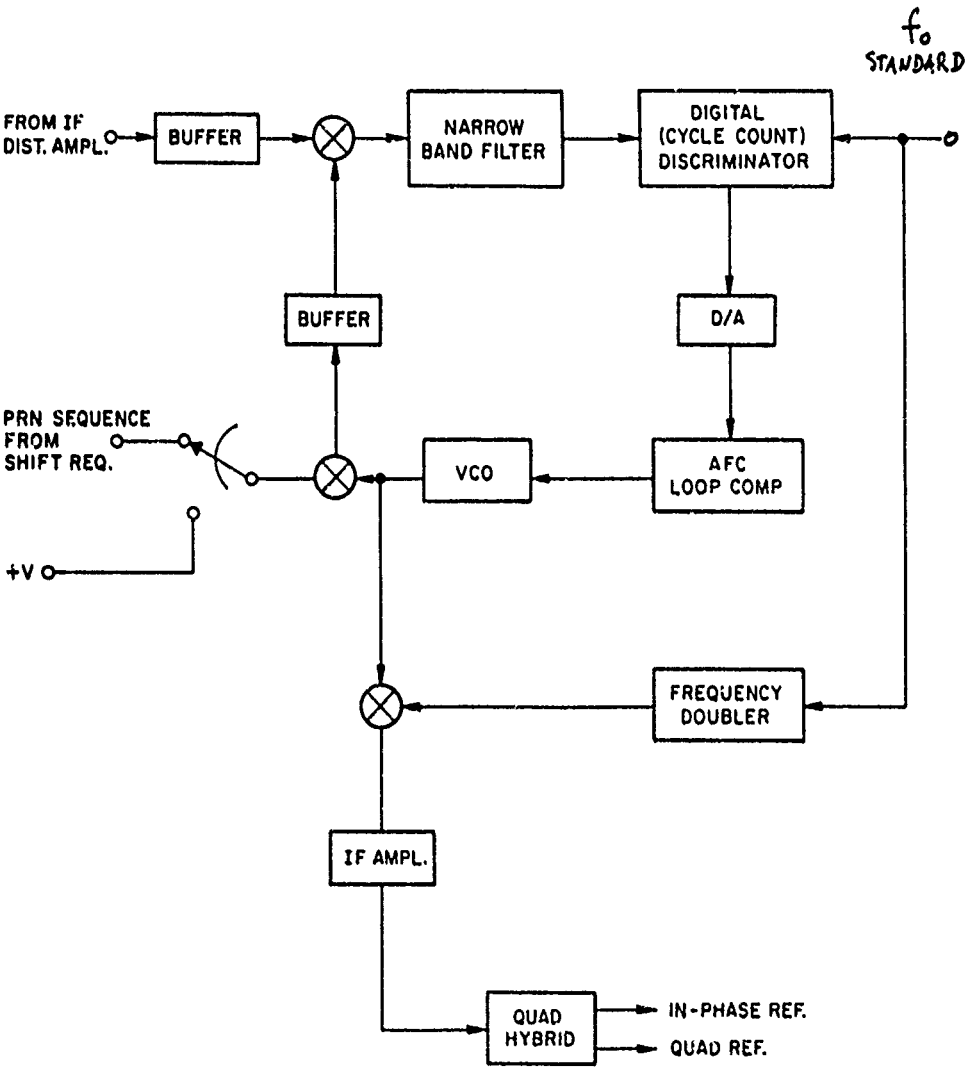

Figure 20. AFC Subsystem

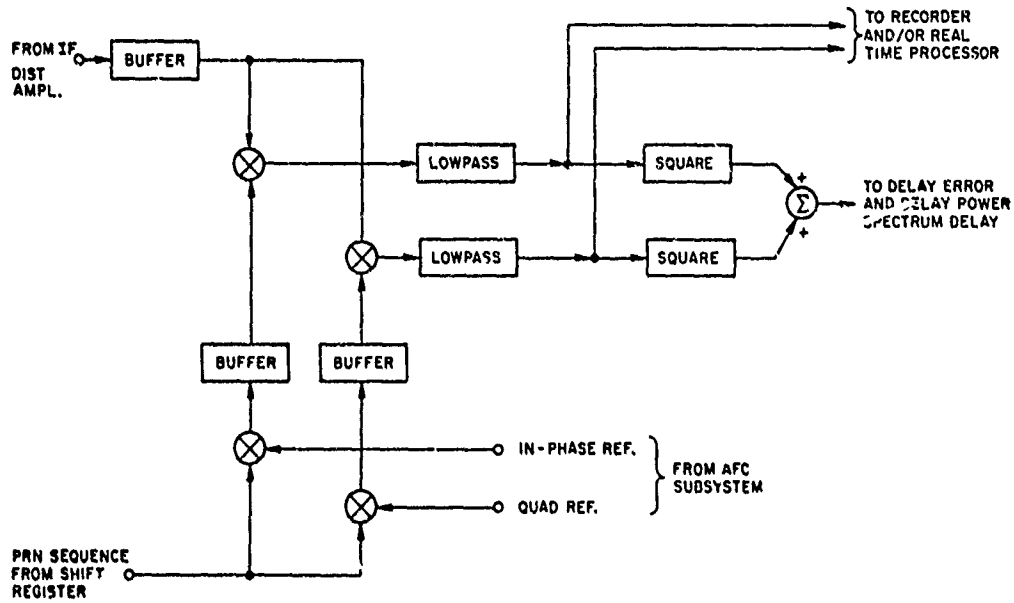

Figure 21. Demodulators I and Q

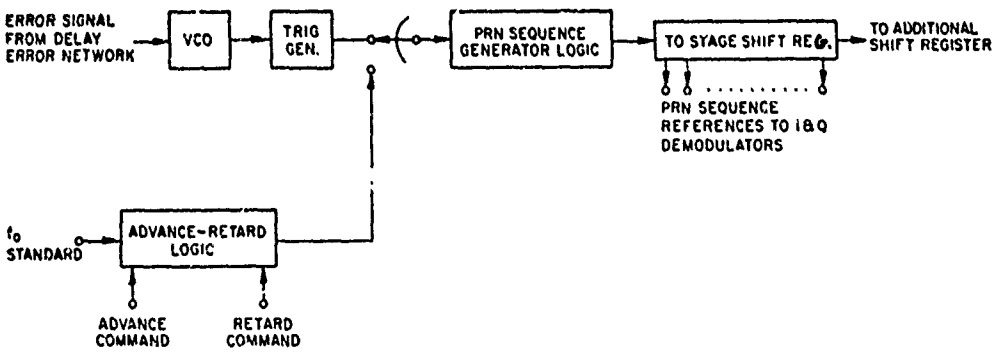

Figure 22. PRN Generator and Shift Registers

Then it can be shown that if the sidelobe interference is neglected,

$$f(nT_o) \approx |g(nT_o, \tau)|^2 \tag{68}$$

Thus, any spectral information obtained from this sequence will relate to the shape of the scattering function for this particular delay τ.

Because of the inherently higher signal-to-noise ratio, it appears that the latter sequence (using simple on-off pulses) offers the best alternative for spectrum analysis. In addition, the total scan time T_o required to probe all channels once is significantly less than for the wideband coded-sequence measurement, thus providing a higher sampling rate and less danger of aliasing effects.

It should be noted that the phase instability of the transmitter oscillator over time intervals of order T_o necessitates the use of an incoherent Doppler measurement. If phase coherence of the oscillator could be assumed, then in-phase and quadrature components generated at each T_o seconds would be used to get the spectral properties directly.

2.4.6 MEASUREMENT OF INSTANTANEOUS IMPULSE RESPONSE

In this section, we discuss the measurement of the instantaneous values of the impulse response of a continuous multipath channel[17] when a periodic train of identically shaped pulses are transmitted. The time duration of the typical pulse is chosen small enough to provide the required resolution to characterize the channel for signals of a specified bandwidth and should also be less than the reciprocal of the Doppler spread. The pulse duration should also be greater than the sum of the channel-impulse response and the transmitted pulse, so as to allow a typical pulse response to become very small before a new pulse arrives.

If the complex envelope of the impulse response of the channel is denoted by $g(t, \xi)$ and the additive noise by $n(t)$, then the complex envelope of the received process is given by

$$w(t) = \sum_k \int p(t - kT - \xi)\, g(t, \xi)\, d\xi + n(t) \tag{69}$$

where $p(t)$ denotes the complex envelope of the typical transmitted pulse. To characterize a channel for use with a signal of bandwidth W, it is only necessary to measure a smeared $g(t, \xi)$, $\hat{g}(t, \xi)$ corresponding to the channel response for a pulse $p(t)$ whose spectrum is flat over the bandwidth W, that is,

$$\hat{g}(t, n) = \int p(n - \xi)\, g(t, \xi)\, d\xi \quad . \tag{70}$$

If the received process w(t) in Eq. (69) is sampled with the periodic impulse train of complex envelope $T = \Sigma \delta(t - \eta - k - T)$, then sampled w(t) is given by

$$Tw(t)\Sigma\delta(t - \eta - kT) = T\Sigma\delta(t - \eta - kT)\, \hat{g}(t, \eta) + T\Sigma\delta(t - \eta - kT)\, \eta(t) \quad . \qquad (71)$$

Thus, the signal component in the complex sampled version of the received process is a sampled version of the desired impulse response. Complex low-pass filtering will then recover the desired impulse response. It is shown in Bello[8] that for a small spread factor of the channel, the impulse response can be measured with a fairly low signal-to-noise ratio of the received r.f. signal.

Another method of measuring the impulse response of the channel is the well-known cross-correlation technique which involves a computation of the short-time cross-correlation function between the output of the channel and the input of the channel. The averaging time is adjusted to be long compared to the time constant of the transmitted probing signal but short compared to the fading-time constant of the channel. To form the short-time cross-correlation function, the received signal is multiplied by a shifted replica of the conjugate of the transmitted signal. The desired channel information is then extracted by filtering the product, using a bandwidth equal to the fading bandwidth.

If the multipath structure of the channel is either discrete, or for all practical purposes, may be regarded as discrete for the class of input-band limited signals for which the channel is to be characterized, the impulse response of such a channel can also be measured by the above-mentioned techniques. If a train of short pulses, short enough to resolve the individual contributions of the discrete paths, is transmitted, the receiver matches the received process by a shifted transmitted pulse train. An integrator notes at which values of shift the maximum outputs occur, and thus determines the set of discrete delays. Once these are determined, the separate paths can be extracted. Similar to the continuous delay case, the discrete paths can also be estimated by the cross-correlation technique.

2.4.7 MULTITONE MEASUREMENT OF THE TIME-VARIANT TRANSFER FUNCTION

The transfer function of the channel can be constructed from frequency-domain samples. A probing signal consisting of tones spaced Ω Hz apart are transmitted and are later extracted from the corresponding received fading tones. The tone spacing should be greater than the Doppler spread to obtain spectrally non-overlapping adjacent tones. The tone spacing should also be less than the reciprocal of the multipath spread.

2.4.8 MEASUREMENT OF CHANNEL-CORRELATION FUNCTIONS

In Section 2.2.2, we outlined three channel-correlation functions: tap-gain correlation function $R(\xi, \tau)$; scattering function $S(\tau_d, f_d)$; and time-frequency correlation function $R(\Omega, \tau)$. If the channel is represented as a WSSUS channel, then the purpose of most channel-probing techniques is to measure one or more of these three channel-correlation functions and associated parameters. These probing techniques are designed to measure the average fading dispersive characteristics of a link. In this section, we discuss four channel-probing techniques, namely the correlation technique, the multitone technique, the chirp technique and the pulse-pair technique. It has been shown in Bello[7] that all these techniques yield essentially the same performance when the measurement error is minimized for a given transmitted energy. The ratio of the square of the maximum value of the channel-correlation function to the mean-square error in the measurement of that channel-correlation function is given for all techniques by the ratio of the average received signal energy and four times the product of the r.f. bandwidth, one-sided noise power density and the channel multipath spread. The measurement times are comparable for the correlation, multitone and the pulse-pair techniques. For the chirp technique, the measurement time is greater by a factor equal roughly to the product of the r.f. bandwidth and the multipath spread.

The Correlation Technique: The correlation technique for the measurement of the tap-gain correlation function $R(\xi, \tau)$ or of the scattering function $S(\tau_d, f_d)$ was originally proposed by Kailath (see Ref. in Bello[7]) and analyzed by Gallagher (see Ref. in Bello[7]). This technique involves the transmission of a sounding signal with an autocorrelation function narrow enough to resolve the multipath structures, for example a pseudo-random sequence of appropriate length. At the receiver, the received waveform is multiplied by a shifted replica of the probing signal at an offset frequency and the difference frequency component is extracted. The autocorrelation function of this extracted component in the variable τ yields the estimate of $R(\xi, \tau)$. Let x(t) be the sounding signal and y(t) be the channel output, then

$$\text{Est}[R(\xi, \tau)] = C_o \int dt\, [x(t - \tau)\, y^*(t)]\, [x^*(t + \xi - \tau)\, y(t + \xi)] \tag{72}$$

and

$$y(t) = \int x(t - \tau')\, g(t, \tau')\, d\tau' \tag{73}$$

where C_o is a constant.

The Multitone Technique: The multitone technique[7] is used to estimate the channel time-frequency correlation function $R(\Omega, \tau)$ by the direct determination of the cross-correlation function between many received tones spaced apart in frequency. The tone spacing should be larger than the Doppler spread and the receiver filter bandwidth.

If $H(j\omega, t)$ is the complex envelope of the received tone, then an estimate of the cross-correlation function between processes corresponding to tones transmitted at frequencies f and $f + \Omega$ Hz from the carrier frequency is given by

$$\text{Est}[R(\Omega, \tau)] = \frac{1}{T} \int_{-T/2}^{T/2} H^*(j\omega, t - \tau/2)\, H(j\omega + j\Omega, t + \tau/2)\, dt \quad . \tag{74}$$

The Chirp Technique: This technique, suggested by Gallagher (ref. in Bello[8]), measures the channel time-frequency correlation function $R(\Omega, \tau)$. This technique involves the transmission of pulses whose frequency varies linearly with time, that is, a sequence of chirp pulses with different frequency slopes. Each received chirp pulse of a given slope is multiplied by a replica generated at the receiver but offset in frequency and the difference frequency component is extracted. The autocorrelation function of this component provides an estimate of $R(\Omega, \tau)$ in the form of $R(\beta\tau, \tau)$ where β is the slope in Hz per second for the chirp pulse $x(t, \beta)$.

Let

$$x(t, \beta) = \exp[j\pi\beta t^2] \qquad |t| < \frac{T_1}{2} \tag{75}$$

where T_1 the pulse duration, is chosen to exceed the integration time T and T must be very much larger than the correlation time of the fading. It is known that fading-correlation time is larger than the path delay. Therefore the estimate of $R(\beta\tau, \tau)$ provided by the chirp-puise technique is given by

$$\text{Est}[R(\beta\tau, t)] = \frac{1}{T} \int_{-T/2}^{T/2} x(t - \tau/2, \beta)\, y^*(t - \tau/2)\, x^*(t + \tau/2, \beta)\, y(t + \tau/2)\, dt \tag{76}$$

where y(t) is received complex envelope given by

$$y(t) = \int x(t - \xi)\, \hat{g}(t, \xi)\, d\xi \quad . \tag{77}$$

The Pulse-Pair Technique: In the pulse-train probing technique, the tap-gain correlation function $R(\xi, \tau)$ is measured by transmitting a sequence (N) of pulse pairs. The separation τ between the members of a pair is chosen larger than the duration of received pulse and the location of the pulse pair is sufficiently separated so that the received signal consists of a distinguishable set of N pulse pairs. The earlier member of the received pair is delayed by τ seconds and multiplied by the conjugate of the later member. From the resulting pulse train, it has been shown in Bello[7] that the tap-gain correlation function can be obtained.

2.5 Discussion of Diversity and Adaptivity

In this report we consider two cases of propagation paths, one characterized by a multipath spread L = 100 microsec, Doppler spread B = 0.1 Hz and path losses 130 dB (correspondent to a midlatitude link) and another characterized by multipath spread L = 1500 microsec, Doppler spread B = 10 Hz and path losses 150 dB to 165 dB (correspondent to a transauroral link). We call the first Case I and the second Case II. In both cases, we have assumed that noise and interference reach overall levels of +30 dB and +45 dB above KTB.

The diversity situation is very different in the two cases. In Case I, the basic diversity cell is a rectangle of size

$$\frac{1}{L} \times \frac{1}{B} = 10^4 \text{ Hz} \times 10 \text{ sec}$$

This means that at a given frequency the fading envelope is correlated for a time interval of 10 seconds, while two frequencies simultaneously emitted are correlated (fading-wise) if their separation is equal to, or less than 10 KHz. In Case II, the cell size is 667 Hz $\times 10^{-1}$ sec. To achieve diversity, the signal's waveform must occupy more than one elementary cell in the diversity grid. This cannot be achieved by lengthening the duration of the waveform (it would not be practical to make the length of a bit several seconds); the only approach available is to choose the spectrum of the radiated waveform to be larger than $1/L$.

By following Kennedy and Lebow[18] we can see in detail how to achieve the required diversity in order to assure an error rate less than a prescribed maximum, for the desired data rate.

To start with, we use FSK modulation. We will extend this analysis to MFSK in a later section of this report. We also assume that the two transmitted FSK signals (mark and space) are composed of n chips, arranged either in time

---

18. Kennedy, R.S. and Lebow, I.L. (1964) Signal desigr for dispersive channels, IEEE Spectrum, Vol. 1, pp. 231-237.

sequence, in parallel, or in some arbitrary series-parallel combination. Let E be the total energy received in all n chips. We also assume that the time-bandwidth product for the radiated waveform is TW = 1. The diversity per chip Z is given by the expressions contained in Table 5. If the mark (space) contains n chips, the total signal diversity is Zn.

Table 5. Expressions to be Used in the Computation of the Diversity Z

If	Then
BT < 1 and LW < 1	Z = 1
BT < 1 and LW > 1	Z = LW
BT > 1 and LW < 1	Z = BT
BT > 1 and LW > 1	Z = BL

In the case of a binary alphabet, the probability of error is computed by using the following expression (also plotted in Figure 23)

$$P_e \cong 0.2\, e^{-\frac{1}{2}\frac{E}{N_o}A(y)} \tag{78}$$

where N_o is the noise-power density (watts/Hz) and the efficiency function A(y) is plotted in Figure 24. The minimum for the probability of error occurs when the function A(y) is at a maximum. From Figure 24, we notice that a broad maximum for A(y) is occurring when $y \cong 0.35$. The corresponding value of A(y) is $A(y) \cong 0.3$.

By making use of the analytical approach illustrated above, let's evaluate how much diversity we need to counteract fading in the case of a binary signalling scheme meant to achieve a data rate R = 24 Kilobits/sec with an error rate 10^{-4}. We assume first to be in Case I path (L = 100 microsec, F = 0.1 Hz, path losses 130 dB).

From Figure 23, in order to achieve $P_e \cong 10^{-4}$, we must have $E/N_o\, A(y) \cong 14$. With the best choice for y ($y \cong 0.35$) we know that $A(y) \cong 0.3$. Therefore, we require

$$\frac{E}{N_o}(0.3) \cong 14 \quad , \quad \frac{E}{N_o} \cong 55 \tag{79}$$

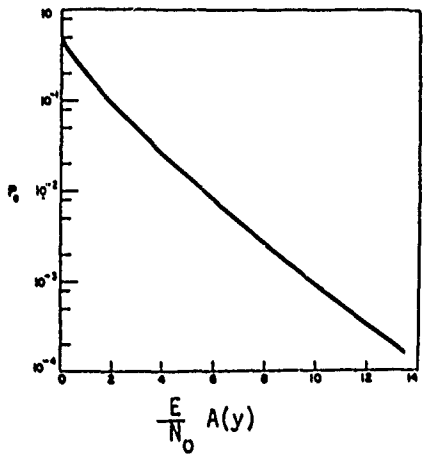

Figure 23. Probability of Error P_e

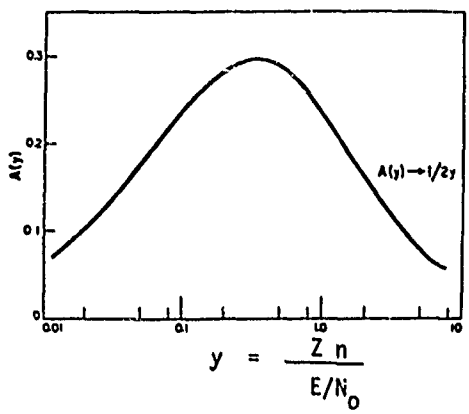

Figure 24. Efficiency Function A(y)

Because, since

$$y = \frac{Zn}{E/N_0} \cong 0.35 \quad , \tag{80}$$

we conclude that we need

$$Zn = 0.35 \times 55 \cong 20 \tag{81}$$

as total signal-waveform diversity. In order to find out how many chips we need, we must obtain from other considerations Z (diversity per chip).

In order to find Z we must determine the products BT and LW, so that we can enter Table 5 and choose the correct expression for Z. We have

$$R = 24 \text{ Kilobit/sec and therefore } T = \frac{1}{R} \cong 41.5 \text{ microsec} \tag{82}$$

This is the length of the mark (and of the space) and the bandwidth that the waveform requires is

$$W = \frac{1}{T} = 24 \text{ KHz} \quad . \tag{83}$$

We are now in a position to compute BT and LW:

$$BT = 0.1 \times 41.5 \times 10^{-6} < 1 \tag{84}$$

$$LW = 10^{-4} \times 24 \times 10^{3} > 1 \tag{85}$$

Therefore from Table 5, we have that $Z = LW$ and consequently, $Z = 2.4$. Because then the required total waveform diversity is $Zn = 20$, we derive immediately how many chips we need

$$n = \frac{20}{Z} \cong 9 \tag{86}$$

This diversity, required to counteract fading, can be achieved for instance by signalling simultaneously on nine carriers, each with a 24-KHz bandwidth. Minimum required separation between two adjacent carriers is $W + B \cong 24$ KHz.

Counteracting fading is not, however, the only problem that we have to solve in order to reliably transmit our 24 Kilobit/sec data rate. In fact, our basic bit length is 41.5 microsec, while the time spread of the channel is 100 microseconds. Therefore, we cannot continue to signal in a certain channel, after the transmission of a bit, for at least 100 microseconds counted from bit's end, or 141.5 microseconds from bit's beginning. Consequently, we need a number of groups of frequencies (each with nine lines) as computed with the formula

$$\frac{T + L}{T} = 1 + \frac{100}{41.5} \cong 4 \tag{87}$$

We have now all the inputs required to make an estimate of the total bandwidth occupancy required by the link, as well as the equipment complexity:

Total bandwidth occupancy:

2	×	9	×	4	×	24 KHz	= 1.728 MHz
mark & space		carriers per group		groups		bandwidth per carrier	

Total number of carriers used: $2 \times 9 \times 4 = 72$.

The above figures apply to simplex communications and must be multiplied by 2 to achieve duplex connection.

In order now to complete the conceptual system design, we must perform an estimate of the required transmitter power. To do this, we compute first the expected noise and interference level in reception. As mentioned in previous sections, we have adopted at HF two values for this level: +30 dB and +45 dB above KTB. Therefore, for the first alternative, we have

$$N_o = 10^3(KT) = 10^3\ 1.38\ 10^{-23}\ 3\ 10^2 = 4.14\ 10^{-18}\ \text{watts/Hz} \quad . \tag{88}$$

The required signal energy is therefore

$$E = 55\ N_o = 2.28\ 10^{-16}\ \text{joules} \tag{89}$$

Consequently, the required signal power is

$$P_r = \frac{E}{T} = 5.48\ 10^{-12}\ \text{watts} \quad . \tag{90}$$

Because the path losses for Case I are 130 dB, inclusive of antenna gains, the transmitter must have a power level

$$P_T = 10^{13}\ P_r = 55\ \text{watts} \quad . \tag{91}$$

Under the assumption that noise and interference amount to +45 dB above KTB, the required level of transmitter power is

$$P_T = 1.74\ \text{K watt} \quad . \tag{92}$$

We have to see now how the situation changes when the propagation path becomes the one of Case II (L = 1500 microsec, B = 10 Hz, path losses 150 dB to 165 dB). These are typical conditions for transauroral propagation. The diversity conditions change radically. We now have

$$\begin{aligned} BT &= 10\ 41.5\ 10^{-6} < 1 \\ LW &= 1.5\ 10^{-3}\ 24\ 10^3 > 1 \end{aligned} \tag{93}$$

and the chip diversity is now Z = LW = 24 1.5 = 36. Table 6 illustrates the transmitter power requirements in this case.

Because the total diversity requirement for the waveform is Z n = 20, a single chip (n = 1) is more than enough. The number of carriers per group is decreased, when going from Case I to Case II, from 9 to 1; however, there is a severe deterioration in the situation of inter-symbol interference. In fact, we need now a much larger number of groups:

Table 6. Transmitter Power Requirements in Transauroral Paths for Binary Waveforms

Path Losses	Noise and Interference Level	Required Transmitter Power
150 dB	+30 dB above KTB +45 dB above KTB	5.5 K watts 174 K watts
165 dB	+30 dB above KTB +45 dB above KTB	174 K watts 5.5 M watts

$$\frac{T + L}{T} = 1 + \frac{1500}{41.5} \cong 38 \qquad (94)$$

This is because we must wait 1500 microsec from the end of a certain bit before being able to go back to signal in the same channel.

The estimate of total bandwidth occupancy and of equipment complexity now yields:

Total bandwidth occupancy:

$$\underset{\substack{\text{mark}\\ \& \\ \text{space}}}{2} \times \underset{\substack{\text{carriers}\\ \text{per}\\ \text{group}}}{1} \times \underset{\text{groups}}{38} \times \underset{\substack{\text{bandwidth}\\ \text{per}\\ \text{carrier}}}{24\ \text{KHz}} = 1.82\ \text{MHz}$$

Total number of carriers used: $2 \times 1 \times 38 = 76$

Not withstanding the large differences between Case I and Case II, as far as the diversity condition is concerned, there is a close similarity between the two cases in terms of total bandwidth occupancy and total number of carriers used. Actually, this is not totally unexpected because going from a path with little time spread to one with large multipath spread, we gain in terms of protection against fading (for a given waveform), but we lose in terms of inter-symbol interference.

These results give a clear indication how the adaptivity of the system could work. If we have available for instance 76 spectral lines in the HF band, each with a bandwidth of 24 KHz, we could arrange 72 of them into four groups of nine carriers when the path is Case I type or we could use all 76 of them (II) in 38 groups, each with a single carrier. This adaptive adjustment to path conditions could be made based on the results of path sounding, channel probing, as well as on the

basis of noise and interference measurements performed for each frequency in use. A control unit would use this information to decide on the best possible arrangements of frequencies and groups, for local use at the terminal where these determinations are made and for transmission to the other terminal, to adapt the parameters of both station equipments to the conditions of the path.

2.6 The Use of M-ary Codes

A substantial improvement in the link's performance can be obtained by using M-ary codes. When the FSK modulation is used, the corresponding approach is called MFSK. With these codes, it is possible in principle to transmit more information through the channel per unit time. The M-ary waveform considered by us consists in the transmission of one out of M frequencies, equally likely, so that the number of bits thus transmitted is $\log_2 M$. It would be $\log_2 2 = 1$ if the transmission were by binary alphabet.

In our study, we have considered a code with M = 8. The adoption of this code makes it possible to achieve a data rate of 2' Kilobit/sec with a pulse length $T = 41.5 \times \log_2 8 = 125$ microsec, corresponding to a bandwidth W = 8 KHz. With M-ary codes, the probability of error is worse than for the binary case. In fact

$$P_{bit, M} = \frac{2^{k-1}}{2^k - 1} (M - 1) P_{bit, Binary} \qquad (95)$$

where $k = \log_2 M$.

If we want to keep $P_{bit, M} = 10^{-4}$ as in the binary case, we must have, for M = 8

$$P_{bit, Binary} = \frac{10^{-4}}{4} = 2.5\ 10^{-5} \quad . \qquad (96)$$

From Figure 23, we have that this probability of error (binary-equivalent) is obtainable with $E/N_o\ A(y) = 17$. The optimum binary-equivalent E/N_o ratio occurs for A(y) = 0.3 and can be derived from the usual equation

$$y = \frac{Z\,n}{E/N_o} = 0.35 \quad .$$

We obtain

$$E/N_o = \frac{Z\,n}{0.35} = \frac{20}{0.35} \cong 57 \quad . \qquad (97)$$

The diversity Z per chip can be computed as follows

Case I

$$LW = 0.8 < 1$$

$$BT = 125\ 10^{-7} < 1 \qquad (98)$$

therefore, $Z = 1$

Case II

$$LW = 1.5\ 10^{-3}\ 8\ 10^{3} = 12 > 1$$

$$BT = 125\ 10^{-6}\ 10 = 12.5\ 10^{-4} < 1 \qquad (99)$$

therefore, $Z = LW = 12$.

We conclude that in Case I, because the required total diversity is $Z_n = 20$, we need only 20 carriers, each with a bandwidth of 8 KHz. In Case II, a total of two carriers is more than enough to counteract path fading. In order to counteract inter-symbol interference, the number of groups that we require can be estimated as follows

Case I

$$\frac{T+I}{T} = 1 + \frac{100}{125} \cong 2 \qquad (100)$$

Case II

$$\frac{T+L}{T} = 1 + \frac{1500}{125} \cong 13 \qquad (101)$$

We have now all the elements to make an estimate of the total bandwidth occupancy required by the MFSK (with M = 8) link, as well as of the equipment complexity

Case I – Total bandwidth occupancy (for simplex)

2	×	8	×	20	×	2	×	8 KHz	= 5.12 MHz
mark & space		M-ary Code		carriers per group		groups		bandwidth per carrier	

Total number of carriers used: $2 \times 8 \times 20 \times 2 = 640$ (for simplex)

Case II – Total bandwidth occupancy (for simplex)

2	×	8	×	2	×	13	×	8 KHz	= 3.33 MHz
mark & space		M-ary Code		carriers per group		groups		bandwidth per carrier	

Total number of carriers used: $2 \times 8 \times 2 \times 13 = 416$ (for simplex)

Concerning then the chip energy, we point out that in the M-ary codes the time duration of the chip is $\log_2 M$ longer than in the binary case. Therefore, we need only

$$\frac{E}{N_o} = \frac{57}{3} = 19 \qquad (102)$$

in the binary-equivalent system.

Because we have for N_o

$$N_o = 4.14 \ 10^{-18} \text{ watts/Hz} \qquad (+30 \text{ dB above KT})$$

or (103)

$$N_o = 1.31 \ 10^{-16} \text{ watts/Hz} \qquad (+45 \text{ dB above KT})$$

the required signal energy levels are respectively

$$E = 8.36 \ 10^{-17} \text{ joules}$$

or (104)

$$E = 2.5 \ 10^{-15} \text{ joules} .$$

The required levels of transmitter power are given in Table 7. It can be seen that there is a factor of almost 10 improvement with respect to the binary-system approach, at the expense of bandwidth occupancy and equipment complexity.

The power densities (watts/Hz) radiated by the proposed M-ary coded emissions are given in the fourth column of Table 7. The equivalent power of a transmitter that would generate equal power density in a 3-KHz voice channel is given in the fifth column of the same table. These levels are relatively low, with the exception of the one on the last line. We have also to point out that our transmitter would be even less bothersome because the emissions would not stay consistently on the same frequencies, but would wander around to follow the adaptivity instructions generated by the microprocessors and control logics.

Table 7. Transmitter Power Requirements in HF Paths for M-ary Transmission With M = 8

Path Losses	Noise and Interference Level	Required Transmitter Power	Radiated Power Density	Equivalent Power in a 3-KHz Channel
Midlatitude Path				
130 dB	+30 dB above KTB	6.67 watts	$1.3\ 10^{-6}$ watts	4 milliwatts
	+45 dB above KTB	211 watts	$4.11\ 10^{-5}$ $\frac{\text{watts}}{\text{Hz}}$	123 milliwatts
Transauroral Path				
150 dB	+30 dB above KTB	667 watts	$2.4\ 10^{-4}$ watts	0.6 watts
	+45 dB above KTB	21.1 Kwatts	$6.34\ 10^{-3}$ $\frac{\text{watts}}{\text{Hz}}$	19 watts
165 dB	+30 dB above KTB	21.1 Kwatts	$6.34\ 10^{-3}$	19 watts
	+45 dB above KTB	667 Kwatts	$2\ 10^{-1}$	600 watts

Note: Pulsewidth = 125 microsec

2.7 Non-Adaptive One-Way Link for Information Transfer Without Feed-Back Acknowledgement

There are cases in which it is neither operationally possible nor advisable to establish a two-way link with feed-back acknowledgement provisions between two terminals. In such cases, adaptivity cannot be embodied into the system and a substantial decrease of communications reliability may result. This is the case that was called Type B Link in Section 2.1.

The way that this case is handled traditionally is to repeat the message on several frequencies. We present in this section an alternative method based on the use of M-ary transmission with a large value of M. Because we have already introduced the M-ary transmission method in Section 2.6 and in Appendix A, we limit ourselves here to a numerical example.

We assume to have M = 64 and we still keep the desired data rate at 24 Kilobit/sec and the specified error rate at 10^{-4}. Pulse length is now T = 41.5. $\log_2 64$ = 249 microsec, that corresponds to a bandwidth of 4 KHz.

We use the same equation for the probability of error that was used in Section 2.6

$$P_{bit,\,M} = \frac{2^{k-1}}{2^k - 1}\,(M - 1)\,P_{bit,\,binary} \tag{105}$$

where, as usual, $k = \log_2 M$. In our case we have therefore that $k = 6$, and

$$P_{bit,\,binary} = \frac{10^{-4}}{32} = 3\ 10^{-6} \tag{106}$$

The function $P_{bit,\,binary}$ is related to the E/N_o ratio by the formula

$$P_{bit,\,binary} = P_e = 0.2 \exp\left\{-\frac{1}{2}\,(E/N_o)\,A(y)\right\} \tag{107}$$

where the symbols have the same meaning as indicated in Section 2.5.

From the formula above, we obtain, by adopting as usual $A(y) = 0.3$

$$E/N_o = 73.77 \tag{108}$$

Therefore, $Z\,n = 0.35\ E/N_o = 26$. For the midlatitude path (Case I), $Z = 1$ (because $LW < 1$ and $BT < 1$), hence $n = 26$. For the transauroral path (Case II, we have $Z = LW = 6$ (because now $LW > 1$, $BT < 1$), hence $n = 5$.

In order to counteract the inter-symbol interference problem, we have to compute

Case I

$$\frac{T + L}{T} = 2 \tag{109}$$

Case II

$$\frac{T + L}{T} = 7 \tag{110}$$

With this, we now have all the parameters necessary for the evaluation of the required bandwidth occupancy and of the number necessary for the carriers:

Case I – Total bandwidth occupancy (for simplex)

$2 \times 64 \times 26 \times 2 \times 4$ KHz = 26.62 MHz

Total number of carriers used (for simplex)

$2 \times 64 \times 26 \times 2 = 6656$ carriers

As the reader can see, this numerical example was worked out to correspond to the total bandwidth occupancy of the entire HF band considered in our study: from 3 MHz to 30 MHz (27-MHz band considered as available in principle). This

was a consequence of the adoption of the value M = 64. A calculation that would be of interest to perform in follow-up activity would be the estimate of the increase in error rate when portions of the HF spectrum (3 to 30 MHz) disappear in propagation outages.

For the transauroral paths, we have

Case II – Total bandwidth occupancy (for simplex)

$$2 \times 64 \times 5 \times 7 \times 4 \text{ KHz} = 17.92 \text{ MHz}$$

Total number of carriers used (for simplex)

$$2 \times 64 \times 5 \times 7 = 4480 \text{ carriers}$$

As far as chip's energy is concerned, we have

$$E/N_o = \frac{73.77}{6} = 12.3 \qquad (111)$$

in the binary-equivalent system. Because the values that we have adopted for N_o are as follows:

$$N_o = 4.14 \ 10^{-18} \text{ watts/Hz} \qquad (+30 \text{ dB above KT})$$

or (112)

$$N_o = 1.31 \ 10^{-16} \text{ watts/Hz} \qquad (+45 \text{ dB above KT})$$

we obtain the required signal energy levels

$$E = 50.9 \ 10^{-18} \text{ joules}$$

or (113)

$$E = 16.11 \ 10^{-16} \text{ joules} .$$

Table 8 provides the values of the transmitter power levels necessary to achieve the signal energies above (pulse width = 249 microsec).

Table 8. Transmitter Power Requirements in HF Paths for Non-Adaptive M-ary Transmission With M = 64

Path Losses	Noise and Interference Level	Required Transmitter Power	Radiated Power Density (watts/Hz)	Equivalent Power in a 3-KHz Channel
Midlatitude Paths				
130 dB	+30 dB above KTB	2 watts	$0.075\ 10^{-6}$	0.225 milliwatts
	+45 dB above KTB	64.4 watts	$2.419\ 10^{-6}$	7.258 milliwatts
Transauroral Paths				
150 dB	+30 dB above KTB	200 watts	$11.16\ 10^{-6}$	33.5 milliwatts
	+45 dB above KTB	6.44 kilowatt	$0.359\ 10^{-3}$	1.1 watts
165 dB	+30 dB above KTB	6.44 kilowatt	$0.359\ 10^{-3}$	1.1 watts
	+45 dB above KTB	203.6 kilowatt	$11.33\ 10^{-3}$	34 watts

Note: Pulsewidth 249 microsec

3. PROPOSED EXPERIMENTAL ACTIVITY

Experiments on the diversity and adaptivity aspects of the proposed scheme could be performed by adopting an evolutionary approach that could start from the analysis of existing digisonde data (records of the IF output are essential in order to perform measurements of the Doppler spread), and from a review of the state-of-the-art of the required instrumentation (frequency-agile transmitters and receivers, broadband HF antennas and matching units, high-speed frequency switching, etc.).

Later on we could construct the breadboard of a one-way link designed according to the principles of the system approach illustrated herewith and we could obtain valuable data of the "path-sounding" and "channel-probing" category. These data would provide a reliable picture of the diversity aspects of midlatitude and transauroral paths.

Fundamental parameters that must be gathered both for the midlatitude and the transauroral case are the following:

1. Statistics of path losses, to be summarized in a diagram "percentage of time that the path losses are lower than the abscissa";

2. Statistics of multipath spread, again leading to the diagram "percentage of time that the multipath spread is smaller than the abscissa";

3. Statistics of Doppler spread, again to be summarized in the diagram "percentage of time that the Doppler spread is smaller than the abscissa";

4. Statistics of the noise and interference levels, leading to the diagram: "percentage of time that the level of noise plus interference is smaller than the abscissa.

The measurements above must be carried out for extended periods both for the midlatitude and the transauroral case, and must be performed at a number of frequencies in the band 3 MHz to 30 MHz at least equal to the number of frequencies mentioned in Table 4. In principle, the separation between two adjacent frequencies should actually be smaller than or equal to the coherent bandwidth of the path (in the models adopted in Section 2, this is 100 KHz for the midlatitude path and only 666 Hz for the transauroral path). However, the adoption of this criterion would lead to rather cumbersome instrumentation, and our suggestion is to start first with a number of frequencies as indicated in the Table 4 mentioned above. This would be sufficient for the limited albeit important scope of exploring the feasibility of the specific scheme proposed in Section 2, where the closest that the spot frequencies were allocated was 8 KHz.

Once that the one-way link tests would be completed, we could perform experiments with an expanded breadboard, that could make it possible to test the adaptivity features of the proposed scheme. This would, of course, require the two-way link between the two terminals.

4. CONCLUSIONS AND RECOMMENDATIONS

The conclusions of our study on adaptive utilization of HF propagation paths indicate that by spreading the radiated power across several MHz of bandwidth occupancy, it is possible to counteract effectively both waveform fading and inter-symbol interference. By this method, data rates of 24 Kbit/sec with 10^{-4} error rates are possible. If this is confirmed by the proposed experimentation, HF would acquire a reliability and channel capacity of the degree that is enjoyed by other communications media. The penalty that must be paid to achieve these results is equipment complexity and bandwidth occupancy. Concerning the first point, modern advances in microprocessor technology, high-density packaging, frequency agility, etc., offer concrete promises. As far as the second point is concerned, the power of the transmitter is so spread that the link would hardly interfere (and for not very long time intervals, because of frequency wandering) with a receiving site.

Our recommendation is that the present study be followed by additional R&D activity in three basic directions: a deeper understanding of the propagation properties of the two types of paths considered, a gathering of experimental data, and an engineering study of the availability and applicability of such modern technological breakthroughs as microprocessors, frequency-agile transmitters and receivers, broadband HF antennas and matching units, switch circuits, decision logics, etc.

References

1. Baghdady, E.J. (1969) Principles of simulation of randomly time-varying channels, IEEE International Conference Communications, Boulder, Colorado, June 9-11, pp. 40-3 to 40-18.
2. Price, R. and Green, P.E. (1958) A communication technique for multipath channels, Proc. IRE, pp. 555-570.
3. Kailath, T. (1959) Sampling Models for Linear Time-Variant Filters, MIT-RLE Report No. 352, Cambridge, Mass.
4. Daly, R.F. (1964) On the Modeling of Time-Varying Frequency-Selective Radio Channels, SRI Project No. 4172, Contract DA 36-039SC-90859.
5. Esposito, R. and Grossi, M.D. (1971) Channel Characterization for Digital Communications in Ground-to-Space HF Paths, 11th Technical Meeting of the Joint Satellite Study Group (JSSG), Florence, Italy, October 4-9.
6. Grossi, M.D. (1971) Experimental HF Back-Up/Emergency Communications System for Space Shuttle/Space Station, Raytheon Prop. ER70-4333.
7. Bello, P.A. and Esposito, R. (1970) Measurement techniques for time-varying dispersive channels, Alta Frequenza, No. II, Vol. XXXIX, pp. 980-996.
8. Lomax, J.B. (1970) HF propagation dispersion, in Phase and Frequency Instabilities in Electromagnetic Wave Propagation, K. Davies, editor, pp. 497-510, AGARD Conference Proceedings No. 33, Techvision Services, Slough, England.
9. Bello, P.A. (1969) Measurement of random time-variant linear channels, IEEE Trans. Info. Th., IT-25, No. 4, July.
10. Davies, K. (1965) Ionospheric Radio Propagation, NBS Monograph No. 80.
11. Dailey, D.K. (1959) The effect of multipath distortion on the choice of operating frequencies for HF communications circuits, IRE Trans. Antenna and Propagation, AP-7, 398.

12. Lomax, J.B. (1970) HF propagation dispersion, in Phase and Frequency Instabilities in Electromagnetic Wave Propagation, K. Davies, editor, pp. 497-510, AGARD Conference Proceedings No. 33, Techvision Services, Slough, England.

13. Shaver, H.N., Tupper, B.C., and Lomax, J.B. (1967) Evaluation of a Gaussian HF channel model, IEEE Trans. on Communications Technology, Vol. 15, No. 1, pp. 79-88.

14. Shepherd, R.A. and Lomax, J.B. (1967) Frequency spread in ionospheric radio propagation, IEEE Trans. on Communications Technology, Vol. 15, No. 2, pp. 268-275.

15. Gupta, A.K. (1979) Dissertation abstract, IEEE Trans. Info. Theory, p. 760.

16. Bello, P.A. (1965) On the rms bandwidth of non-linearly envelope detected narrowband Gaussian noise, IEEE Trans. on Info. Theory, pp. 236-239.

17. Bello, P.A. (1965) Some techniques for the instantaneous real-time measurement of multipath and Doppler spreads, IEEE Trans. on Comm. Tech., Vol. 13, No. 3, pp. 155-192.

18. Kennedy, R.S. and Lebow, I.L. (1964) Signal design for dispersive channels, IEEE Spectrum, Vol. 1, pp. 231-237.

Appendix A

M-ary Transmission Methods

A1. GENERAL

In this appendix, the performance of three basic data-transmission methods, namely, m-level Phase Shift Keyed, m-level Amplitude Shift Keyed and m-level (orthogonal) Frequency Shift Keyed are compared. The problem addressed is one of detecting a known signal in a white noise background with minimum probability of error. The approach adopted is that of Arthurs and Dym[A1] who address this problem from a geometric point of view.

The analysis of data-transmission systems is commonly based on the following model. There is assumed to exist a message source generating a stream of equally likely messages, M_1, M_2, ..., M_m, into a waveform generator having available an alphabet of m distinct waveforms, $S_1(t)$, $S_2(t)$, ..., $S_m(t)$, each of duration T (and necessarily finite energy). One waveform is transmitted every T seconds, the choice of waveform depending in some fashion on the incoming message and possibly on the waveforms transmitted in preceding time slots. The medium coupling the transmitter to the receiver is assumed to add stationary white-zero mean-Gaussian noise to the transmitted signal but otherwise is assumed to be distortion free. It is generally further assumed that the receiver is time-synchronized with

---

A1. Arthurs, E. and Dym, H. (1962) On the optimum detection of digital signals in the presence of white Gaussian noise, IRE Trans. on Communications Systems, Vol. CS-10, pp. 336-372.

the transmitter (synchronous detection). Sometimes it is also assumed that the receiver is phase-locked to the transmitter (coherent detection). Here we shall always assume time synchronism but shall distinguish between coherent and incoherent detection.

The problem we are generally interested in solving, given this model (see Figure A1), is how to design the receiver so that it makes as few errors as possible. Furthermore, assuming than an optimum receiver (optimum in the sense that it will make fewer errors in the long run than any other receiver) is constructed, we are interested in calculating its error rate.

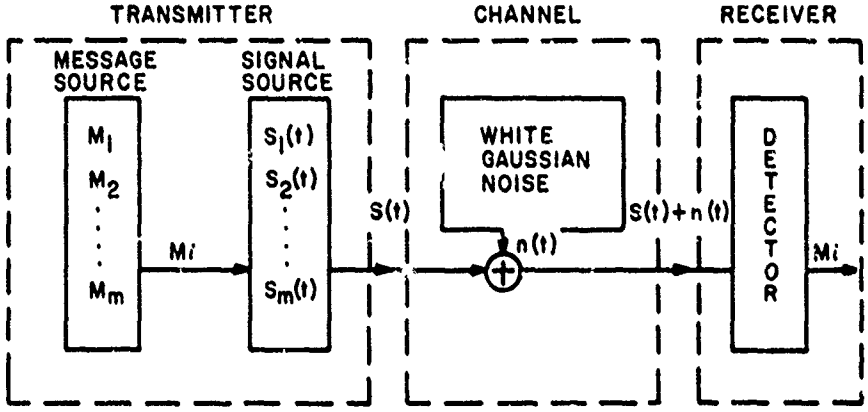

Figure A1. Idealized Model of a Data-Transmission System

In this model, following assumptions are made:

1. Each signal waveform is transmitted with equal probability.

2. The transmitter is subject to an average power limitation, E/T (watts), where T is the duration of each transmitted signal waveform.

3. The received signal is the sum of the transmitted signal and stationary white-zero mean-Gaussian with double-sided spectral density N_o (watts/Hz).

4. The receiver is in time synchronism with the transmitter; however, the distinction is made whether the receiver is phase-locked to the transmitter.

5. The received signal is processed by a maximum-likelihood detector except in the ASK incoherent case.

6. In FSK and PSK cases, the transmitted sinusoidal pulses contain equal energy E whereas in the ASK case the amplitudes (square root of the energy) of the transmitted pulses are uniformly spaced starting with zero. Furthermore, FSK signals are orthogonal.

A2. DISCUSSION

A2.1 Introductory Remarks

In the following discussions, we will compare the performance of the M-ary data-transmission systems, when a fixed-waveform duration is transmitted, and when waveform duration is varied to maintain a fixed-signalling rate. In Sections A2.2 and A2.3 we will provide the curves (only for FSK case) of the probability of error ($10 \log_{10} p_e$) as a function of signal-to-noise ratio (in decibels), with the number of levels m appearing as a parameter. In Section A2.4 we compare these systems on the basis of bandwidth.

A2.2 Comparisons Assuming Fixed-Waveform Duration

It is known that increasing m (the number of waveforms transmitted in anytime T) tends to increase the probability of error whereas increasing the energy content in each transmitted signal (that is, the signal-to-noise ratio) tends to decrease the probability of error. Increasing m introduces the most degradation in the ASK case, somewhat less degradation in the PSK case and comparatively little degradation in the FSK case (Figures A2 and A3). In fact, for large m, the average probability of error of an FSK system should be smaller than that of a PSK or an ASK system. If one compares these systems on the basis of coherency vs. incoherency, the PSK system suffers the most degradation in performance due to lack of coherence. Calculations show that for large m, the cost of incoherence is a 3-dB degradation in signal-to-noise ratio. For small m, the degradation is somewhat less. In the ASK and FSK cases (Figure A4) it has been shown that for a small probability of error (say, $p_e < 10^{-5}$) the degradation between coherent and incoherent is of the order of a decibel or less.

A2.3 Comparisons Assuming a Fixed-Signaling Rate

Instead of maintaining the duration of each transmitted pulse at a fixed value T independent of m, we now consider the equally valid constraint of a fixed rate R (we are still assuming that the transmitter is average-power limited). Under this constraint, we can allow a longer time duration for each waveform in a multilevel system and, hence, increase the energy content of the transmitted signals. Assuming that the rate at which data is being transmitted,

$$R = \frac{\log_2 m}{T_m} \quad \text{(bits/sec)} \quad , \tag{A1}$$

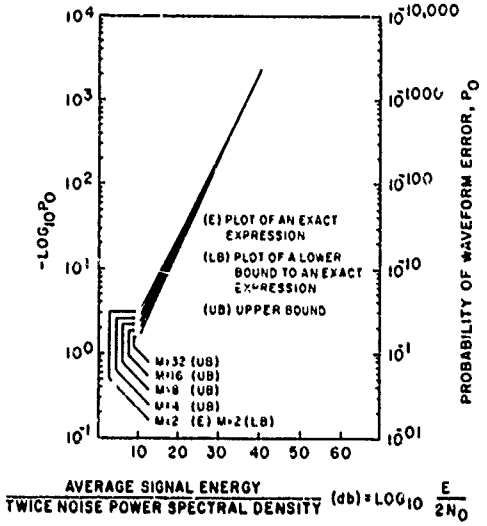

Figure A2. Probability of Waveform Error (m-Level FSK Coherent) Assuming That the Duration of Each Signal Is Fixed Independently of m

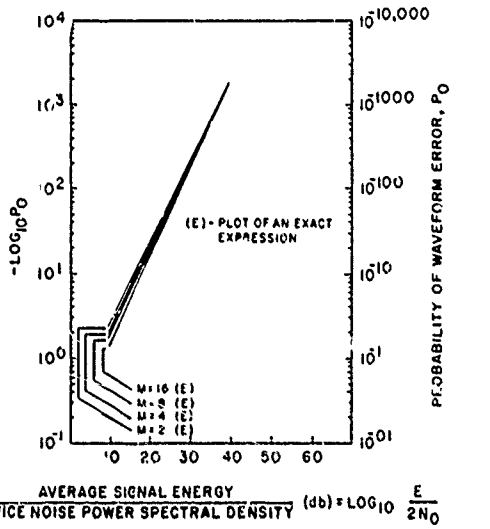

Figure A3. Probability of Waveform Error (m-Level FSK Incoherent) Assuming That the Duration of Each Signal Is Fixed Independently of m

is maintained constant, it follows that

$$T_2 = \frac{1}{R} \tag{A2}$$

and, therefore, that

$$T_m = T_2 \log_2 m \tag{A3}$$

since the transmitter is average-power limited,

$$\frac{E_m}{T_m} = \frac{E_2}{T_2} \quad . \tag{A4}$$

Combining Eqs. (A3) and (A4) yields

$$E_m = E_2 \log_2 m \tag{A5}$$

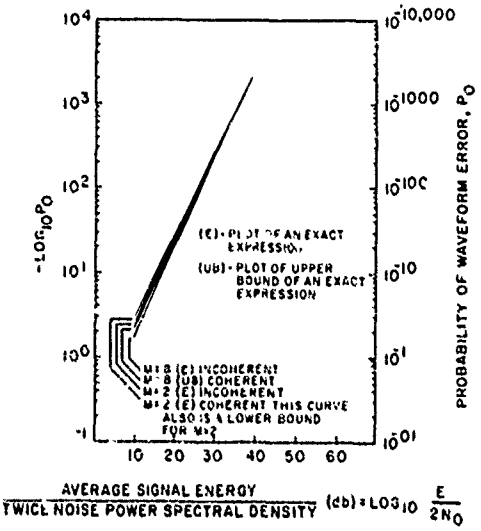

Figure A4. Comparison of Coherent FSK and Incoherent FSK

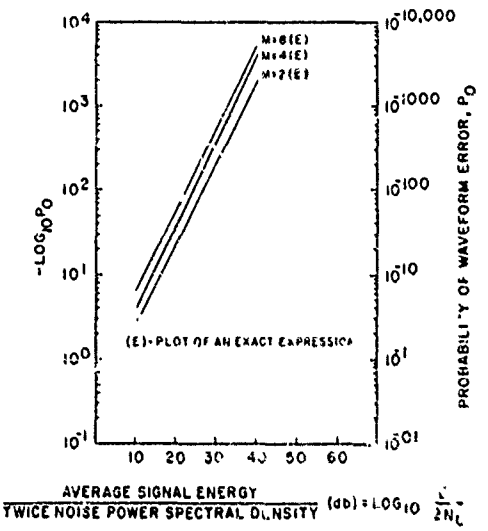

Figure A5. Probability of Waveform Error (m-Level FSK Incoherent) Assuming That Signal Duration Is Adjusted to Keep the Data Rate Constant

from which it follows that

$$10 \log_{10} \left(\frac{E_m}{2 N_o} \right) = 10 \log \frac{E_2}{2 N_o} + 10 \log_{10} (\log_2 m) \qquad (A6)$$

That is to say, under the assumptions of constant rate an m-level system has a signal-to-noise ratio advantage of $10 \log_{10} (\log_2 m)$ dB over its two-level counterpart. If one computes the probability of error for these cases, one finds that the multilevel PSK and ASK systems are inferior in performance to their two-level counterparts whereas FSK systems seem to improve in performance with increasing m (see Figure A5).

A2.4 Discussion of Bandwidth

Thus far, all comparisons have been made under the assumption that a distortionless "wideband" Gaussian channel is available. In practice, the bandwidth allotted to any one transmitter is generally limited and, hence, the relative efficiency with which it uses the available bandwidth of prime interest. The parameter

r is defined as the ratio of the rate at which information is being transmitted, $R = \log_2 m/T$ bits/sec, to the Nyquist rate of transmission, 2B bits/sec, that is

$$r = \frac{R}{2B} = \frac{\log_2 m}{2BT} \quad . \tag{A7}$$

It is quite difficult to define B precisely; for the purposes of the present discussion, if a sinusoid of duration T and frequency f_o will be passed with negligible distortion by an ideal filter with passband 1.5/T centered around f_o. It follows therefore, that for the PSK and ASK modulation schemes wherein the frequency of the pulses sent in each time slot is fixed the required transmitter bandwidth $B \cong 1.5/T$ and, correspondingly, the bandwidth efficiency

$$r = \frac{\log_2 m}{3} \quad . \tag{A8}$$

In the FSK case, however, assuming a separation of 1/T between adjacent tones, an m-level transmitter requires a bandwidth

$$B = \frac{m + 0.5}{T} \quad , \tag{A9}$$

and which case

$$r = \frac{\log_2 m}{2m + 1} \quad . \tag{A10}$$

In the FSK coherent case, however, adjacent signals need only be separated by a frequency difference of 1/2T to maintain orthogonality and, hence, the required bandwidth may be reduced to

$$B = \frac{m + 2}{2T} \quad , \tag{A11}$$

resulting in a bandwidth efficiency of

$$r = \frac{\log_2 m}{2 + m} \quad . \tag{A12}$$

It is apparent from Figure A6 that simple multilevel orthogonal FSK systems, even under idealized operating conditions, are inefficient users of bandwidth. Physically, the reason is clear; in any time period T only a fraction of the total system bandwidth, namely, that occupied by the particular tone transmitted, is utilized. Thus, we see that although the number of levels of an FSK system may be increased with relatively little degradation in performance, there is corre spondingly an increase in the bandwidth required by the system to operate. In contrast, multilevel ASK and PSK modulation schemes utilize the bandwidth more efficiently but the probability of error increases with m.

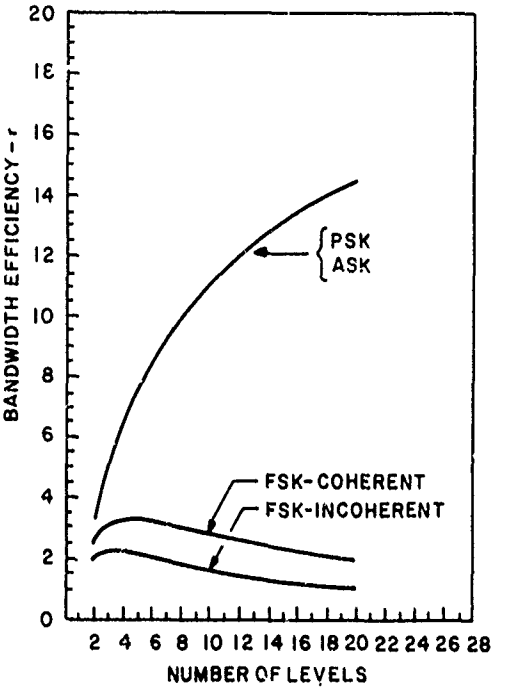

Figure A6. Plot of Bandwidth Efficiency as a Function of the Number of Levels

A2.5 Signal Selection for M-ary Transmission

For the complete evaluation of a communi cation system and the related coding schemes, one needs to determine not only the error probability as a function of the signal-to-noise ratio and data rate, but also the bandwidth occupancy of the transmission channel. The most direct definition of bandwidth occupancy of a given channel is the minimum frequency separation between channels such that signals of one channel have no effect on the coder of any other. Let a signal of the α-th channel be denoted by $x_{\alpha}^{(i)}(t)$ and one of another channel $x_{\beta}^{(j)}(t)$. The α-th channel decoder operates on any received signal y(t) with the M possible transmitted signals $x_{\alpha}^{(i)}(t)$ of the given channel to form the quantities

$$\frac{1}{T}\int_{0}^{T} y(t)\, x_{\alpha}^{(i)}(t)\, dt \quad . \tag{A13}$$

Thus, there will be no effect on the decoder of either channel due to the signal of the adjacent channel provided

$$\int_0^T x_\alpha^{(i)}(t)\, x_\beta^{(j)}(t)\, dt = 0 \tag{A14}$$

for all i and j and for all α and β. Denoting the elementary signals of the α^{th} channel by S_o and S_1, and those of the β^{th} by S_o' and S_1', the condition becomes

$$\int_0^{T/n} S_r(t)\, S_m(t)\, dt = 0 \tag{A15}$$

for r and m + 0, 1, where each output signal $x^{(i)}(t)$ of duration T seconds consists of a sequence of n signals, each of duration T/n seconds, chosen randomly from the two elementary signals $S_o(t)$ and $S_1(t)$. Thus the bandwidth occupied by $x^{(i)}(t)$ depends on the time functions $S_o(t)$ and $S_1(t)$.

The above orthogonal condition is satisfied if the elementary signals of the α-th channel are taken to be

$$S_r(t) = \sqrt{2S}\cos\left(\frac{\alpha\pi n}{T}\right)t \tag{A16}$$

those of the other channel are

$$S_r'(t) = -\sqrt{2S}\cos\left(\frac{\beta\pi n}{T}\right)t \quad . \tag{A17}$$

Thus it is clear that the minimum frequency separation or the bandwidth occupancy of each channel is $(\pi n/T)$[rad/sec] or $(n/2T)$[Hz]. Other channels can obviously be placed at radian frequencies which are multiplies of $\pi n/T$ away.

The transmitted signals are readily generated by coding each elementary signal which itself is generated either by balanced modulating the carrier or by phase modulating it by $\pm 90^o$. At this point it is useful to review and discuss briefly the basic physical parameters. A set of $M = 2^K$ equiprobable signals $x^{(i)}(t)$, each of duration T seconds are received at a power level of S watts with additive stationary white Gaussian noise of spectral density N_o watts/Hz. The relationships among signals which are pertinent to the reception problem are their normalized inner products

$$\rho_{ij} = \frac{\int_0^T x^{(i)}(t)\, x^{(j)}(t)\, dt}{ST} \quad . \tag{A18}$$

The error probability P_E for the optimal decoder is a function of ST/N_o and the $[\rho_{ij}]$ matrix. When $x^{(i)}(t)$ is generated as a sequence of n elementary binary signals ρ_{ij} is expressible in terms of the number of agreements and disagreements in the binary-code vectors from which $x^{(i)}(t)$ and $x^{(j)}(t)$ was generated. For, in this case

$$\rho_{ij} = \frac{1}{ST} \sum_{r=1}^{n} \int_{(r-1)T/n}^{r(T/n)} x^{(i)}(t)\, x^{(j)}(t)\, dt \quad . \tag{A19}$$

For the elementary signals, each term of the summation is either +ST/n or -ST/n, depending on whether the code symbols for $x^{(i)}$ and $x^{(j)}$ during the specific sub-interval were the same or different. Hence for binary signals,

$$\rho_{ij} = \frac{\text{\# agreements} - \text{\# disagreements}}{n} \quad . \tag{A20}$$

Any one of the M equiprobable transmitted signals contains $\log_2 M$ bits of information. Since each signal requires T seconds for transmission, the transmitted information rate is given by

$$R = \frac{\log_2 M}{T} = \frac{K}{T} \text{ bits/sec} \quad . \tag{A21}$$

The time required to transmit one bit is

$$T_\beta = \frac{T}{\log_2 M} = \frac{T}{K} \text{ sec/bit} \quad . \tag{A22}$$

In order to compare communication systems properly for different values, the error probability should be considered as a function of ST_β/N_o, which is the received signal energy per bit, divided by the noise spectral density. This will be one measure of comparison for signal sets of different size, M, and different matrices $[\rho_{ij}]$. The other basic parameter is the ratio of bandwidth occupancy-to-data rate W/R. Bandwidth occupancy was shown above to be n/2T Hz, where n is the number of sub-intervals of the code signal. Taking the ratio of this to the rate, it follows that

$$\frac{W}{R} = \frac{n}{2 \log_2 M} = \frac{n}{2K} \quad . \tag{A23}$$

In general, the aim will be to find classes of codes which produce as low an error probability as possible for a given K and ST_β/N_o ratio, under a constraint of the W/R ratio.

A2.6 Performance of Orthogonal Code Signals for M → ∞

Although orthogonal signals are not optimal for communication over the Gaussian channel, for large numbers of signals M they nearly achieve the highest degree of trans-orthogonality because the maximum correlation coefficient can be no smaller than $-1/(M-1)$, which is very nearly zero for large M. Also their performance is simplest to analyze because the correlation matrix $[\rho_{ij}] = I$ and consequently the expression for error probability reduces[A2] to

$$1 - P_E = P_C = \int_{-\infty}^{+\infty} \frac{\exp[-v_1^2/2]}{\sqrt{2\pi}} \left[\int_{-\infty}^{v_1+\sqrt{2ST/N_o}} \frac{e^{-v^2/2}}{\sqrt{2\pi}} \right]^{M-1} dv_1$$

$$= \int_{-\infty}^{\infty} \frac{\exp[-v_1^2/2]}{\sqrt{2\pi}} \operatorname{erf}\left[\left(v_1 + \sqrt{\frac{2ST}{N_o}}\right)\right]^{M-1} dv_1 \qquad \text{(A24)}$$

P_E is independent of which signal was transmitted since v_1 is merely a dummy variable of integration. The above equation has been integrated numerically using an IBM computer for $M = 2^K$ for K = 1 through 10 and for K = 15 and 20. For proper comparison of the results for different values of M, the independent variable should be ST_β/N_o where $T_\beta = T/\log_2 M$. Figure A7 presents results and demonstrates that for all but very low values of ST_B/N_o, the error probability decreases with the number of signals in the set, M, or the data-vector dimension K.

It is particularly interesting to consider the limiting behavior of P_E as M approaches ∞. The similar results shown below, are also true for noncoherent reception of M-ary transmission. The optimum receiver in this case consists of a set of M-envelope correlation detectors returning to the above equation

---

A2. Golomb, S.W., editor (1964) Digital Communications with Space Applications, Prentice Hall, New York, N.Y., Chapter 7.

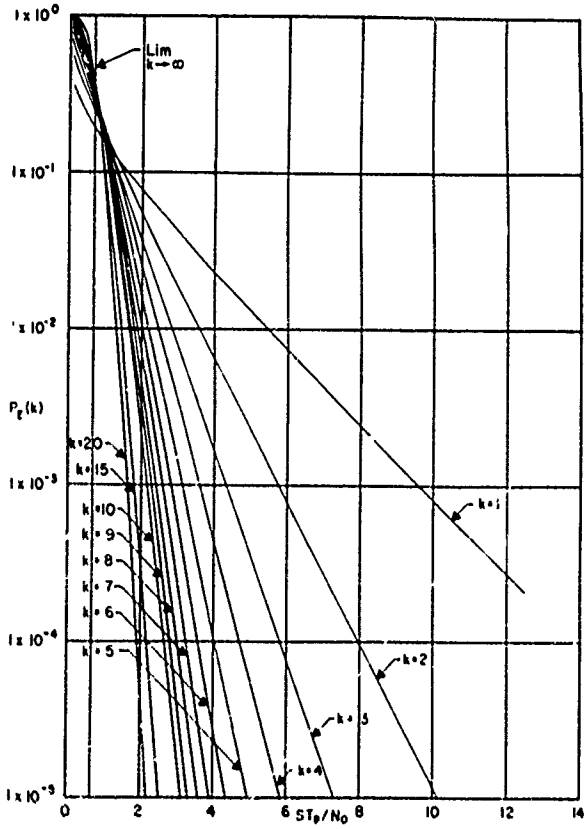

Figure A7. $P_E(k)$ as a Function of k, Showing That for All But Very Low Values of ST_B/N_0, P_E Decreases With M or k

$$\lim_{M \to \infty} P_C = \lim_{M \to \infty} \int_{-\infty}^{\infty} \frac{\exp[-v_1^2/2]}{\sqrt{2\pi}} \left[\operatorname{erf}\left(v_1 + \sqrt{\frac{2ST_\beta \log_2 M}{N_o}} \right) \right]^{M-1} dv_1$$

$$= \int_{-\infty}^{\infty} \frac{\exp[-v_1^2/2]}{\sqrt{2\pi}} \lim_{M \to \infty} \left[\operatorname{erf}\left(v_1 + \sqrt{\frac{2ST_\beta \log_2 M}{N_o}} \right) \right]^{M-1} dv_1 \qquad \text{(A25)}$$

Let $ST_B/N_o \to \beta$ and consider the limit of the logarithm of the expression in brackets of Eq. (A25)

$$\lim_{M \to \infty} \ln \left[\operatorname{erf} \left(v_1 + \sqrt{2\beta \log_2 M} \right) \right]^{M-1}$$

$$= \lim_{M \to \infty} \frac{\ln \left[\operatorname{erf} \left(v_1 + \sqrt{2\beta \log_2 M} \right) \right]}{\frac{1}{M-1}} \tag{A26}$$

Taking M as a continuous variable and using ℓ Hospital's rule produced the above limit as

$$= \begin{cases} -\infty & \text{if} \quad \beta < \ln 2 \\ \\ 0 & \text{if} \quad \beta > \ln 2 \end{cases} \qquad \text{for} \quad -\infty < v_1 < \infty \quad . \tag{A27}$$

Since this is the limit of the logarithm of the expression in brackets in Eq. (A25), the limit of the expression itself is

$$\lim_{M \to \infty} \left[\operatorname{erf} \left(v_1 + \sqrt{2\beta \log_2 M} \right) \right] = \begin{cases} 0 & \text{if} \quad \beta < \ln 2 \\ \\ 1 & \text{if} \quad \beta > \ln 2 \end{cases} \qquad \text{for } -\infty < v_1 < \infty \tag{A28}$$

which implies of Eq. (A25) that

$$\lim_{M \to \infty} P_C = \begin{cases} 0 & \text{if} \quad \beta = \dfrac{ST_\beta}{N_o} < \ln 2 \\ \\ 1 & \text{if} \quad \beta = \dfrac{ST_\beta}{N_o} > \ln 2 \end{cases} \tag{A29}$$

or in terms of error probability

$$\lim_{M \to \infty} P_E = \begin{cases} 1 & \text{if} \quad \dfrac{ST_\beta}{N_o} < \ln 2 \\ \\ 0 & \text{if} \quad \dfrac{ST_\beta}{N_o} > \ln 2 \end{cases} \tag{A30}$$

The stepwise limiting behavior is shown in Figure A7. The limiting behavior is particularly significant from an information theoretic viewpoint. Shanon's formula for the channel capacity of a channel of bandwidth W perturbed by additive Gaussian noise of uniform spectral density N_o is

$$C = W \log_2 \left(1 + \frac{S}{N_o W}\right) . \tag{A31}$$

This represents the maximum rate for error-free transmission in the limit as the message duration becomes infinite. Letting the bandwidth also approach infinity yields

$$\begin{aligned} \underset{W \to \infty}{C} &= \underset{W \to \infty}{\text{Lim}} \frac{S}{N_o} \frac{N_o W}{S} \log_2 \left(1 + \frac{S}{N_o W}\right) \\ &= \underset{W \to \infty}{} \frac{S}{N_o} \log_2 \left(1 + \frac{S}{N_o W}\right)^{\frac{N_o W}{S}} \\ &= \frac{S}{N_o} \log_2 e = \frac{S}{N_o \ln 2} \end{aligned} \tag{A32}$$

Thus from Eqs. (A30) and (A32) it follows that orthogonal codes achieve error-free transmission in the limit as $M \to \infty$ provided the data rate

$$R = \frac{1}{T_\beta} < \frac{S}{N_o \ln 2} = \underset{M \to \infty}{\text{Lim}} C . \tag{A33}$$

Of course, as $M \to \infty$, the message duration also approaches infinity since $T = T_\beta \log_2 M$. Also the bandwidth approaches ∞. Thus if no bandwidth constraint is placed on the code signal set, orthogonal codes exhibit the best possible behavior in the limit as M approaches infinity, since they provide error-free transmission rates up to channel capacity.

A2.7 The Sequential vs. Bit Error Probability

The significant measure of any communication system's performance depends upon its use. If a set of K-bit messages such as teletype or sampled data is to be sent, the sequence-error probability, that is, the probability that a decoding error was made in at least one bit in a sequence of K bits, is the important parameter. On the other hand, if a sequence of independent bits is sent, the bit-error probability should be determined.

For orthogonal coding, since all errors are equally probable, the expected number of bits in error when a K-bit coded word has been detected incorrectly is

$$\frac{\sum_{i=1}^{k} i \binom{k}{i}}{\sum_{i=1}^{k} \binom{k}{i}} = \frac{K\,2^{K-1}}{2^K - 1} \quad . \tag{A34}$$

Thus the conditional probability that a given bit is in error when the K-bit word within which it was encoded is incorrect is $2^{K-1}/(2^K - 1)$.

Thus in terms of the word-error probability $P_E(K)$ for a K-bit orthogonal code word, the bit-error probability[A2] is

$$P_B(K) = \frac{2^{K-1}}{2^K - 1}\, P_E(K) \tag{A35}$$

where $K = \log_2 M$. $P_B(k)$ is plotted in Figure A8 for various values of k.

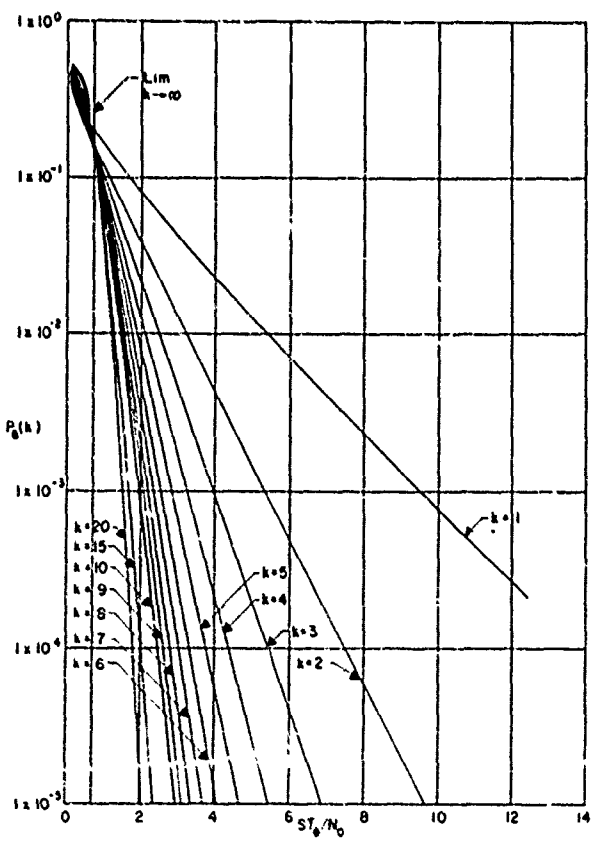

Figure A8. $P_B(k)$ as a Function of k

To conclude, symbol-error probability is related to binary-error probability by the formula

$$P_E(k) = (M - 1)\, P_{E,b} \tag{A36}$$

where $P_{E,b}$ is the binary-error probability; we now have

$$P_B(k) = \frac{2^{k-1}}{2^k - 1}\,(M - 1)\, P_{E,b} \tag{A37}$$

or

$$P_{E,b} = \frac{1}{2^{k-1}}\, P_B(k) \ . \tag{A38}$$

A2.8 M-ary Transmission Over Fading Channels

The following situation is considered. A transmitter sends one of M equal energy waveform over a linear, randomly time-varying channel. These waveforms are all frequency shifts of the same basic waveform. The channel is assumed to have stationary statistics and stationary behavior in frequency. The transmitted waveform will be corrupted in a statistically identical manner no matter which of the M frequency translates is sent. In addition to the time variations of the impulse response of the channel which cause a multiplication disturbance, the signal is also corrupted by additive white noise.

The receiver measures the received energy at each of the M frequencies and yields an output symbol corresponding to the largest measured value. These energy measurements are performed by correlating the received signal with the appropriate frequency translates of a finite set of orthonormal functions and then squaring and adding the correlator outputs. It will be assumed that the frequency separation of the M-possible transmitted waveforms is chosen sufficiently large so that the signal energy appearing in one set of correlator outputs as a result of transmitting a pulse at a different frequency can be ignored.

Under these conditions Pierce[A3] showed that, for a fixed transmitted energy per bit, as the alphabet size is allowed to become arbitrarily large, the probability of correct reception depends only on the noise density and the probability distribution of the energy per bit contained in the projection of the signal on the subspace spanned by the orthogonal functions sufficiently large, the error probability

---

A3. Pierce, J.N. (1966) Ultimate performance of M-ary transmission on fading channels, IEEE Trans. on Information Theory, Vol. 12, No. 1.

can be made as small as desired as long as the expectations of total received energy per bit exceeds (log 2) times the thermal noise density. The result is somewhat surprising in that it is independent of how badly the waveforms are corrupted by the multiplicative channel and of the exact fading distribution. It is also shown that this limiting capacity cannot be exceeded by any other type of combining method if the possible transmitted symbols are equiprobable. This is due to the fact that the performance achievable with the pure energy addition is the same as the performance attainable on the infinite-bandwidth nonfading channel.

A3. CONCLUDING REMARKS

There are additional factors which have been ignored in the present analysis which tend to limit the performance of actual communication systems. Among these are distortion in the received signal and inter symbol interference due to nonlinear delay, band limiting, and fluctuations in the gain of the medium that couples the transmitter to the receiver. Furthermore, the received signal is processed in less than ideal fashion by the detector due to imperfections in the hardware and time recovery. It is noted that all these factors ultimately manifest themselves at the detector simply as a perturbation in the position of the transmitted message point. As such, the effects are similar to those produced by the noise and may largely be compensated for by an additional margin of signal-to-noise ratio at the detector.

Conversely, we might say that some fraction of the total signal-to-noise ratio available at the detector is needed to compensate for effects of the type listed above which were not accounted for in the basic analysis. Consequently, only the remaining fraction of the signal-to-noise ratio is available for combating Gaussian noise. It is to be expected, therefore, that any predictions of the probability of error based on estimates of the total signal-to-noise ratio available at the detector will be unduly optimistic.

Appendix B

Preliminary Estimates of Error Rates in Asymmetrical, Doppler-Shifted, Transauroral, HF Propagation Paths

This appendix discusses the influence of a Doppler-shifted asymmetrical fading spectrum on the binary-error probabilities of incoherent FSK and differentially coherent phase-reversal matched-filter receivers.

B1. INTRODUCTORY REMARKS

Recently, Gupta[B1] has developed a complex filtering technique to simulate Asymmetrical Doppler-Shifted Narrow-Band Gaussian (ADS-NBG) channels. With this technique, it became possible to account for some additional channel parameters not considered before, such as the non-zero centroid and the skewness of fading spectrun. (or of the spectrum of the extended channel comprising the fading channel and receiver processing filters). Such spectral shapes are known to occur in troposcatter channels (see references in Gupta[B1]) and in the HF transauroral channels, of direct interest here.[B2]

B1. Gupta, A.K. (1979) Complex Envelope Simulation of Scatter Channels, presented at the IEEE National Telecommunications Conference, Washington, DC, November 27-29.

B2. Lomax, J.B. (1970) HF Propagation Dispersion, in "Phase and Frequency Instabilities in Electromagnetic Propagation," K. Davies, Editor, pp. 497-510, AGARD Conference Proceedings, Number Thirty-Three, Techvision Services, Slough, England.

The reasons for this non-zero Doppler shift and for the asymmetry in the spectrum of the baseband process are:

1. Doppler shift (see Figure B1). This may be due to "offset" in the tuning of the link's oscillators, to time changes in the refractive/scattering properties of the medium, etc.;

2. Asymmetry in the spectrum (see Figure B2). This may be due to geometrical asymmetries in the link (off-great-circle-path superimposition to the main path), asymmetries in the receiver filters (RF, IF or baseband), etc.

Theoretical interpretations developed thus far account only for the Doppler shift due to the frequency offset in the local oscillator at the receiver. No analytical description had been worked out before in order to account for the shift due to propagation medium and for the asymmetry in the received baseband spectrum.

Figure B3 shows a typical representation available in the literature for the received spectrum which is clearly symmetrical. This spectrum is then shifted by the "spectral-shift unit" to simulate the frequency offset in the receiver oscillators. In Gupta[B1] an analytical representation of the channel has been developed that fully accounts for all aspects of the two phenomena mentioned above, thereby removing the limitations in the present channel simulators.

In this section, we investigate the effects of non-zero centroid and skewness of the fading spectrum on the binary-error probabilities of incoherent and differentially coherent phase-reversal matched-filter receivers employing post-detection diversity combining.

In this analysis, flat fading is assumed. The expressions of the binary-error probabilities, derived here, are the extension of the results for the case of the Gaussian fading correlation function of Bello and Nelin.[B3] The general expressions for the binary-error probabilities of incoherent and differentially coherent matched-filter receivers are derived. In Bello and Nelin,[B3] the signal-to-noise degradation (due to fading) curves are given as a function of fading bandwidth. However, we also obtain the signal-to-noise degradation expressions due to non-zero centroid and skewness of the spectrum.

Recently Gupta[B4] has approximated an asymmetrical Doppler-shifted fading spectrum by its Edgeworth expansion. This expansion has the property that the second through fourth central spectral moments are identical to that of the spectrum approximated. If m_1 is the centroid (first simple moment) and m_2, m_3 and

---

B3. Bello, P.A. and Nelin, B.D. (1962) The influence of fading spectrum on the binary error probabilities of incoherent and differentially coherent matched filter receivers, IRE Trans. Communications Systems, Vol. CS-10, pp. 160-168, June.

B4. Gupta, A.K. (1979) Dissertation abstract, IEEE Transaction on Information Theory, November, p. 760.

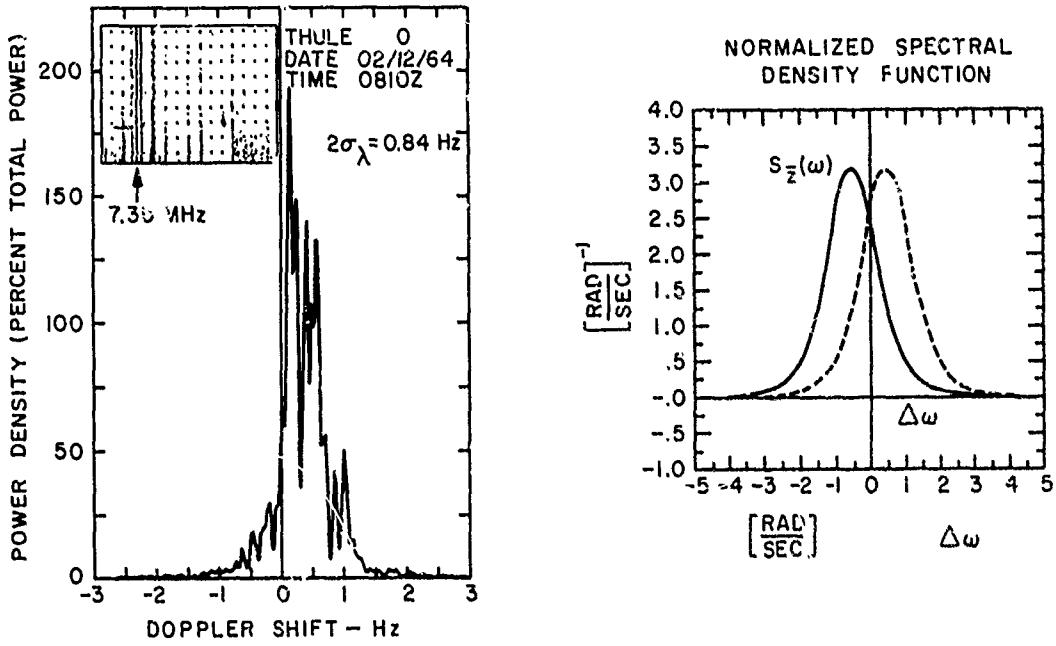

Figure B1. Doppler-Shifted Spectrum in a Transauroral Path and an Example of Computer Simulation

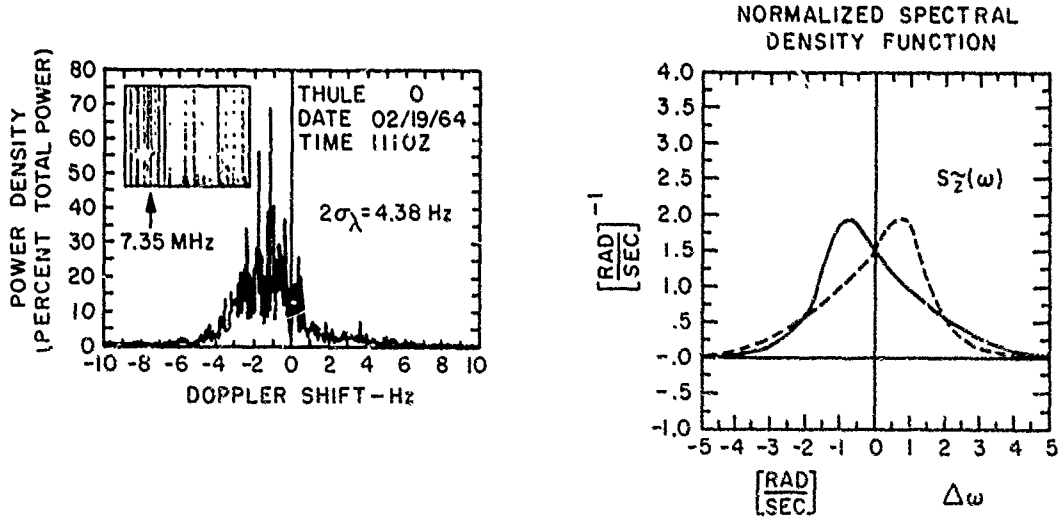

Figure B2. Example of Skewed Asymmetrical Spectrum in Transauroral Path and a Computer Simulation

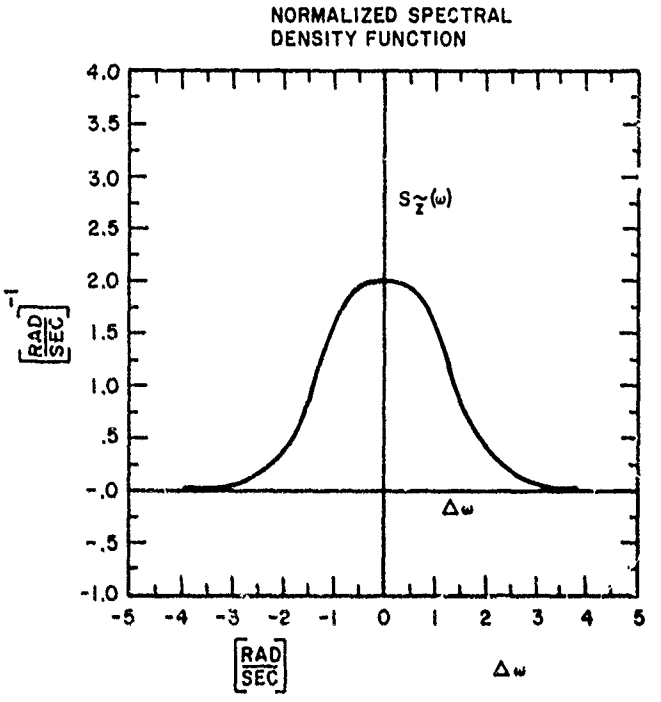

Figure B3. Typical Symmetrical Spectra Considered Thus Far in the Literature

m_4 are second through fourth central spectral moments, then the Edgeworth expansion of the spectrum $S(\omega)$ is given by

$$S(\omega) = 2\sigma^2\sqrt{\frac{2\pi}{m_2}}\ \exp\left\{-\frac{1}{2}\left(\frac{\omega - m_1}{\sqrt{m_2}}\right)^2\right\}\left\{1 + \frac{sk}{6}\,He_3\left(\frac{\omega - m_1}{\sqrt{m_2}}\right)\right\}$$

$$+ \frac{Ex}{24}\,He_4\left(\frac{\omega - m_1}{\sqrt{m_2}}\right) + \frac{s_k^2}{72}\,He_6\left(\frac{\omega - m_1}{\sqrt{m_2}}\right)\Bigg\}. \qquad \text{(B1)}$$

In Eq. (B1) $He_n(y)$ is a Hermite polynominal of degree n defined by $He_n(y) = \exp(y^2/2)(-d/dy)^n \exp(-y^2/2)$.

The Fourier inverse transform of $S(\omega)$ is given by

$$R_1(\tau) = 2\sigma^2 \exp\left(jm_1\tau - \frac{1}{2}m_2\tau^2\right)\left[1 - j\left(\frac{s_k m_2^{1.5}}{6}\right)\tau^3 + \frac{Ex\, m_2^2\tau^4}{24}\right.$$

$$\left. - \frac{s_k^2 m_2^3 \tau^6}{72}\right] \qquad \text{(B2)}$$

where, as in probabilistic analysis, s_k and Ex are the skew coefficient and the coefficient of excess respectively. For simplicity, we will assume that Ex = 0 and that the last term in the bracket of Eq. (B2) is negligible. Therefore $R_1(\tau)$ in Eq. (B2) will consist of the sum of two terms:

1. the term involving the Doppler-shifted but symmetric spectrum
2. the additive interference term involving the asymmetry of the spectrum.

Therefore $R_1(\tau)$ is approximated to

$$R(\tau) = 2\sigma^2 \exp\left(jm_1\tau - \frac{1}{2} m_2 \tau^2\right)[1 + a\tau^3] \tag{B3}$$

where $a = -j(s_k m_2^{1.5}/6)$ denotes the magnitude of interference.

Now we obtain the probability-of-error expressions for the incoherent FSK and differentially coherent phase-reversal matched-filter receivers. It is to be noted that in Bello and Nelin,[B3] m_1 and s_k are assumed to be zero.

B2. ERROR PROBABILITIES FOR INCOHERENT MATCHED FILTER RECEIVERS

A simplified block diagram of an incoherent matched-filter receiver is shown in Figure B4. Two matched filters are indicated, each matched to one of the two possible waveforms that are successively repeated to form the transmitted binary communication signal. The outputs of the matched filters are envelope-detected and subtracted. Diversity-combining is performed by summing the outputs for all the diversity receivers. It is assumed that bit synchronism exists. Based upon the stationary complex-valued Gaussian fading statistics, the error probability for a received binary waveform occupying the interval of bit duration are calculated in Bello and Nelin.[B3] For the case of FSK transmission, the transmitted waveforms are given by

$$S_o(t) = \sqrt{\frac{2E}{T}}\; e^{j\left(\frac{n\pi}{T}\right)}$$

$$S_1(t) = \sqrt{\frac{2E}{T}}\; e^{-j\left(\frac{n\pi}{T}\right)t} \quad ; \quad o < t < T \tag{B4}$$

where the integer n is equal to the frequency separation between the mark and space frequencies normalized with respect to the data rate 1/T.

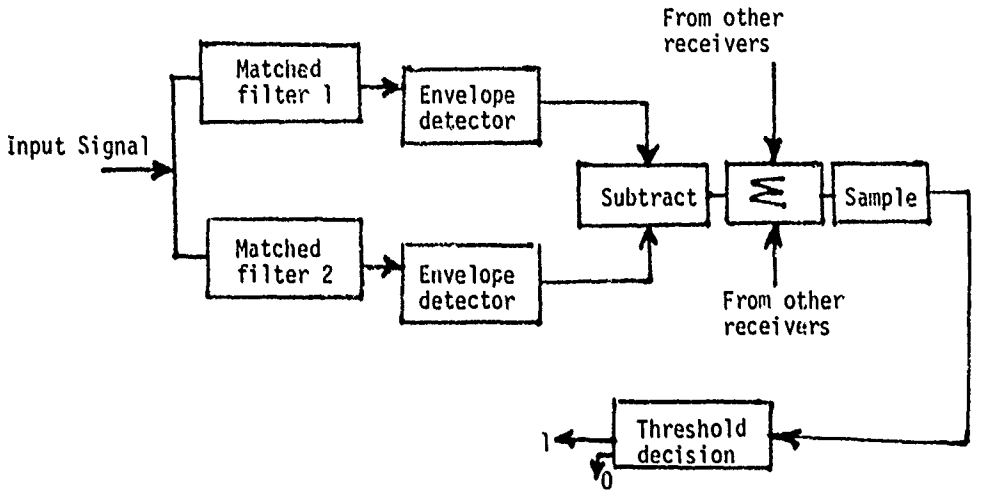

Figure B4. Block Diagram of an Incoherent Matched-Filter Receiver

For the waveforms given in Eq. (B4), the required m_{rs} and λ_{rs} functions, are defined in Bello and Nelin[B3] as

$$\lambda_{rs}(\tau) = \int_{o}^{T} S^{*}(t)\, S_{s}(t)\, S(t+\tau)\, S_{r}^{*}(t+\tau)\, dt \quad , \quad r, s = 0, 1$$

$$m_{rs} = \int_{-T}^{T} R(\tau)\, \lambda_{rs}(\tau)\, d\tau + 4\, N_{o}\, E_{rs} \quad , \tag{B5}$$

$$E_{rs} = \int_{o}^{T} S_{s}^{*}(t)\, S_{r}(t)\, dt \quad , \quad \text{where } N_{o} \text{ is the spectral density of additive noise.}$$

and S(t) could be either $S_1(t)$ or $S_o(t)$, are given by

$$\lambda_{oo}^{o}(\tau) = \frac{4E^2}{T}\left(1 - \frac{|\tau|}{T}\right) \qquad |\tau| < T$$

$$\lambda_{1o}^{o}(\tau) = \frac{4E^2}{2jn\pi T}\left(1 - e^{\frac{2jn\pi}{T}\tau}\right) \quad , \quad 0 < \tau < T$$

$$= \frac{4E^2}{2jn\pi T}\left(e^{\frac{2jn\pi}{T}\tau} - 1\right) \qquad -T < \tau < 0$$

$$\lambda_{11}^{o}(\tau) = \frac{4E^2}{T}\left(1 - \frac{|\tau|}{T}\right) e^{\frac{2jn\pi}{T}\tau} \quad , \quad |\tau| < T$$

$$\lambda_{oo}^{1}(\tau) = \text{complex conjugate of } \lambda_{11}^{o}(\tau) \text{ or } [\lambda_{11}^{o}(\tau)]^*$$

$$\lambda_{11}^{1}(\tau) = \lambda_{oo}^{o}(\tau) \ .$$

$$\lambda_{1o}^{1}(\tau) = \frac{4E^2}{2jn\pi T}\left[e^{\frac{-2jn\pi}{T}\tau} - 1\right] \quad , \quad 0 < \tau < T$$

$$- \frac{4E^2}{2jn\pi T}\left[1 - e^{\frac{-2jn\pi}{T}\tau}\right] \quad , \quad -T < \tau < 0 \ . \tag{B6}$$

In Eq. (B6), the superscript "o" denotes $S(t) = S_o(t)$, $o < t < T$, "1" denotes $S(t) = S_1(t)$, $o < t < T$ and

$$E = \frac{1}{2}\int_o^T |S_o(t)|^2 \, dt = \frac{1}{2}\int_o^T |S_1(t)|^2 \, dt \ . \tag{B7}$$

Substituting $R(\tau)$ in Eq. (B3) in m_{rs} Eq. (B5), one obtains (letting $\rho = \sigma^2 E/N_o$)

$$m_{oo}^{o}(\tau) = 16\, E^2 \sigma^2 \left[\frac{1}{2\rho} + \frac{1}{2T}\left\{\frac{2\cos(m_1 T)\, e^{-(1/2)m_2 T^2} - 2}{m_2 T}\right\}\right.$$

$$\left. + \left(1 - \frac{jm_1}{m_2 T}\right) I_o + \left(1 + \frac{jm_1}{m_2 T}\right) I_o \,\middle|_{m_1 \text{ replaced by } -m_1}\right]$$

$$+ \frac{8E^2\sigma^2}{T}\, a \left[\frac{-10jm_1 m_2 + 2jm_1^3}{m_2^4 T} + I_1 - I_1 \,\middle|_{m_1 \text{ replaced by } -m_1}\right.$$

$$\left. + I_2 - I_2 \,\middle|_{m_1 \text{ replaced by } -m_1}\right] \tag{B8}$$

In Eq. (B8)

$$I_o = \int_o^T \exp\left(jm_1\tau - \frac{1}{2}\, m_2\tau^2\right) d\tau = \frac{1}{2}\sqrt{\frac{2\pi}{m_2}}\; e^{-m_1^2/2m_2}$$

$$\operatorname{erf}\left(\sqrt{\frac{m_2}{2}}\, T - \frac{jm_1}{\sqrt{2m_2}}\right) - \operatorname{erf}\left(\frac{-jm_1}{\sqrt{2m_2}}\right)\Bigg] \quad ,$$

$$I_1 = \left(\frac{3jm_1}{m_2^2} - \frac{jm_1^3}{m_2^3} - \frac{3}{m_2^2 T} + \frac{6m_1^2}{m_2^3 T} - \frac{m_1^4}{Tm_2^4}\right) I_o$$

$$I_2 = \exp\left(jm_1 T - \frac{1}{2}\, m_2 T^2\right)\left\{\frac{1}{m_2} + \frac{5jm_1}{m_2^3 T} - \frac{jm_1^3}{m_2^4 T}\right\} \tag{B9}$$

and

$$m_{11}^o = m_{oo}^o\Big|_{m_1 \text{ replaced by } m_1 + \frac{2\pi n}{T}} \tag{B10}$$

and

$$m_{10}^o = \frac{4E^2\sigma^2}{jn\pi T}\left[\left(I_o - I_o\Big|_{\substack{m_1 \text{ replaced by} \\ m_1 + \frac{2n\pi}{T}}} + I_o\Big|_{\substack{m_1 \text{ replaced by} \\ -\left(m_1 + \frac{2n\pi}{T}\right)}} - I_o\Big|_{\substack{m_1 \text{ replaced} \\ \text{by } -m_1}}\right)\right.$$

$$\left. + a\left\{I_3 + I_3\Big|_{\substack{m_1 \text{ replaced} \\ \text{by } -m_1}} - I_3\Big|_{\substack{m_1 \text{ replaced} \\ \text{by } m_1 + \frac{2n\pi}{T}}} - I_3\Big|_{\substack{m_1 \text{ replaced by} \\ -\left(m_1 + \frac{2n\pi}{T}\right)}}\right\}\right] \tag{B11}$$

where

$$I_3 = \frac{2m_2 - m_1^2}{m_2^3} - \left[\frac{2m_2 - m_1^2 + T^2 m_2^2 + jm_1 m_2 T}{m_2^3}\right] \cdot$$

$$\cdot \exp\left(jm_1 T - \frac{1}{2} m_2 T^2\right) + \left(\frac{jm_1}{m_2}\right)\left(\frac{2m_2 - m_1^2}{m_2^2}\right) I_o$$

Similarly one can obtain

$$m_{oo}^1 = m_{11}^o \Big|_{\substack{n \text{ replaced by} \\ -n}} \tag{B12}$$

$$m_{11}^1 = m_{oo}^o \tag{B13}$$

and

$$m_{10}^1 = \frac{4E^2\sigma^2}{jn\pi T}\left[\left(I_o\Big|_{\substack{m_1 \text{ replaced} \\ \text{by } m_1 - \frac{2n\pi}{T}}} - I_o + I_o\Big|_{\substack{m_1 \text{ replaced} \\ \text{by } -m_1}} - I_o\Big|_{\substack{m_1 \text{ replaced} \\ \text{by } -\left(m_1 - \frac{2n\pi}{T}\right)}}\right)\right.$$

$$\left. + a\left(I_3\Big|_{\substack{m_1 \text{ replaced} \\ \text{by } m_1 - \frac{2n\pi}{T}}} - I_3\Big|_{\substack{m_1 \text{ replaced} \\ \text{by } -m_1}} - I_3 + I_3\Big|_{\substack{m_1 \text{ replaced by} \\ -\left(m_1 - \frac{2n\pi}{T}\right)}}\right)\right] \tag{B14}$$

B3. PROBABILITY OF ERROR FORMULATION FOR INCOHERENT RECEPTION

To compute the probability of error, one requires[B3] parameter r as

$$r = \frac{2(m_{11} - m_{oo})}{\sqrt{(m_{11} - m_{oo})^2 + 4\left(m_{11}m_{oo} - |m_{10}|^2\right)} - (m_{11} - m_{oo})} \tag{B15}$$

Depending upon the superscripts on $m_{r,s}(r, s = o, 1)$, one obtains r_o, r_1. The significance of r_o and r_1 will be outlined below.

The probability of error expression for zero-fading bandwidth and square-law combined diversity was derived by Pierce.[B5] If p_1 is the probability that a "o" is printed given that a "1" is sent and p_o is the probability that a "1" is printed given that a "o" is sent, then for zero-fading bandwidth $p_o = p_1 = p$ where

$$p = \sum_{m=o}^{M-1} \frac{(2M - 1)!(-1)^m}{(M - 1)!\,(M - 1 - m)!\,m!\,(M + m)}\,(2 + \rho)^{-M-m} \tag{B16}$$

In Eq. (B16), M is the order of diversity and ρ is the ratio of the signal power in data channel and the noise power in data channel. The noise power in the data channel is defined as the noise power in a rectangular bandpass filter of unity gain and bandwidth $1/T$. At a large signal-to-noise ratio, SNR, the leading terms predominate and we have, to a good approximation

$$p = \frac{(2M - 1)!}{(M - 1)!\,M!}\,(\rho)^{-M} \quad , \quad \rho \gg 1 \quad . \tag{B17}$$

For the case of general fading and general binary signals,[B3] one may determine p_1 by using an "equivalent" signal-to-noise ratio ρ_1 in the zero-fading bandwidth expression for p_1 (Eqs. (B16) or (B17)). This equivalent SNR is given by

$$\rho_1 = r_1 \quad . \tag{B18}$$

Similarly p_o for general fading can be determined by using an equivalent SNR ρ_o, in the slow fading expression for p_1 where

$$\rho_o = \frac{r_o}{1 + r_o} \tag{B19}$$

In general $p_o \neq p_1$. Thus in the presence of an asymmetrical spectrum and/or a non-zero centroid, asymmetric binary channel may result.

B5. Pierce, J. N. (1958) Theoretical Diversity Improvement in Frequency-Shift Keying, Proc. IRE, Vol. 45, pp. 903-910, May.

B4. ERROR PROBABILITIES FOR A PHASE-REVERSAL KINEPLEX SYSTEM

A simplified block diagram of the differentially coherent matched-filter receiver is shown in Figure B5. It is assumed that only two possible pulses $S_1(t)$, $S_0(t)$ are transmitted as with the incoherent matched-filter receiver. However, the transmitted bit is encoded into the change or lack of change of successive adjacent pulses. Thus a transmission of the pairs $S_1(t)$ or $S_0(t)$, $S_1(t)$ denotes a "0", say, while the pairs $S_1(t)$, $S_1(t)$ and $S_0(t)$, $S_0(t)$ denote a "1". The receiver consists in part of two separate coherent matched-filter receivers with filters matched to waveforms S_1 and S_0 but differing by an input delay of one band duration. Thus, the two receivers are operating upon adjacent bands. The actual detector output is obtained by using the output of one coherent receiver as a reference for the other. In the special case when the pulses $S_0(t)$, $S_1(t)$ are ± 1 over the band duration, the differentially coherent system specializes to the differentially coherent phase-reversal Kineplex system.

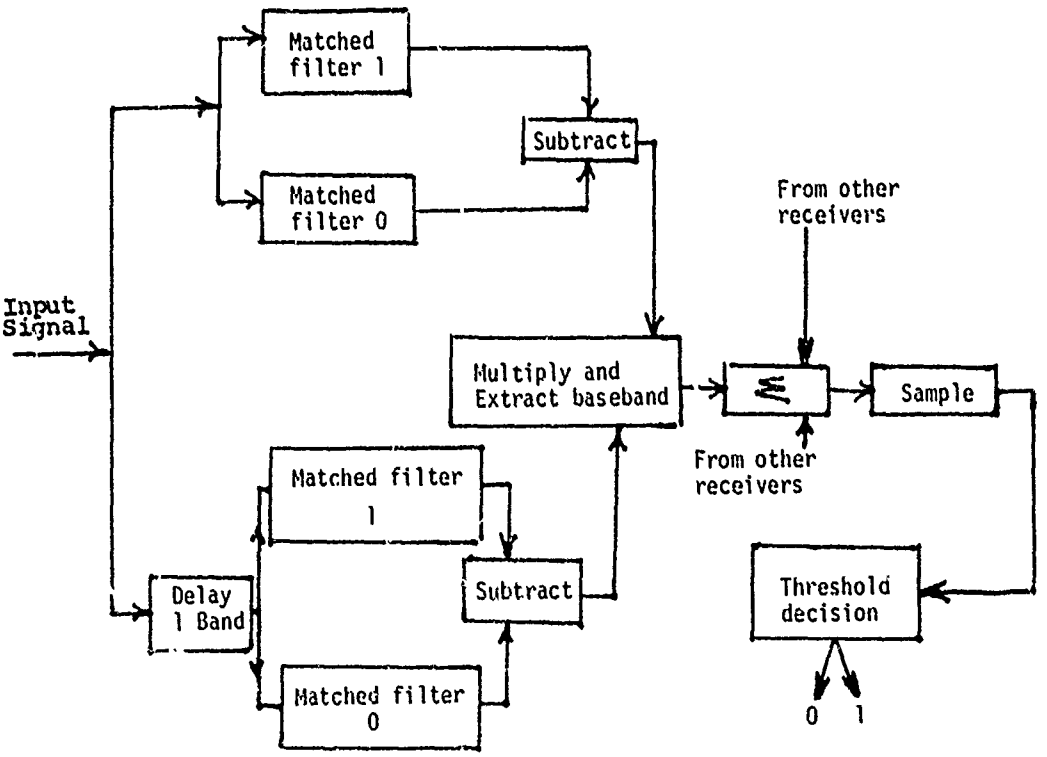

Figure B5. Block Diagram of a Differentially Coherent Matched-Filter Receiver

In the following discussion, we will compute the expression of the probability of error for DPSK or phase-reversal Kineplex system. Due to antipodal nature of binary waveforms

$$S_1(t) = \sqrt{\frac{2E}{T}} \quad \text{and} \quad S_o(t) = -S_1(t) \quad \text{for} \quad o < t < T \ , \tag{B20}$$

binary symmetric operation will exist (that is, $p_o = p_1$) for all fading correlation functions. As in the FSK incoherent case, the following results are the extension of the results given in Bello and Nelin.[B3] The reader is referred to Bello and Nelin[B3] for a detailed analysis.

For the case of general fading and general binary signals, p_o and p_1 can be determined, similar to the FSK case, by using "equivalent" SNR in Eqs. (B16) or (B17). The error-probability expression in Eq. (B16) was derived for noncoherent FSK reception with "square law" diversity combining and slow fading (zero-fading bandwidth). The equivalent SNR ρ_{11} is given[B3] as

$$\rho_{11} = \frac{2(m_{1o} + m_{1o}^*)}{\sqrt{(m_{1o}+m_{1o}^*)^2 + 4(m_{11}m_{oo} - |m_{1o}|^2) - (m_{1o} + m_{1o}^*)}} \tag{B21}$$

where

$$m_{oo} = m_{11} = 32\,E^2\sigma^2 \left[\frac{1}{\rho} + \frac{1}{T} \left\{ \frac{2\cos(m_1 T)\, e^{-(1/2)m_2 T^2} - 2}{m_2 T} + \left(1 - \frac{jm_1}{m_2 T}\right) I_o \right.\right.$$

$$\left. + \left(1 + \frac{jm_1}{m_2 T}\right) I_o \right|_{\substack{m_1 \text{ replaced} \\ \text{by } -m_1}} \Bigg\}$$

$$+ \frac{a}{T} \left\{ \frac{-10jm_1m_2 + 2jm_1^3}{m_2^4 T} + I_1 - I_1 \right|_{\substack{m_1 \text{ replaced} \\ \text{by } -m_1}} + I_2 - I_2 \Big|_{\substack{m_1 \text{ replaced} \\ \text{by } -m_1}} \Bigg\}$$

(B22)

and letting $m_1' = m_1 + j m_2 T$

$$m_{1o} = \frac{32 E^2 \sigma^2}{T} \exp\left(j m_1 T - \frac{1}{2} m_2 T^2\right) \left\{ \left[\frac{2 \cos (m_1' T)\, e^{-(1/2) m_2 T^2} - 2}{m_2 T} \right.\right.$$

$$+ \left(1 - \frac{j m_1'}{m_2 T}\right) I_o \Big|_{\substack{m_1 \text{ replaced} \\ \text{by } m_1'}} + \left(1 + \frac{j m_1'}{m_2 T}\right) I_o \Big|_{\substack{m_1 \text{ replaced} \\ \text{by } -m_1'}} \left.\right]$$

$$+ \frac{a}{T} \left[\left(\frac{2 j m_1'^3}{m_2^4} - \frac{10 j m_1'}{m_2^3} + \frac{6 m_1'^2}{m_2^3} - \frac{2T^3}{m_2} - \frac{12T}{m_2^2} - \frac{6 j T^2 m_1'}{m_2^2} \right) \right.$$

$$+ \left(\frac{T^3}{m_2} + \frac{3 j m_1' T^2}{m_2^2} + \frac{7T}{m_2^2} + \frac{5 j m_1'}{m_2^3} - \frac{3 m_1'^2 T}{m_2^3} - \frac{j m_1'^3}{m_2^4} \right)$$

$$\cdot \exp (j m_1' T - \tfrac{1}{2} m_2 T^2)$$

$$+ \left(\frac{T^3}{m_2} + \frac{3 j m_1^2 T^2}{m_2^2} + \frac{5T}{m_2^2} + \frac{5 j m_1'}{m_2^3} - \frac{3 T m_1'^3}{m_2^3} - \frac{j m_1'^3}{m_2^4} \right)$$

$$\cdot \exp (-j m_1' T - \tfrac{1}{2} m_2 T^2)$$

$$+ \left(T^4 + \frac{2 j m_1'}{m_2} T^3 - \frac{6 j m_1' T}{m_2^2} - \frac{3}{m_2^2} + \frac{6 m_1'^2}{m_2^3} + \frac{2 j T m_1'^3}{m_2^3} - \frac{m_1'^4}{m_2^4} \right)$$

$$I_o \Big|_{\substack{m_1 \text{ replaced} \\ \text{by } m_1'}}$$

$$+\left(T^4+\frac{4jm_1'}{m_2}T^3+\frac{12jm_1'T}{m_2^2}+\frac{3}{m_2^2}-\frac{6m_1'^2}{m_2^3}+\frac{6T^2}{m_2}-\frac{6m_1'^2}{m_2^2}T^2\right.$$

$$\left.\left.-\frac{4jm_1'^3}{m_2^3}T+\frac{m_1'^4}{m_2^4}\right)I_o\left|\begin{array}{l}m_1 \text{ replaced}\\ \text{by } -m_1'\end{array}\right.\right]\Bigg\} \qquad \text{(B23)}$$

To recapitulate, the probability of error for a skewed and Doppler-shifted channel (incoherent FSK modulation), can be computed as follows:

1st Step—Compute the Doppler shift of the received spectrum. This is called m_1 (rad sec^{-1});

2nd Step—Compute the parameter a, as defined by

$$a = -j\left(\frac{s_k\, m_2^{1.5}}{6}\right)$$

where

m_2 is the fading rate (= Doppler spread of the received spectrum, in rad/sec)

s_k is the skewness of the spectrum, as defined in Eq. (22), Section 2.4.2.

3rd Step—Compute the quantities $m_{r,s}$ (where r and s acquire the values 0 and 1) by using Eqs. (B10) through (B14). (Note that $m^o_{r,s}$ refers to bit "0" and $m^1_{r,s}$ refers to bit "1").

4th Step—Compute the function r from Eq. (B15).

5th Step—Compute ρ_1 and ρ_o from Eqs. (B18) and (B19) (ρ_o refers to bit "0" and ρ_1 refers to bit "1").

6th Step—Compute p_1 and p_o (equivalent binary probability of error) from Eqs. (B16) or (B17) (again, p_o refers to bit "0" and p_1 refers to bit "1").

Similar to what has been just described for the incoherent FSK modulation case, the probability of error can be computed for the case of a coherent-differential Kineplex system. Since, in this case, p_o and p_1 for all shapes of the fading spectrum, the computation of either one of them is sufficient. First, m_{11}, m_{10} and m_{oo} are computed by using the Eqs. (B22) and (B23) as a function of the spectral parameters. Then, ρ_{11} is computed from Eq. (B21). Since ρ_{11} can be thought of as an "equivalent signal-to-noise ratio," the probability of error can be computed from the Pierce formula, given in Eq. (B16).